The transition state and regulation of γ-TuRC-mediated microtubule nucleation revealed by single molecule microscopy

Akanksha Thawani[1], Michael J Rale[2], Nicolas Coudray[3], Gira Bhabha[3], Howard A Stone[4], Joshua W Shaevitz[5,6], Sabine Petry[2,*]

[1]Department of Chemical and Biological Engineering, Princeton University, Princeton NJ, USA

[2]Department of Molecular Biology, Princeton University, Princeton NJ, USA

[3]Department of Cell Biology, New York University School of Medicine, New York NY, USA

[4]Department of Mechanical and Aerospace Engineering, Princeton University, Princeton NJ, USA

[5]Lewis-Sigler Institute for Integrative Genomics and [6]Department of Physics, Princeton University, Princeton NJ, USA

* Correspondence: spetry@princeton.edu

Abstract

Determining how microtubules (MTs) are nucleated is essential for understanding how the cytoskeleton assembles. While the MT nucleator, γ-tubulin ring complex (γ-TuRC) has been identified, precisely how γ-TuRC nucleates a MT remains poorly understood. Here we developed a single molecule assay to directly visualize nucleation of a MT from purified *Xenopus laevis* γ-TuRC. We reveal a high γ-/αβ-tubulin affinity, which facilitates assembly of a MT from γ-TuRC. Whereas spontaneous nucleation requires assembly of 8 αβ-tubulins, nucleation from γ-TuRC occurs efficiently with a cooperativity of 4 αβ-tubulin dimers. This is distinct from pre-assembled MT seeds, where a single dimer is sufficient to initiate growth. A computational model predicts our kinetic measurements and reveals the rate-limiting transition where laterally-associated αβ-tubulins drive γ-TuRC into a closed conformation. Putative activation domain of CDK5RAP2, NME7 and TPX2 do not enhance γ-TuRC-mediated nucleation, while XMAP215 drastically increases the nucleation efficiency by strengthening the longitudinal γ-/αβ-tubulin interaction.

Introduction

Microtubules (MTs) enable cell division, motility, intracellular organization and transport. Half a century ago, MTs were found to be composed of αβ-tubulin dimers, yet how MTs are nucleated in the cell to assemble the cellular structures remains poorly understood[1,2]. The universal nucleator, γ-tubulin efficiently nucleates MTs *in vivo*[3–5] by forming a 2.2 megadalton, ring-shaped complex with γ-tubulin complex proteins (GCPs), known as the γ-Tubulin Ring Complex (γ-TuRC)[6–11]. Structural studies[9,12–15] have revealed that γ-TuRC positions a lateral array of 13 γ-tubulin molecules that are thought to template MT assembly by binding αβ-tubulin dimers and promoting their lateral interaction to result in nucleation of a MT[9,12,16–18]. Despite this model being widely accepted, MT nucleation from γ-TuRC molecules has not been directly visualized in real time and the dynamics of nucleation of a MT from αβ-tubulin dimers remains to be characterized. In particular, determining the critical nucleus, i.e., the rate-limiting transition state, for γ-TuRC nucleation is of tremendous interest, as it has important implications for how MT nucleation is spatiotemporally regulated in the cell (Fig. 1A).

In the absence of γ-TuRC, MTs can also nucleate spontaneously from high concentrations of αβ-tubulin *in vitro*. In this process, which displays a nucleation barrier, the assembly of many αβ-tubulin dimers is thought to occur to form lateral and longitudinal contacts[19–22]. It has long been speculated whether γ-TuRC-mediated nucleation occurs similarly, or follows a distinct reaction pathway[18,22–25]. Moreover, the structure of native γ-TuRC shows an *open* conformation where adjacent γ-tubulin do not form a lateral interaction[13–15], raising further questions on how the conformational mismatch impacts γ-TuRC's nucleation activity (Fig. 1A). It has been widely proposed that γ-TuRC may transition to a *closed* conformation during MT assembly to match the geometry of αβ-tubulin dimers arranged laterally in the MT lattice[10,13]. This transition could further

51 provide a mode of regulation through several putative MT-associated proteins (MAPs) that have
52 been proposed to promote a closed conformation of γ-TuRC's[10,13,18] and regulate γ-TuRC's
53 nucleation activity[9,10,13,26–28]. Finally, the interaction affinity between γ-tubulin and αβ-tubulin and
54 its role on MT nucleation remain unknown[18,23] (Fig. 1A).

55 Investigating the molecular biophysics of MT nucleation by γ-TuRC at the single-molecule
56 level and with computational modeling have the potential to address these questions. By
57 identifying transition states and reaction intermediates during the γ-TuRC-mediated nucleation
58 reaction, important insights into the dynamics of MT nucleation can be revealed. Yet, technical
59 challenges in both purifying γ-TuRC at high yield, as well as the inability to visualize MT
60 nucleation events from individual γ-TuRC molecules in real time and at high resolution, have
61 posed limitations. In this work, we overcome these longstanding challenges to reconstitute MT
62 nucleation from γ-TuRC and visualize the reaction live at the resolution of single molecules. We
63 use computational models to gain further mechanistic insights into MT nucleation and to identify
64 the molecular composition and arrangement of the rate-limiting transition state in γ-TuRC. Finally,
65 we examine the roles of various MAPs, particularly the co-nucleation factor XMAP215, in γ-
66 TuRC-mediated MT nucleation and comprehensively examine how specific biomolecular features
67 govern how MT nucleation from γ-TuRC occurs.
68

Results

Visualizing microtubule nucleation from γ-TuRC with single molecule microscopy

To study how γ-TuRC nucleates a MT, we purified endogenous γ-TuRC from *Xenopus* egg extracts and biotinylated the complexes to immobilize them on functionalized glass (Fig. 1-figure supplement 1A-B). Upon perfusing fluorescent αβ-tubulin, we visualized MT nucleation live with total internal reflection fluorescence microscopy (TIRFM) (Fig. 1B). Strikingly, MT nucleation events occurred specifically from γ-TuRC molecules that were either unlabeled (Fig. 1B and Video 1) or fluorescently labelled during the purification (Fig. 1-figure supplement 1C and Video 2). Kymographs revealed that single, attached γ-TuRC molecules assembled αβ-tubulin into a MT *de novo* starting from zero length within the diffraction limit of light microscopy (Fig. 1C), ruling out an alternative model where MTs first spontaneously nucleate and then become stabilized via γ-TuRC. By observing fiduciary marks on the MT lattice (Fig. 1C) and generating polarity-marked MTs from attached γ-TuRC (Fig. 1- figure supplement 1D), we show that γ-TuRC caps the MT minus-end while only the plus-end polymerizes, as supported by previous works[16,17]. Notably, the detachment of γ-TuRC molecules and re-growth of the MT minus-ends were not observed, and γ-TuRC persists on the MT minus-end for the duration of our experiments. Altogether, our results demonstrate that γ-TuRC directly nucleates a MT.

Molecular composition of the transition state during γ-TuRC-mediated nucleation

To determine how γ-TuRC nucleates a MT, we measured the kinetics of MT nucleation for a constant density of γ-TuRC molecules and increasing αβ-tubulin concentrations (Fig. 2A and Video 3). γ-TuRCs nucleated MTs starting from 7 μM tubulin (Fig. 2A-B), which is higher than

92 the minimum tubulin concentration (C^*) needed for growth from a pre-formed MT plus-end (C^*
93 = 1.4 μM, Fig. 2B). Furthermore, the number of MTs nucleated from γ-TuRC increased non-
94 linearly with αβ-tubulin concentration as opposed to the linear increase in MT's growth speed with
95 tubulin concentration (Fig. 2B). By measuring the number of MTs nucleated over time with
96 varying αβ-tubulin concentration (Fig. 2C), we calculated the rate of MT nucleation. The power-
97 law dependence on αβ-tubulin concentration (Fig. 2D) yields the number of tubulin dimers, 3.9 ±
98 0.5, that compose the rate-limiting, transition state during MT assembly from γ-TuRC (Fig. 2D).
99 Thus, the cooperative assembly of nearly 4 αβ-tubulin subunits on γ-TuRC represents the most
100 critical, rate-limiting step in MT nucleation.
101
102 **γ-TuRC-mediated nucleation is more efficient than spontaneous nucleation**
103 Based on the traditional assay where MTs are nucleated, fixed and visualized, a large variability
104 in γ-TuRC's MT nucleation activity has been observed. With this setup, γ-TuRC has often been
105 reported to be a poor nucleator with a similar activity as spontaneous MT nucleation[6,8–11,13,14,26,29].
106 With our live TIRFM assay, we aimed to quantitatively compare the efficiency of γ-TuRC-
107 mediated MT nucleation with spontaneous MT nucleation (Fig. 3A). In contrast to γ-TuRC-
108 mediated nucleation, a higher concentration of 14 μM tubulin was required for any spontaneous
109 assembly of MTs, after which both the plus- and minus-ends polymerize (Fig. 3B, Fig. 3-figure
110 supplement 1A and Video 4). The number of MTs assembled as a function of the αβ-tubulin
111 concentration displayed a power-law dependence with an even larger exponent of 8.1 ± 0.9 (Fig.
112 3C), indicating a highly cooperative process that requires 8 αβ-tubulin dimers in a rate-limiting
113 intermediate, in agreement with previous reports[19,20]. Further, direct comparison and measurement
114 of spontaneous MT assembly with γ-TuRC-mediated nucleation (Fig. 3- figure supplement 1B-C)

115 clearly demonstrates that γ-TuRC nucleates MTs significantly more efficiently. Notably, specific
116 attachment of γ-TuRC to coverslips is also required to observe the nucleation activity (Fig. 3-
117 figure supplement 1C). In sum, γ-TuRC-mediated nucleation occurs efficiently and its critical
118 nucleus requires less than half the number of αβ-tubulin dimers compared to spontaneous
119 assembly.
120
121 **Contribution of end architecture of γ-TuRC to microtubule nucleation**
122 The MT plus-end architecture, which ranges from blunt to tapered, is critical for MT
123 polymerization dynamics[30–32], and was recently proposed to be critical for MT nucleation[25]. To
124 investigate how the blunt-end geometry of γ-TuRC contributes to its nucleation kinetics and
125 transition state, we generated Alexa-568 labelled, stable MT seeds with blunt ends as described
126 previously[25] and compared MT assembly from seeds upon addition of Cy5-labelled αβ-tubulin
127 dimers (Fig. 3C) side-by-side with γ-TuRC-mediated nucleation. At a minimum concentration of
128 2.45μM, approaching the critical concentration needed for polymerization of a MT plus-end, a
129 large proportion of pre-formed MT seeds assemble MTs (Fig. 3C-D, Fig. 3-figure supplement 1D
130 and Video 5). At 7 μM tubulin, the rate of assembly of MTs from the blunt seeds increased to reach
131 the maximum rate that could be temporally resolved, i.e. all of the MT seeds immediately
132 assembled a MT (Fig. 4D). This is in contrast to the kinetics of γ-TuRC-mediated nucleation at
133 7μM tubulin concentration, where minimal nucleation activity was observed (Fig. 2C-D). The
134 measured reaction kinetics as a function of the αβ-tubulin concentration (Fig. 3D) was used to
135 obtain the power-law of the nucleation rate, 1 ± 0.3 (Fig. 3E). This suggests that in our assay
136 condition, blunt MT ends assemble tubulin dimers into the MT lattice non-cooperatively. In other
137 words, the addition of a single αβ-tubulin dimer suffices to overcome the rate-limiting barrier,

138 which also occurs during the polymerization phase of MT dynamics. Notably, when this
139 experiment was replicated with the coverslip preparation and assay conditions reported
140 previously[25], a high concentration of tubulin was necessary for seeds to assemble MTs in
141 agreement with the previous work[25]. However, our assay conditions, that were used to compare
142 seed-templated MT assembly with γ-TuRC-mediated nucleation side-by-side, result in a low,
143 minimal tubulin concentration that is needed for seed-mediated MT assembly. To conclude, while
144 the γ-TuRC positions a blunt plus-end of γ-tubulins, the contribution of this specific end
145 architecture in defining the kinetics of nucleation from γ-TuRC and its transition state is minimal.

146 In summary, because γ-TuRC positions an array of γ-tubulins at its nucleation interface
147 that are thought to stabilize intrinsically weak, lateral αβ/αβ-tubulin interaction[9,10,13,14,18,22,23], MT
148 nucleation by γ-TuRC has been proposed to function similar to polymerization of a MT end. Here
149 we show several lines of evidence that γ-TuRC-mediated nucleation has distinct characteristics
150 from MT polymerization and assembly from blunt MT seeds. While growth speed of MTs
151 nucleated from γ-TuRC or templated from MT seeds is similar (Fig. 3-figure supplement 1D), γ-
152 TuRC molecules do not nucleate MTs at low tubulin concentration where MT polymerization can
153 occur. Further increasing tubulin concentration results in a non-linear increase in the number of γ-
154 TuRCs molecules that nucleate MT, as opposed to a linear increase in rate of assembly from seeds.
155 At the highest tubulin concentrations, approximately 10-15% of γ-TuRCs nucleate MTs in the
156 TIRF assays. While these results were obtained with endogenous γ-TuRCs purified from cytosol,
157 it remains possible that specific factors at MTOCs can modulate γ-TuRC's conformation and
158 kinetics. In summary, the rate-limiting transition state on γ-TuRC is composed of four αβ-tubulin
159 dimers in contrast with MT polymerization where one tubulin dimer suffices to overcome the
160 slowest step.

161

162 **γ-tubulin has a high affinity for αβ-tubulin**

163 Consequently, specific biochemical features of γ-TuRC must govern its nucleation activity and the
164 composition of the transition state during nucleation. To address this, we first measured the
165 interaction affinity between γ-tubulin and αβ-tubulin, which could provide insight into γ-TuRC's
166 nucleation interface and its role in MT nucleation. To begin, we performed size-exclusion
167 chromatography where γ-tubulin alone elutes as a broad peak in fractions I-N (Fig. 4A (i), pseudo-
168 colored profile in green) at low concentration. Interestingly, in the presence of either 10 μM (low)
169 or 35 μM (high) concentrations of αβ-tubulin, the γ-tubulin binds to αβ-tubulin (pseudo-colored
170 profile in cyan) and elutes earlier, specifically in fraction H (Fig. 4A (ii-iii), yellow arrow). Further,
171 the overall elution profile of γ-tubulin is altered to follow αβ-tubulin, showing that γ-tubulin binds
172 to αβ-tubulin at both the low and high concentrations we tested. To compare this with αβ-/αβ-
173 tubulin's longitudinal interaction, we performed chromatography of αβ-tubulin alone (Fig. 4-
174 figure supplement 1A). At a lower concentration (10μM), αβ-tubulin elutes only as a single subunit
175 in fractions H-K (Fig. 4-figure supplement 1A (i)). Only at high αβ-tubulin concentration (35μM)
176 did we detect a small population of αβ-tubulin bound to another αβ-tubulin (Fig. 4-figure
177 supplement 1A (i), fractions B-C denoted with red arrows). This suggests that the heterogeneous
178 γ-/αβ-tubulin affinity is higher than the αβ-/αβ-tubulin.

179 To further investigate how γ-tubulin and αβ-tubulin interact, we turned to single molecule
180 microscopy. We attached biotinylated αβ-tubulin dimers to a coverslip, added either fluorescently-
181 labelled αβ-tubulin (Fig. 4B(i)) or γ-tubulin (Fig. 4B(ii)) to the solution, and visualized the binding
182 of single fluorescent molecules to αβ-tubulin molecules on the coverslip. While both fluorescent
183 αβ-tubulin and γ-tubulin specifically bind to surface-attached αβ-tubulin, 15-fold more γ-tubulin

184 molecules were bound than αβ-tubulin molecules (Fig. 4C), further supporting a stronger γ-/αβ-
185 tubulin interaction. Finally, these results were confirmed with a biolayer interferometry assay,
186 where lower concentrations of γ-tubulin were detected to interact with probe-bound αβ-tubulin,
187 while a much higher concentration of αβ-tubulin was necessary to measure an interaction between
188 αβ-/αβ-tubulin dimers (Fig. 4-figure supplement 1B). These results are congruent with *in vivo* γ-
189 /αβ-tubulin affinity measurements made in yeast cells[33].

190 In performing the above experiments, we unexpectedly found that purified γ-tubulin on its
191 own, at high concentrations and at 33 °C, efficiently nucleated MTs from αβ-tubulin subunits (Fig.
192 4-figure supplement 2A) and capped MT minus-ends while allowing plus-ends to polymerize (Fig.
193 4-figure supplement 2B). Besides its ability to form higher order oligomers in a physiological
194 buffer[29], γ-tubulin at high concentrations also forms filaments *in vitro* of variable widths (Fig. 4-
195 figure supplement 2C; Moritz and Agard, unpublished results) as assayed by negative stain
196 electron microscopy (EM). The formation of filaments *in vitro* is consistent with the previous *in*
197 *vivo* observations where γ-tubulin was over-expression and immunoprecipited[34–36]. To understand
198 the nature of these filaments, we generated 3D reconstructions, which revealed that γ-tubulins self-
199 assemble into lateral arrays with a repeating unit of approximately 54Å (Fig. 4-figure supplement
200 2D-E). This closely matches the lateral tubulin repeats in the MT lattice (PDB:6DPU[37,38]) and in
201 γ-tubulin crystal contacts (52Å, PDB:1Z5W[39,40]), but not the longitudinal αβ-tubulin repeat (40Å).
202 This suggests that laterally associated γ-tubulin are sufficient to efficiently nucleate MTs.

203 In sum, at the nucleation interface of γ-TuRC, γ-tubulin has a higher longitudinal affinity
204 for αβ-tubulin compared to αβ-tubulin's affinity for itself, which promotes MT nucleation from γ-
205 TuRC.

206

207 **Monte Carlo simulations recapitulate the dynamics microtubule nucleation from γ-TuRC**

208 To further probe the dynamics of MT nucleation, we developed Monte Carlo simulations to model
209 MT nucleation from γ-TuRC. Our model was based on one previously developed for the plus-end
210 dynamics of a MT[31,41,42]. A 13-protofilament geometry for the MT lattice and γ-TuRC were used
211 with a pitch of 3 tubulins (Fig. 5A). αβ-tubulin dimers arrive with a constant on rate, k_{on} ($\mu M^{-1}s^{-}$
212 ^{1}) on each protofilament. The interactions between αβ-tubulins was assumed to occur with
213 longitudinal and lateral bond energies, $\Delta G_{Long,\alpha\beta-\alpha\beta}$ and $\Delta G_{Lat,\alpha\beta-\alpha\beta}$, respectively, similar to
214 previous literature[31,41,42]. The longitudinal bond energy between γ-/αβ-tubulin, $\Delta G_{Long,\gamma-\alpha\beta}$
215 determines the dwell time of αβ-tubulin dimers on γ-TuRC. An open conformation of native γ-
216 TuRC was assumed, as observed in recent structural work[13,14], where lateral interactions between
217 tubulins on neighboring sites were not allowed. A thermodynamic barrier, $\Delta G_{\gamma TuRC-conf}$ and a
218 pre-factor rate constant $k_{\gamma TuRC-conf}$ (s^{-1}) determine the transition from this open to *closed* γ-TuRC
219 conformation where lateral tubulin interactions can occur (Fig. 5A). As αβ-tubulin dimers
220 assemble on γ-TuRC, the free energy of this transition decreases by the total energy of all n lateral
221 bonds that can be formed, $\Delta G_{\gamma TuRC-conf} - n\Delta G_{Lat,\alpha\beta-\alpha\beta}$.

222 MT growth parameters were determined by fitting to experimental growth speed curves
223 (Fig. 5-figure supplement 1A), and were found to be similar to previous estimates[31,41]. Based on
224 our biochemical measurement (Fig. 4), $\Delta G_{Long,\gamma-\alpha\beta}$ was estimated to be higher than
225 $\Delta G_{Long,\alpha\beta-\alpha\beta}$, while a wide range was explored for the other parameters. The resulting model
226 produces a sharp transition from zero-MT length to a continuously growing MT upon γ-TuRC
227 closure (Fig. 5B) that occurs at variable time points for each realization of the model (Fig. 5B and
228 Fig. 5-figure supplement 1B-C(i)). This qualitatively recapitulates the dynamics of γ-TuRC-
229 mediated nucleation events observed experimentally.

230 Nucleation kinetics and the power-law dependence on αβ-tubulin concentration was
231 obtained by simulating hundreds of model realizations. While $k_{\gamma TuRC-conf}$ and $\Delta G_{Long,\gamma-\alpha\beta}$ do
232 not alter the power-law exponent significantly, they set the rate of nucleation at a specific αβ-
233 tubulin concentration (Fig. 5-figure supplement 1B-C). The thermodynamic barrier, $\Delta G_{\gamma TuRC-conf}$
234 instead determines the power-law exponent and the number of αβ-tubulins in the rate-limiting,
235 transition state (Fig. 5C). At $\Delta G_{\gamma TuRC-conf} < 2.5k_BT$, cooperative assembly of 1-2 αβ-tubulins
236 suffice to nucleate MTs, while at high $\Delta G_{\gamma TuRC-conf} > 20k_BT$, more than 5 αβ-tubulins assemble
237 cooperatively for successful MT nucleation. At an intermediate $\Delta G_{\gamma TuRC-conf} = 10k_BT$, MT
238 nucleation kinetics and its power-law dependence recapitulates our experimental measurements
239 (compare Fig. 5-figure supplement 2A with Fig. 2C-D). Here γ-TuRCs minimally nucleate MTs
240 at 7μM tubulin, MT nucleation increases non-linearly with tubulin concentration, and 4 ± 0.4 αβ-
241 tubulins compose the transition state (Fig. 5-figure supplement 2A and Fig. 5C, green curve
242 highlighted with an asterisk).
243 As a further validation of our model, we simulated the dynamics of MT nucleation from
244 blunt MT seeds. Here we assumed that MT assembly begins from a closed γ-TuRC geometry
245 where all longitudinal bond energies were set equal to $\Delta G_{Long,\alpha\beta-\alpha\beta}$ (Fig. 5-figure supplement
246 2B). The simulations predict near complete MT assembly at minimal αβ-tubulin concentration of
247 2μM and transition state of 1.1 ± 0.1 αβ-tubulins (Fig. 5-figure supplement 2B), in agreement with
248 MT assembly from blunt seeds that we measured experimentally (Fig. 3D-E). Thus, our Monte
249 Carlo simulations accurately capture the detailed dynamics of MT nucleation from γ-TuRC.
250
251 **Arrangement of αβ-tubulin dimers in transition state for γ-TuRC-mediated microtubule**
252 **nucleation**

253 We next characterized the dynamics of αβ-tubulins during MT nucleation from γ-TuRC by
254 examining the time traces from individual model simulations. First, prior to MT nucleation, we
255 observe longitudinal association of individual αβ-tubulins either to the γ-tubulin sites on the open
256 γ-TuRC or, less frequently, with existing αβ-tubulin in a protofilament (Fig. 5B, left insets). These
257 αβ-tubulins dissociate rapidly in the absence of additional lateral bond energy. Once a MT lattice
258 is assembled, persistence of αβ-tubulin dimers with both longitudinal and lateral contacts drive the
259 growth of plus-end. Analogous observations during growth of a MT plus-end also show rapid
260 dissociation of αβ-tubulin that form only a longitudinal contact, while ones with additional lateral
261 contacts persist[31]. At the sharp transition prior to MT assembly (Fig. 5B, right insets), we find that
262 many αβ-tubulin dimers stochastically assemble on neighboring sites on γ-TuRC. Favorable Gibbs
263 free energy from the lateral interaction between these αβ-tubulin dimers overcomes the energy
264 penalty of the conformational change and transitions γ-TuRC into a closed state.

265 Finally, we characterize the arrangement of αβ-tubulin dimers in the rate-limiting, transition
266 state that results in a closed γ-TuRC conformation prior to MT polymerization. A variable total
267 number of αβ-tubulin dimers with an average of 5.2 ± 1 (n=2119 simulations) were present on γ-
268 TuRC at the transition state (Fig. 5D, left). To our surprise, αβ-tubulin subunits in the transition
269 state assemble on neighboring sites into laterally-arranged groupings (Fig. 5D, right). The most
270 probable transition state is composed of four αβ-tubulin arranged on neighboring sites that form 3
271 lateral bonds when the γ-TuRC conformation changes to a closed one. The other probable states
272 have 5 αβ-tubulins arranged laterally in two groups of 2 and 3 dimers each, or in two groups of 1
273 and 4 dimers each, and 6 αβ-tubulins arranged in two groups of 2 and 4 dimers, or in two groups
274 of 3 dimers each. Most importantly, in these transition states, the free energy gained from the
275 lateral bonds between αβ-tubulins compensates for the thermodynamic barrier posed by γ-TuRC's

276 open conformation to allow for MT nucleation. Notably, the laterally-arranged group of 4 αβ-
277 tubulin dimers physically represents the power-law exponent measured from the average
278 nucleation kinetics (Fig. 2D).
279
280 **Role of putative activation factors in γ-TuRC mediated nucleation**
281 Next, we investigated how accessory factors regulate γ-TuRC-dependent MT nucleation. While
282 several activation factors[26,27,43] have been proposed to enhance the MT nucleation activity of γ-
283 TuRC, the function of these putative activation factors remains to be tested with a sensitive and
284 direct assay. We incubated the purified γ-TuRC activation domain (γ-TuNA)[26] from *Xenopus*
285 *laevis* protein CDK5RAP2 with γ-TuRC at high concentrations to maximally saturate the binding
286 sites on γ-TuRC (Fig. 6A), and further supplemented additional γ-TuNA with αβ-tubulin used
287 during the nucleation assay. Measurement of nucleation activity revealed that CDK5RAP2's γ-
288 TuNA domain increases γ-TuRC-mediated nucleation only by 1.4 (± 0.02) -fold (mean ± std, n =
289 2) at t = 180 seconds, falling within the 95% confidence intervals of the control reactions (Fig. 6A-
290 B and Video 6). Another putative activator, NME7[27], when added to γ-TuRC at saturating
291 concentrations[44] (Fig. 6-figure supplement 1 and Video 6), did not increase γ-TuRC's nucleation
292 activity (Fig. 6B). Finally, we assessed the protein TPX2 that not only contains a split γ-TuNA and
293 overlapping SPM[43], but also functions as an anti-catastrophe factor *in vitro*[25,45] and was proposed
294 to stimulate γ-TuRC-mediated nucleation[43,46,47]. TPX2 also had a small increase on the nucleation
295 activity of γ-TuRC by 1.2 (± 0.3) -fold (mean ± std, n = 3) at t = 180 seconds, but bound strongly
296 along the MT lattice (Fig. 6C-D and Video 6). While high concentration of TPX2 forms
297 condensates with αβ-tubulin and promotes spontaneous MT nucleation[45,48], near its endogenous
298 concentration of TPX2[49] used here, TPX2 is able to saturates the MT lattice, yet it does not

299 significantly increase γ-TuRC-mediated nucleation, in agreement with the physiological
300 observations[43]. Thus, the putative activation motif of CDK5RAP2, full-length NME7 or TPX2 all
301 have minor effects on γ-TuRC's MT nucleation activity.
302
303 **XMAP215 promotes microtubule nucleation by strengthening the longitudinal bond energy**
304 **between γ-TuRC and αβ-tubulin**
305 Recently, XMAP215 was discovered to be a nucleation factor that synergizes with γ-TuRC in *X.*
306 *laevis* and *S. cerevisiae*[29,50], or works in an additive manner with γ-tubulin[51]. To investigate how
307 XMAP215 participates in MT nucleation, we performed single molecule experiments with
308 XMAP215 and γ-TuRC. At low tubulin concentrations of 3.5μM and 7μM, where none or little
309 MT nucleation occurs from γ-TuRCs alone (Fig. 7A and Fig. 7-figure supplement 1A), as shown
310 earlier. Strikingly, the addition of XMAP215 induced many surface-attached γ-TuRCs to nucleate
311 MTs, resulting in a drastic increase in number of nucleated MTs by 25 (±9) -fold (mean ± std, n =
312 3) within t = 120 seconds (Fig. 7A-B, Fig. Fig. 7-figure supplement 1B and Video 7). By directly
313 visualizing γ-TuRC and XMAP215 molecules during the nucleation reaction (Fig. 7C), we found
314 that XMAP215 and γ-TuRC molecules first form a complex from which a MT was then nucleated
315 (Fig. 7C and Video 8). For 76% of the events (n=56), XMAP215 visibly persisted between 3 to
316 ≥300 seconds on γ-TuRC before MT nucleation. After MT nucleation, XMAP215 molecules
317 polymerize and track with the MT plus-end. For 50% of nucleation events (n=58), some
318 XMAP215 molecules remained on the minus-end together with γ-TuRC, while for the other 50%
319 of events, XMAP215 was not observed on the minus-end after nucleation. This suggests that
320 XMAP215 molecules nucleate with γ-TuRC and then continue polymerization of the plus-end.

321 How does XMAP215 enable MT nucleation from γ-TuRC? We titrated αβ-tubulin at
322 constant γ-TuRC and XMAP215 concentrations and measured the kinetics of nucleation (Fig. 7-
323 figure supplement 1C and Fig. 7D). XMAP215 effectively decreases the minimal tubulin
324 concentration necessary for MT nucleation from γ-TuRC to 1.6μM (Fig. 7-figure supplement 1C),
325 very close to the minimal concentration for plus-end polymerization. As before, we calculated the
326 composition of the transition state by measuring the power-law dependence between the MT
327 nucleation rate and tubulin concentration with a resulting cooperative assembly of 3.3 ± 0.8 αβ-
328 tubulin dimers occurs (Fig. 7E). This suggests that XMAP215 does not lower the thermodynamic
329 barrier to nucleation by altering the geometry of γ-TuRC. Further, neither the N-terminus,
330 containing TOG1-4 domains, nor the C-terminus of XMAP215, containing the TOG5 and C-
331 terminal domain that directly interact with γ-tubulin[29], stimulate additional nucleation from γ-
332 TuRC (Fig. 7-figure supplement 1D-E).

333 Finally, we used our simulations to understand the thermodynamics underlying the MT
334 nucleation activity of XMAP215. Based on its role in accelerating both MT polymerization and
335 nucleation[29,50], we implicitly modeled the thermodynamic effect of XMAP215's activity by
336 strengthening the longitudinal tubulin bonds, as described previously[41]. The simulation where only
337 the longitudinal αβ-/αβ-tubulin bond is strengthened does not capture the enhancement of MT
338 nucleation by XMAP215 (Fig. 7D, left). Instead, simulations where both the longitudinal γ-/αβ-
339 tubulin and αβ-/αβ-tubulin bond energies are increased by 1.2-fold captures the accelerated
340 kinetics of MT nucleation at low αβ-tubulin concentrations. These simulations also predict a
341 similar transition state composition as measured experimentally (Fig. 7D-E, left), supporting
342 XMAP215's role in strengthening γ-/αβ-tubulin interactions at the nucleation interface.
343 Altogether, our results confirm that XMAP215 indeed functions synergistically with γ-TuRC, in

344 agreement with recent works[15,29,50]. Most importantly, our results show that, while the transition
345 state is defined by γ-TuRC's conformation, XMAP215 strengthens the longitudinal γ-/αβ-tubulin
346 bond to function as a bona-fide nucleation factor.
347
348 **Inhibition of γ-TuRC mediated nucleation by specific microtubule associated proteins**
349 Finally, we asked whether specific MAPs could have an inhibitory effect on MT nucleation from
350 γ-TuRC. The two most abundant inhibitory MAPs in the cytosol, MCAK and Stathmin function
351 by removing αβ-tubulin dimers from the MT lattice[52,53] or sequestering αβ-tubulin dimers[54,55],
352 respectively. We find that addition of either sub-endogenous concentration of MCAK, or near-
353 endogenous Stathmin concentration (Fig. 7F, Fig. 7-figure supplement 2 and Video 9) was
354 sufficient to nearly abolish MT nucleation from all γ-TuRC molecules. Thus, γ-TuRC-mediated
355 nucleation is inhibited by MAPs that inhibit MT polymerization.

356 **Discussion**

357 Decades after the discovery of MTs, their αβ-tubulin subunits and the identification of γ-TuRC as
358 the universal MT nucleator[3,6–8,16,17], it has remained poorly understood how MTs are nucleated and
359 how this process is regulated in the cell[18,22,46]. Here we establish a single-molecule assay to study
360 MT nucleation and combine it with computational modelling to identify the rate-limiting,
361 transition state of γ-TuRC-mediated nucleation . We examine how biochemical features of γ-TuRC
362 contribute to its the nucleation activity and regulation.

363 New methods and direct measurements developed in this study reconcile several prior
364 observations for γ-TuRC-mediated MT nucleation. First, the nucleation activity of γ-TuRC has
365 been found as variable and often low and similar to spontaneous MT assembly[6,8,10,13–15,18,22], and
366 γ-TuRC's requirement in the cell has been debated[4,45,56–58]. Low concentration of γ-TuRC
367 molecules obtained from endogenous purifications and lack of live observation of a growing or
368 capped MT minus-end, which is needed to distinguish between γ-TuRC-mediated and spontaneous
369 nucleation, could affect the assessment of γ-TuRC's nucleation activity. Second, because of
370 technical challenges in the traditional setup where MTs are nucleated, fixed and spun down onto
371 a coverslip[6,8–10,13,26,27,29], variable assessment of the role of accessory factors[13,26,27] has been
372 reported. Here, by developing a high resolution assay that provides specific live information to
373 visualize MT nucleation events from γ-TuRC and distinguish between non-γ-TuRC nucleated
374 MTs, analyses system to measure its nucleation activity independent of concentration, as well as
375 direct visualization of MAPs bound to γ-TuRC or the MT lattice allows us to unambiguously study
376 γ-TuRC mediated nucleation and its regulation by MAPs.

377 While the molecular architecture of γ-TuRC was revealed by recent cryo-EM structures[9,13–
378 15], the dynamics of MT nucleation from γ-TuRC and how it relates to γ-TuRC's specific

379 biochemical features has remained unknown. By combining biochemical investigation with
380 computational modeling, we show that 4 αβ-tubulin heterodimers on neighboring sites form the
381 critical nucleus, i.e. the rate-limiting transition state on γ-TuRC. A model, in which γ-TuRC
382 stochastically changes its conformation from an *open* to *closed* state, where the latter is stabilized
383 by lateral αβ-tubulin interactions, comprehensively explains our experimental measurements.
384 While native γ-TuRC purified from cytosol was used here, further activated γ-TuRC isolated from
385 MTOCs may result in cooperativity between fewer αβ-tubulin dimers for successful nucleation.
386 Likewise, MT assembly from pre-assembled, blunt seeds, could resemble nucleation from already
387 closed γ-TuRCs. We find that the subsequent transition of the growing MT end from blunt- to
388 tapered one, is not the major, rate-limiting step during nucleation from γ-TuRC. Notably, a parallel
389 work also reported MT nucleation from single, human γ-TuRC molecules recently[15]. While the
390 majority of findings agree with our work, 6.7 dimers were required in the critical nucleus and an
391 overall lower activity of γ-TuRC (0.5%) was found[15]. Low structural integrity of purified γ-TuRC
392 from incorporation of BFP-tagged GCP2 and a higher ratio of γ-tubulin sub-complexes, or species-
393 specific variation in γ-TuRC properties could explain these differences.

394 Our simulations further predict that a hypothetical low affinity between γ-/αβ-tubulin[23] is
395 insufficient to induce any MT nucleation because αβ-tubulins that bind to γ-TuRC dissociate
396 rapidly. Instead, our biochemical investigation show that the high affinity of γ-/αβ-tubulin
397 interaction increases the dwell time of αβ-tubulin dimers on γ-TuRC and promotes γ-TuRC's MT
398 nucleation activity, as predicted by our modeling. Finally, this net mechanism is
399 thermodynamically favorable compared to spontaneous MT nucleation as the free energy of
400 longitudinal γ-/αβ-tubulin interactions, $13(\Delta G_{Long,\gamma-\alpha\beta})$, exceeds the energy penalty from
401 conformational rearrangement of γ-TuRC, $\Delta G_{\gamma TuRC-conf}$. In sum, building on the recent structural

402 work[13–15], our results show that the open γ-TuRC conformation and its transition to a closed one
403 defines γ-TuRC's nucleation activity and transition state. In the future, it will be important to study
404 how γ-TuRC transitions to a closed conformation with high resolution structural studies, as well
405 as how other biochemical properties, in addition to those modeled here, govern its nucleation
406 activity. Our single molecule assay, kinetic analyses and computational modeling will be essential
407 to complement and place atomic structures into a mechanism that explains how MT nucleation γ-
408 TuRC occurs and how it is regulated.

409 Whereas spatial regulation of MT nucleation is achieved by localizing γ-TuRC to specific
410 MTOC as shown previously[18,24,46,59], temporal regulation of MT nucleation had been proposed to
411 occur through activation factors that modify γ-TuRC's conformation and upregulate its
412 activity[18,26,27,46,59]. While several putative activation factors do not significantly enhance of γ-
413 TuRC's nucleation activity as shown here, new factors, that are yet to be identified, may serve this
414 role to alter γ-TuRC's conformation at MTOCs. Alternatively, we postulate another mechanism
415 for temporal control governing the availability and localization of αβ-tubulin. In this model, locally
416 concentrating soluble αβ-tubulin could upregulate the levels of γ-TuRC-mediated MT nucleation,
417 e.g. as recently shown through accumulation of high concentration of tubulin dimers at the
418 centrosome by MAPs[58,60] and by co-condensation of tubulin on MTs by TPX2 during branching
419 MT nucleation[48], and finally via specific recruitment of tubulin on γ-TuRC through the binding of
420 XMAP215 as shown here[29,50].

421 **Supplementary Materials**

422 Supplementary Materials includes nine figures, nine videos, MATLAB code for simulations and
423 source data.

424

425 **Acknowledgements**

426 We thank Brian Mahon and Sophie Travis for advice on processing of electron microscopy data,
427 David Agard, Michelle Moritz and Petry lab members for discussions. This work was supported
428 by an American Heart Association predoctoral fellowship 17PRE33660328 and a Princeton
429 University Honorific Fellowship (both to AT), a Howard Hughes Medical Institute Gilliam
430 fellowship and a National Science Foundation graduate research fellowship (both to MJR),
431 NIGMS R00GM112982 (to GB), NIH New Innovator Award 1DP2GM123493, Pew Scholars
432 Program in the Biomedical Sciences 00027340, David and Lucile Packard Foundation 2014-40376
433 (all to SP), and the Center for the Physics of Biological Function sponsored by the National Science
434 Foundation grant PHY-1734030.

435

436 **Competing financial interests**

437 The authors declare no competing financial interests.

438

439 **Abbreviations List**

440 Microtubule (MT)

441 Microtubule associated protein (MAP)

442 Gamma-tubulin (γ-tubulin) and Gamma-tubulin ring complex (γ-TuRC)

443 Gamma-tubulin complex protein (GCP)

Microtubule organizing center (MTOC)

Protofilament (pf)

Electron microscopy (EM)

447 **References**

448 1. Petry, S. Mechanisms of Mitotic Spindle Assembly. *Annu. Rev. Biochem.* **85**, 659–683 (2016).

449 2. Wu, J. & Akhmanova, A. Microtubule-Organizing Centers. *Annu. Rev. Cell Dev. Biol.* **33**, 51–
450 75 (2017).

451 3. Oakley, C. E. & Oakley, B. R. Identification of gamma-tubulin, a new member of the tubulin
452 superfamily encoded by mipA gene of Aspergillus nidulans. *Nature* **338**, 662–664 (1989).

453 4. Hannak, E. *et al.* The kinetically dominant assembly pathway for centrosomal asters in
454 Caenorhabditis elegans is gamma-tubulin dependent. *J. Cell Biol.* **157**, 591–602 (2002).

455 5. Groen, A. C., Maresca, T. J., Gatlin, J. C., Salmon, E. D. & Mitchison, T. J. Functional
456 overlap of microtubule assembly factors in chromatin-promoted spindle assembly. *Mol. Biol.*
457 *Cell* **20**, 2766–2773 (2009).

458 6. Moritz, M., Braunfeld, M. B., Sedat, J. W., Alberts, B. & Agard, D. A. Microtubule nucleation
459 by gamma-tubulin-containing rings in the centrosome. *Nature* **378**, 638–640 (1995).

460 7. Moritz, M., Zheng, Y., Alberts, B. M. & Oegema, K. Recruitment of the gamma-tubulin ring
461 complex to Drosophila salt-stripped centrosome scaffolds. *J. Cell Biol.* **142**, 775–786 (1998).

462 8. Zheng, Y., Wong, M. L., Alberts, B. & Mitchison, T. Nucleation of microtubule assembly by
463 a gamma-tubulin-containing ring complex. *Nature* **378**, 578–583 (1995).

464 9. Kollman, J. M., Polka, J. K., Zelter, A., Davis, T. N. & Agard, D. A. Microtubule nucleating
465 gamma-TuSC assembles structures with 13-fold microtubule-like symmetry. *Nature* **466**,
466 879–882 (2010).

467 10. Kollman, J. M. *et al.* Ring closure activates yeast γTuRC for species-specific microtubule
468 nucleation. *Nat. Struct. Mol. Biol.* **22**, 132–137 (2015).

469 11. Oegema, K. *et al.* Characterization of two related Drosophila gamma-tubulin complexes that
470 differ in their ability to nucleate microtubules. *J. Cell Biol.* **144**, 721–733 (1999).
471 12. Moritz, M., Braunfeld, M. B., Guénebaut, V., Heuser, J. & Agard, D. A. Structure of the
472 gamma-tubulin ring complex: a template for microtubule nucleation. *Nat. Cell Biol.* **2**, 365–
473 370 (2000).
474 13. Liu, P. *et al.* Insights into the assembly and activation of the microtubule nucleator γ-TuRC.
475 *Nature* **578**, 467–471 (2020).
476 14. Wieczorek, M. *et al.* Asymmetric Molecular Architecture of the Human γ-Tubulin Ring
477 Complex. *Cell* **180**, 165-175.e16 (2020).
478 15. Consolati, T. *et al.* Microtubule Nucleation Properties of Single Human γTuRCs Explained
479 by Their Cryo-EM Structure. *Dev. Cell* (2020) doi:10.1016/j.devcel.2020.04.019.
480 16. Keating, T. J. & Borisy, G. G. Immunostructural evidence for the template mechanism of
481 microtubule nucleation. *Nat. Cell Biol.* **2**, 352–357 (2000).
482 17. Wiese, C. & Zheng, Y. A new function for the gamma-tubulin ring complex as a microtubule
483 minus-end cap. *Nat. Cell Biol.* **2**, 358–364 (2000).
484 18. Kollman, J. M., Merdes, A., Mourey, L. & Agard, D. A. Microtubule nucleation by γ-tubulin
485 complexes. *Nat. Rev. Mol. Cell Biol.* **12**, 709–721 (2011).
486 19. Voter, W. A. & Erickson, H. P. The kinetics of microtubule assembly. Evidence for a two-
487 stage nucleation mechanism. *J. Biol. Chem.* **259**, 10430–10438 (1984).
488 20. Flyvbjerg, H., Jobs, E. & Leibler, S. Kinetics of self-assembling microtubules: an 'inverse
489 problem' in biochemistry. *Proc. Natl. Acad. Sci. U.S.A.* **93**, 5975–5979 (1996).
490 21. Portran, D., Schaedel, L., Xu, Z., Théry, M. & Nachury, M. V. Tubulin acetylation protects
491 long-lived microtubules against mechanical ageing. *Nat. Cell Biol.* **19**, 391–398 (2017).

492 22. Roostalu, J. & Surrey, T. Microtubule nucleation: beyond the template. *Nat. Rev. Mol. Cell*
493 *Biol.* **18**, 702–710 (2017).
494 23. Rice, L., Moritz, M. & Agard, D. A. *Microtubules form by progressively faster tubulin*
495 *accretion, not by nucleation-elongation*. http://biorxiv.org/lookup/doi/10.1101/545236
496 (2019) doi:10.1101/545236.
497 24. Wiese, C. & Zheng, Y. Microtubule nucleation: gamma-tubulin and beyond. *J. Cell. Sci.*
498 **119**, 4143–4153 (2006).
499 25. Wieczorek, M., Bechstedt, S., Chaaban, S. & Brouhard, G. J. Microtubule-associated
500 proteins control the kinetics of microtubule nucleation. *Nat. Cell Biol.* **17**, 907–916 (2015).
501 26. Choi, Y.-K., Liu, P., Sze, S. K., Dai, C. & Qi, R. Z. CDK5RAP2 stimulates microtubule
502 nucleation by the gamma-tubulin ring complex. *J. Cell Biol.* **191**, 1089–1095 (2010).
503 27. Liu, P., Choi, Y.-K. & Qi, R. Z. NME7 is a functional component of the γ-tubulin ring
504 complex. *Mol. Biol. Cell* **25**, 2017–2025 (2014).
505 28. Lynch, E. M., Groocock, L. M., Borek, W. E. & Sawin, K. E. Activation of the γ-tubulin
506 complex by the Mto1/2 complex. *Curr. Biol.* **24**, 896–903 (2014).
507 29. Thawani, A., Kadzik, R. S. & Petry, S. XMAP215 is a microtubule nucleation factor that
508 functions synergistically with the γ-tubulin ring complex. *Nat. Cell Biol.* **20**, 575–585
509 (2018).
510 30. Gardner, M. K. *et al.* Rapid Microtubule Self-Assembly Kinetics. *Cell* **159**, 215 (2014).
511 31. Mickolajczyk, K. J., Geyer, E. A., Kim, T., Rice, L. M. & Hancock, W. O. Direct
512 observation of individual tubulin dimers binding to growing microtubules. *Proc. Natl. Acad.*
513 *Sci. U.S.A.* **116**, 7314–7322 (2019).

514 32. Brouhard, G. J. & Rice, L. M. Microtubule dynamics: an interplay of biochemistry and
515 mechanics. *Nat. Rev. Mol. Cell Biol.* **19**, 451–463 (2018).
516 33. Erlemann, S. *et al.* An extended γ-tubulin ring functions as a stable platform in microtubule
517 nucleation. *J. Cell Biol.* **197**, 59–74 (2012).
518 34. Lindström, L. & Alvarado-Kristensson, M. Characterization of gamma-tubulin filaments in
519 mammalian cells. *Biochim Biophys Acta Mol Cell Res* **1865**, 158–171 (2018).
520 35. Chumová, J. *et al.* γ-Tubulin has a conserved intrinsic property of self-polymerization into
521 double stranded filaments and fibrillar networks. *Biochim Biophys Acta Mol Cell Res* **1865**,
522 734–748 (2018).
523 36. Pouchucq, L., Lobos-Ruiz, P., Araya, G., Valpuesta, J. M. & Monasterio, O. The chaperonin
524 CCT promotes the formation of fibrillar aggregates of γ-tubulin. *Biochimica et Biophysica*
525 *Acta (BBA) - Proteins and Proteomics* **1866**, 519–526 (2018).
526 37. Zhang, R., LaFrance, B. & Nogales, E. Separating the effects of nucleotide and EB binding
527 on microtubule structure. *Proc. Natl. Acad. Sci. U.S.A.* **115**, E6191–E6200 (2018).
528 38. Zhang, R. & Nogales, E. 6DPU: Undecorated GMPCPP microtubule. *Protein Data Bank:*
529 *www.rcsb.org/structure/6DPU* (2018) doi:10.2210/pdb6DPU/pdb.
530 39. Aldaz, H., Rice, L. M., Stearns, T. & Agard, D. A. Insights into microtubule nucleation from
531 the crystal structure of human gamma-tubulin. *Nature* **435**, 523–527 (2005).
532 40. Aldaz, H., Rice, L. M., Stearns, T. & Agard, D. A. 1Z5W: Crystal Structure of gamma-
533 tubulin bound to GTP. *Protein Data Bank: www.rcsb.org/structure/1Z5W* (2005)
534 doi:10.2210/pdb1Z5W/pdb.
535 41. VanBuren, V., Odde, D. J. & Cassimeris, L. Estimates of lateral and longitudinal bond
536 energies within the microtubule lattice. *Proc. Natl. Acad. Sci. U.S.A.* **99**, 6035–6040 (2002).

537 42. Ayaz, P. *et al.* A tethered delivery mechanism explains the catalytic action of a microtubule
538 polymerase. *Elife* **3**, e03069 (2014).
539 43. Alfaro-Aco, R., Thawani, A. & Petry, S. Structural analysis of the role of TPX2 in branching
540 microtubule nucleation. *J. Cell Biol.* **216**, 983–997 (2017).
541 44. Wühr, M. *et al.* Deep proteomics of the Xenopus laevis egg using an mRNA-derived
542 reference database. *Curr. Biol.* **24**, 1467–1475 (2014).
543 45. Roostalu, J., Cade, N. I. & Surrey, T. Complementary activities of TPX2 and chTOG
544 constitute an efficient importin-regulated microtubule nucleation module. *Nat. Cell Biol.* **17**,
545 1422–1434 (2015).
546 46. Tovey, C. A. & Conduit, P. T. Microtubule nucleation by γ-tubulin complexes and beyond.
547 *Essays Biochem.* **62**, 765–780 (2018).
548 47. Zhang, R., Roostalu, J., Surrey, T. & Nogales, E. Structural insight into TPX2-stimulated
549 microtubule assembly. *Elife* **6**, (2017).
550 48. King, M. R. & Petry, S. Phase separation of TPX2 enhances and spatially coordinates
551 microtubule nucleation. *Nat Commun* **11**, 270 (2020).
552 49. Thawani, A., Stone, H. A., Shaevitz, J. W. & Petry, S. Spatiotemporal organization of
553 branched microtubule networks. *Elife* **8**, (2019).
554 50. Gunzelmann, J. *et al.* The microtubule polymerase Stu2 promotes oligomerization of the γ-
555 TuSC for cytoplasmic microtubule nucleation. *Elife* **7**, (2018).
556 51. King, B. R. *et al. XMAP215 and γ-tubulin additively promote microtubule nucleation in*
557 *purified solutions*. http://biorxiv.org/lookup/doi/10.1101/2020.05.21.109561 (2020)
558 doi:10.1101/2020.05.21.109561.

559 52. Hunter, A. W. *et al.* The kinesin-related protein MCAK is a microtubule depolymerase that
560 forms an ATP-hydrolyzing complex at microtubule ends. *Mol. Cell* **11**, 445–457 (2003).
561 53. Howard, J. & Hyman, A. A. Microtubule polymerases and depolymerases. *Curr. Opin. Cell*
562 *Biol.* **19**, 31–35 (2007).
563 54. Jourdain, L., Curmi, P., Sobel, A., Pantaloni, D. & Carlier, M. F. Stathmin: a tubulin-
564 sequestering protein which forms a ternary T2S complex with two tubulin molecules.
565 *Biochemistry* **36**, 10817–10821 (1997).
566 55. Belmont, L. D. & Mitchison, T. J. Identification of a protein that interacts with tubulin
567 dimers and increases the catastrophe rate of microtubules. *Cell* **84**, 623–631 (1996).
568 56. Rogers, G. C., Rusan, N. M., Peifer, M. & Rogers, S. L. A multicomponent assembly
569 pathway contributes to the formation of acentrosomal microtubule arrays in interphase
570 Drosophila cells. *Mol. Biol. Cell* **19**, 3163–3178 (2008).
571 57. Raff, J. W. Phase Separation and the Centrosome: A Fait Accompli? *Trends Cell Biol.* **29**,
572 612–622 (2019).
573 58. Woodruff, J. B. *et al.* The Centrosome Is a Selective Condensate that Nucleates Microtubules
574 by Concentrating Tubulin. *Cell* **169**, 1066-1077.e10 (2017).
575 59. Petry, S. & Vale, R. D. Microtubule nucleation at the centrosome and beyond. *Nat. Cell Biol.*
576 **17**, 1089–1093 (2015).
577 60. Baumgart, J. *et al.* Soluble tubulin is significantly enriched at mitotic centrosomes. *J. Cell*
578 *Biol.* **218**, 3977–3985 (2019).
579 61. Tan, S., Kern, R. C. & Selleck, W. The pST44 polycistronic expression system for producing
580 protein complexes in Escherichia coli. *Protein Expr. Purif.* **40**, 385–395 (2005).

581 62. Ohi, R., Sapra, T., Howard, J. & Mitchison, T. J. Differentiation of cytoplasmic and meiotic
582 spindle assembly MCAK functions by Aurora B-dependent phosphorylation. *Mol. Biol. Cell*
583 **15**, 2895–2906 (2004).
584 63. Reber, S. B. *et al.* XMAP215 activity sets spindle length by controlling the total mass of
585 spindle microtubules. *Nat. Cell Biol.* **15**, 1116–1122 (2013).
586 64. Hannak, E. & Heald, R. Investigating mitotic spindle assembly and function in vitro using
587 Xenopus laevis egg extracts. *Nat Protoc* **1**, 2305–2314 (2006).
588 65. Murray, A. W. & Kirschner, M. W. Cyclin synthesis drives the early embryonic cell cycle.
589 *Nature* **339**, 275–280 (1989).
590 66. Bieling, P., Telley, I. A., Hentrich, C., Piehler, J. & Surrey, T. Fluorescence microscopy
591 assays on chemically functionalized surfaces for quantitative imaging of microtubule, motor,
592 and +TIP dynamics. *Methods Cell Biol.* **95**, 555–580 (2010).
593 67. Thévenaz, P., Ruttimann, U. E. & Unser, M. A pyramid approach to subpixel registration
594 based on intensity. *IEEE Trans Image Process* **7**, 27–41 (1998).
595 68. Zanic, M. Measuring the Effects of Microtubule-Associated Proteins on Microtubule
596 Dynamics In Vitro. *Methods Mol. Biol.* **1413**, 47–61 (2016).
597 69. Le Maire, M., Aggerbeck, L. P., Monteilhet, C., Andersen, J. P. & Møller, J. V. The use of
598 high-performance liquid chromatography for the determination of size and molecular weight
599 of proteins: a caution and a list of membrane proteins suitable as standards. *Anal. Biochem.*
600 **154**, 525–535 (1986).
601 70. Ovesný, M., Křížek, P., Borkovec, J., Svindrych, Z. & Hagen, G. M. ThunderSTORM: a
602 comprehensive ImageJ plug-in for PALM and STORM data analysis and super-resolution
603 imaging. *Bioinformatics* **30**, 2389–2390 (2014).

604 71. Punjani, A., Rubinstein, J. L., Fleet, D. J. & Brubaker, M. A. cryoSPARC: algorithms for
605 rapid unsupervised cryo-EM structure determination. *Nat. Methods* **14**, 290–296 (2017).
606 72. Zhang, K. Gctf: Real-time CTF determination and correction. *J. Struct. Biol.* **193**, 1–12
607 (2016).
608 73. Pettersen, E. F. *et al.* UCSF Chimera--a visualization system for exploratory research and
609 analysis. *J Comput Chem* **25**, 1605–1612 (2004).
610

611 **Methods**

612

613 **Purification of recombinant proteins**

614 Full-length TPX2 with N-terminal Strep II-6xHis-GFP-TEV site tags was cloned into pST50Tr-
615 STRHISNDHFR (pST50) vector[61] using Gibson Assembly (New England Biolabs). N-terminal
616 6xHis-tagged, *Xenopus laevis* Stathmin 1A was a gift from Christiane Wiese (University of
617 Madison). N-terminal tagged 6xHis-TEV MCAK plasmid was a gift from Ryoma Ohi[62]. Wild-
618 type XMAP215 with C-terminal GFP-7xHis plasmid was a gift from Simone Reber[63] and was used
619 to clone XMAP215 with C-terminal SNAP-TEV-7xHis-StrepII tags as well as with C-terminal
620 TEV-GFP-7xHis-StrepII tags, first into pST50 vector and further into pFastBac1 vector. TOG5-
621 CT truncation of XMAP215 was produced by cloning amino acids 1091-2065 into pST50 vector
622 with C-terminal GFP-7xHis-Strep tags. Human γ-tubulin TEV-Strep II-6xHis tags was codon-
623 optimized for Sf9 expression, synthesized (Genscript), and further cloned into pFastBac1 vector.
624 6xHis tagged γ-TuNA (N-terminal aa 56-89 of *Xenopus laevis* CDK5RAP2) was also cloned into
625 pST50 and expressed in *E. coli* Rosetta2 cells. Dual StrepII-6xHis-tagged *Xenopus laevis* NME7
626 was cloned into pFastBac1 vector, expressed, and purified from Sf9 cells.

627 TPX2, Stathmin and truncations of XMAP215 (TOG5-CT and TOG1-4) used in this study
628 were expressed in *E. coli* Rosetta2 cells (EMD Millipore) by inducing with 0.5-1 mM IPTG for
629 12-18 hours at 16°C or 7 hours at 25°C. Wild-type XMAP215, MCAK and γ-tubulin were
630 expressed and purified from Sf9 cells using Bac-to-Bac system (Invitrogen). The cells were lysed
631 (EmulsiFlex, Avestin) and *E. coli* lysate was clarified by centrifugation at 13,000 rpm in Fiberlite
632 F21-8 rotor (ThermoFisher) and Sf9 cell lysate at 50,000 rpm in Ti70 rotor (Beckman Coulter) for
633 30-45 minutes.

634 TPX2 was first affinity purified using Ni-NTA beads in binding buffer (50mM Tris-HCl
635 pH 8.0, 750mM NaCl, 15mM Imidazole, 2.5mM PMSF, 6mM BME) and eluted with 200mM
636 Imidazole. All protein was pooled and diluted 4-fold to 200mM final NaCl. Nucleotides were
637 removed with a Heparin column (HiTrap Heparin HP, GE Healthcare) by binding protein in
638 250mM NaCl and isocratic elution in 750mM NaCl, all solutions prepared in Heparin buffer
639 (50mM Tris-HCl, pH 8.0, 2.5mM PMSF, 6mM BME). Peak fractions were pooled and loaded on
640 to Superdex 200 pg 16/600, and gel filtration was performed in CSF-XB buffer.

641 XMAP215-GFP-7xHis was purified using His-affinity (His-Trap, GE Healthcare) by
642 binding in buffer (50mM $NaPO_4$, 500mM NaCl, 20mM Imidazole, pH 8.0) and eluting in 500mM
643 Imidazole. Peak fractions were pooled and diluted 5-fold with 50mM Na-MES pH 6.6, bound to a
644 cation-exchange column (Mono S 10/100 GL, GE Healthcare) with 50mM MES, 50mM NaCl, pH
645 6.6 and eluted with a salt-gradient up to 1M NaCl. Peak fractions were pooled and dialyzed into
646 CSF-XB buffer. XMAP215-SNAP-TEV-7xHis-StrepII or XMAP215-TEV-GFP-7xHis-StrepII
647 was first affinity purified with StrepTrap HP (GE Healthcare) with binding buffer (50mM $NaPO_4$,
648 270mM NaCl, 2mM $MgCl_2$, 2.5mM PMSF, 6mM BME, pH 7.2), eluted with 2.5mM D-
649 desthiobiotin. Peak fractions were pooled, concentrated and further purification via gel filtration
650 (Superdex 200 10/300 GL) in CSF-XB buffer containing 150mM KCl. For fluorescent labelling
651 of SNAP-tag in XMAP215-SNAP-TEV-7xHis-StrepII, StrepTrap elution was cation-exchanged
652 (Mono S 10/100 GL), peak fractions pooled and reacted with 2-molar excess SNAP-substrate
653 Alexa-488 dye (S9129, NEB) overnight at 4°C, followed by purification via gel filtration
654 (Superdex 200 10/300 GL) in CSF-XB buffer. Approximately 70% labeling efficiency of the
655 SNAP-tag was achieved.

656 γ-tubulin was purified by binding to HisTrap HP (GE Healthcare) in binding buffer (50
657 mM KPO_4 pH 8.0, 500 mM KCl, 1 mM $MgCl_2$, 10% glycerol, 5mM Imidazole, 0.25 μM GTP, 5
658 mM BME, 2.5mM PMSF), washing first with 50 mM KPO_4 pH 8.0, 300 mM KCl, 1 mM $MgCl_2$,
659 10% glycerol, 25 mM imidazole, 0.25 μM GTP, 5 mM BME), and then with 50 mM K-MES pH
660 6.6, 500 mM KCl, 5mM $MgCl_2$, 10% glycerol, 25 mM imidazole, 0.25 μM GTP, 5 mM BME) and
661 eluted in 50 mM K-MES pH 6.6, 500 mM KCl, 5mM $MgCl_2$, 10% glycerol, 250 mM imidazole,
662 0.25 μM GTP, 5 mM BME. Peak fractions were further purified with gel filtration (Superdex 200
663 10/300 GL) in gel filtration buffer (50 mM K-MES pH 6.6, 500 mM KCl, 5 mM $MgCl_2$, 1 mM K-
664 EGTA, 1 μM GTP, 1 mM DTT). For covalent labelling of γ-tubulin with Alexa-568 or Alexa-488
665 dye, peak gel filtration fractions were pooled and dialyzed into labelling buffer (50mM KPO_4 pH
666 8.0, 500mM KCl, 1mM MgCl2, 2% glycerol, 25μM GDP, 5mM BME), reacted with 5 to 20-fold
667 excess of Alexa-568 or Alexa-488 NHS ester (catalog # A20003, A20000, GE Healthcare) for 1
668 hour at 4°C, and unreacted dye was separated with size exclusion Superdex 200 10/300 GL in gel
669 filtration buffer as above. 7% labelling of γ-tubulin was achieved.

670 γ-TuNA motif from CDK5RAP2 was purified by binding to Ni-NTA resin in binding
671 buffer buffer (50mM Tris-HCl pH 8, 500mM NaCl, 20mM Imidazole), eluted with 250 mM
672 Imidazole and further purified by gel filtration into storage buffer (50mM Tris-HCl pH 7.5,
673 200mM NaCl). NME7 was purified similar to γ-TuNA by first Ni-NTA affinity followed by size
674 exclusion, as described for γ-TuNA, except with salt concentration of 150mM NaCl and additional
675 0.05% Tween-20, and further dialyzed into BRB80 for storage.

676 MCAK was first affinity purified by binding to His-Trap HP (GE Healthcare) in binding
677 buffer (50mM NaPO4, 500mM NaCl, 6mM BME, 0.1mM MgATP, 10mM Imidazole, 1mM
678 MgCl2, 2.5mM PMSF, 6mM BME, pH to 7.5), eluting with 300mM Imidazole, followed by gel-

679 filtration (Superdex 200 10/300 GL, GE Healthcare) in storage buffer (10 mM K-HEPES pH 7.7,
680 300 mM KCl, 6mM BME, 0.1 mM MgATP, 1mM $MgCl_2$, 10% w/v sucrose).
681 Stathmin was purified using His-affinity (His-Trap HP, GE Healthcare) by first binding in
682 binding buffer (20mM $NaPO_4$ pH 8.0, 500mM NaCl, 30mM Imidazole, 2.5mM PMSF, 6mM
683 BME) and eluting with 300mM Imidazole, followed by gel filtration (HiLoad 16/600 Superdex,
684 GE Healthcare) into CSF-XB buffer (100mM KCl, 10mM K-HEPES, 5mM K-EGTA, 1mM
685 $MgCl_2$, 0.1mM $CaCl_2$, pH 7.7 with 10% w/v sucrose).
686 All recombinant proteins were flash-frozen and stored at -80°C, and their concentration
687 was determined by analyzing a Coomassie-stained SDS-PAGE against known concentration of
688 BSA (A7906, Sigma).
689 Bovine brain tubulin was labelled with biotin-, Cy5-, Alexa-488 or Alexa-568 NHS esters
690 (GE Healthcare) as described previously[49].
691
692 **Purification, biotinylated and fluorescent labeling of γ-TuRC**
693 Endogenous γ-TuRC was purified from *Xenopus* egg extracts and labeled with the following steps
694 at 4°C. 7-8 ml of meiotic extract from *Xenopus* laevis eggs, prepared as described previously[64,65],
695 was first diluted 5-fold with CSF-XBg buffer (10mM K-HEPES, 100mM KCl, 1mM $MgCl_2$, 5mM
696 K-EGTA, 10% w/v sucrose, 1mM DTT, 1mM GTP, 10 μg/ml LPC protease inhibitors, pH 7.7),
697 centrifuged to remove large aggregates at 3500 rpm (Thermo Sorvall Legend XTR) for 10 minutes,
698 and the supernatant filtered sequentially with 1.2 μm and 0.8 μm Cellulose Acetate filters
699 (Whatman) followed by 0.22 μm PES filter (ThermoFisher). γ-TuRC was precipitated by
700 incubating with 6.5% w/v PEG-8000k (Sigma) for 30 minutes and centrifuged at 17,000 rpm (SS-
701 34 rotor, ThermoScientific) for 20 minutes. γ-TuRC-rich pellet was resuspended in CSF-XB buffer

702 with 0.05% v/v NP-40 using a mortar & pestle homogenizer, PEG was removed via centrifugation
703 at 136,000 xg for 7 minutes in TLA100.3 (Beckman Ultracentrifuge), and supernatant was pre-
704 cleared by incubating with Protein A Sepharose beads (GE LifeSciences #17127901) for 20
705 minutes. Beads were removed, γ-TuRC was incubated with 4-5 mg of a polyclonal antibody
706 custom-made against C-terminal residues 413-451 of *X. laevis* γ-tubulin (Genscript) for 2 hours
707 on gentle rotisserie, and further incubated with 1ml washed Protein A Sepharose bead slurry for 2
708 hours. γ-TuRC-bound beads were washed sequentially with 30 ml of CSF-XBg buffer, 30 ml of
709 CSF-XBg buffer with 250 mM KCl (high salt wash), 10 ml CSF-XBg buffer with 5mM ATP
710 (removes heat-shock proteins), and finally 10 ml CSF-XBg buffer before labeling. For
711 biotinylation of γ-TuRC, beads were incubated with 25 μM NHS-PEG4-biotin (A39259,
712 ThermoFisher) in CSF-XBg buffer for 1 hour at 4°C, and unbound biotin was removed by washing
713 with 30 ml CSF-XBg buffer prior to elution step. For combined fluorescent and biotin labeling of
714 γ-TuRC, the wash step after ATP-wash consisted of 10 ml of labelling buffer (10mM K-HEPES,
715 100mM KCl, 1mM $MgCl_2$, 5mM K-EGTA, 10% w/v sucrose, 0.5mM TCEP, 1mM GTP, 10 μg/ml
716 LPC, pH 7.1) and fluorescent labelling was performed by incubating the beads with 1 μM Alexa-
717 568 C_5 Maleimide (A20341, ThermoFisher). Unreacted dye was removed with 10 ml CSF-XBg
718 buffer, beads were incubated with 25 μM NHS-PEG4-biotin (A39259, ThermoFisher) in CSF-
719 XBg buffer for 1 hour at 4°C, and unreacted biotin removed with 30 ml CSF-XBg buffer. Labeled
720 γ-TuRC was eluted by incubating 2-3ml of γ-tubulin peptide (residues 413-451) at 0.4-0.5mg/ml
721 in CSF-XBg buffer with beads overnight. After 10-12 hours, γ-TuRC was collected by adding 1-
722 2ml CSF-XBg buffer to the column, concentrated to 200 μl in 30k NMWL Amicon concentrator
723 (EMD Millipore) and layered onto a continuous 10-50 w/w % sucrose gradient prepared in a 2.2
724 ml ultra-clear tube (11x34 mm, Beckman Coulter) using a two-step program in Gradient Master

725 108 machine. Sucrose gradient fractionation of γ-TuRC was performed by centrifugation at
726 200,000xg in TLS55 rotor (Beckman Coulter) for 3 hours. The gradient was fractionated from the
727 top in 11-12 fractions using wide-bore pipette tips and peak 2-3 fractions were identified by
728 immunoblotting against γ-tubulin with GTU-88 antibody (Sigma). γ-TuRC was concentrated to 80
729 µl in 30k NMWL Amicon concentrator (EMD Millipore) and fresh purification was used
730 immediately for single molecule assays. Cryo-preservation of γ-TuRC molecules resulted in loss
731 of ring assembly and activity.
732
733 **Assessment of γ-TuRC with protein gel, immunoblot and negative stain electron microscopy**
734 To assess the purity of γ-TuRC, 3-5 µl of purified γ-TuRC was visualized on an SDS-PAGE with
735 SYPRO Ruby stain (ThermoFisher) following the manufacturer's protocol. Biotinylated subunits
736 of γ-TuRC were assessed by immunoblotting with Streptavidin-conjugated alkaline phosphatase
737 (S921, ThermoFisher). For further conjugation of Alexa-568 dye to γ-TuRC, fluorescently labelled
738 subunits were assessed by visualizing an SDS-PAGE gel with Typhoon FLA 9500 (GE
739 Healthcare) with LPG filter and 100 µm pixel size. γ-TuRC purification was also assessed by
740 visualizing using electron microscopy. 4 µl of peak sucrose gradient fraction of γ-TuRC was
741 pipetted onto CF400-Cu grids (Electron Microscopy Sciences), incubated at room temperature for
742 60 seconds and then wicked away. 2% uranyl acetate was applied to the grids for 30 seconds,
743 wicked away, and the grids were air-dried for 10 minutes. The grids were imaged using Phillips
744 CM100 TEM microscope at 64000x magnification.
745
746 **Preparation of functionalized coverslips**

747 22x22 mm, high precision coverslips (170±5 μm, Carl Zeiss, catalog # 474030-9020-000) were
748 functionalized for single molecule assays based on a recent protocol[45,66] with specific
749 modifications. Briefly, coverslips were labelled on the surface to be functionalized by scratching
750 "C" on right, bottom corner, placed in Teflon racks, sonicated with 3N NaOH for 30 minutes,
751 rinsed with water and sonicated in piranha solution (2 parts of 30 w/w % hydrogen peroxide and
752 3 parts sulfuric acid) for 45 minutes. Coverslips were rinsed thrice in water, and all water was
753 removed by spin drying completely in a custom-made spin coater. Pairs of coverslips were made
754 to sandwich 3-glycidyloxypropyl trimethoxysilane (440167, Sigma) on the marked sides, placed
755 in glass petri dishes, and covalent reaction was performed in a lab oven at 75°C for 30 minutes.
756 Coverslips were incubated for 15 minutes at room temperature, the sandwiches were separated,
757 incubated in acetone for 15 minutes, then transferred to fresh acetone and quickly dried under
758 nitrogen stream. Coverslip sandwiches were prepared with a small pile of well mixed HO-PEG-
759 NH_2 and 10% biotin-CONH-PEG-NH_2 (Rapp Polymere) in glass petri dishes, warmed to 75°C in
760 the lab oven until PEG melts, air bubbles were pressed out and PEG coupling was performed at
761 75°C overnight. The following day, individual coverslips were separated from sandwiches,
762 sonicated in MilliQ water for 30 minutes, washed further with water until no foaming is visible,
763 dried with a spin dryer, and stored at 4°C. Functionalized coverslips were used within 1 month of
764 preparation.

765 Imaging chambers were prepared by first assembling a channel on glass slide with double
766 sided tape strips (Tesa) 5 mm apart, coating the channel with 2mg/ml PLL(20)-g[3.5]- PEG(2)
767 (SuSOS) in dH_2O, incubating for 20 minutes, rinsing out the unbound PEG molecules with dH_2O
768 and drying the glass slide under the nitrogen stream. A piece of functionalized coverslip was cut

769 with the diamond pen and assembled functionalized face down on imaging chamber. The prepared
770 chambers were stored at 4°C and used within a day of assembly.
771
772 **Microtubule nucleation assay with purified γ-TuRC**
773 The imaging channel was prepared as follows. First, 5% w/v Pluronic F-127 in dH_2O was
774 introduced in the chamber (1 vol = 50 µl) and incubated for 10 minutes at room temperature. The
775 chamber was washed with 2 vols of assay buffer (80mM K-PIPES, 1mM $MgCl_2$, 1mM EGTA,
776 30mM KCl, 0.075% w/v methylcellulose 4000 cp, 1% w/v D-(+)-glucose, 0.02% w/v Brij-35,
777 5mM BME, 1mM GTP) with 0.05 mg/ml κ-casien (casein buffer), followed by 1 vol of 0.5 mg/ml
778 NeutrAvidin (A2666, ThermoFisher) in casein buffer, incubated on a cold block for 3 minutes,
779 and washed with 2 vols of BRB80 (80mM K-PIPES, 1mM $MgCl_2$, 1mM EGTA pH 6.8). 5-fold
780 dilution of γ-TuRC in BRB80 was introduced in the flow chamber and incubated for 10 minutes.
781 Unattached γ-TuRC molecules were washed with 1 vol of BRB80.
782 During the incubations, nucleation mix was prepared containing desired concentration of
783 αβ-tubulin (3.5-21 µM) purified from bovine brain with 5% Cy5-labeled tubulin along with
784 1mg/ml BSA (A7906, Sigma) in assay buffer, centrifuged for 12 minutes in TLA100 (Beckman
785 Coulter) to remove aggregates, a final 0.68 mg/ml glucose oxidase (SERVA, catalog # SE22778),
786 0.16 mg/ml catalase (Sigma, catalog # SRE0041) was added, and reaction mixture was introduced
787 into the flow chamber containing γ-TuRC.
788
789 **Total internal reflection fluorescence (TIRF) microscopy and analysis of microtubule**
790 **nucleation from γ-TuRC**

791 Nucleation of MTs was visualized with inverted Nikon TiE TIRF microscope using a 100X, 1.49
792 NA TIRF objective. An objective heater collar was attached (Bioptechs, model 150819-13) and
793 the temperature set-point of 33.5°C was used for experiments. Time-lapse videos were recorded
794 for 10 minutes at 0.5-1 frame per second using Andor iXon DU-897 camera with EM gain of 300
795 and exposure time of 50-200 ms each frame. Reference time-point zero (0 seconds) refers to when
796 the reaction was incubated at 33.5°C on the microscope, and for most reactions, imaging was
797 started within 30 seconds.

798 Growth speed of the plus-ends of MTs nucleated by γ-TuRC was measured by generating
799 kymographs in ImageJ. For few specific datasets with notable in-plane drift, an ImageJ plugin,
800 StackReg[67], was to correct a minor translational drift before proceeding with the analysis. Region
801 of interest (ROI) for individual MTs were selected and resliced to generate a length-time plot and
802 a line was fit to the growing MT plus-end. The slope of this line represents growth speed. The
803 kinetics of MT nucleation from γ-TuRC was measured as follows. A kymograph was generated
804 for every MT nucleated in the field of view. For most nucleation events, the time of nucleation of
805 the MT was obtained from observing the kymograph and manually recording the initiation time
806 point (see Fig. 1C for examples). For MTs where nucleation occurred before the timelapse movie
807 began or where the initiation was not clearly observed in the kymograph, the shortest length of the
808 MT that was clearly visible in the timelapse was measured and measured average growth speed of
809 MTs was used to estimate the time of nucleation. We verified that this procedure accurately
810 estimates the nucleation time for test case MTs where the nucleation event was visible. The
811 measurement of number of MTs ($N(t)$) nucleated versus time was generated from a manual log
812 containing the nucleation time for all MTs observed in the field of view. To represent the
813 theoretical field-to-field heterogeneity in the number of MTs nucleated, we assumed that binding

814 of γ-TuRC and subsequent nucleation follows a Poisson distribution with mean n MTs and
815 standard deviation $\sqrt{n}$ MTs. 95% confidence interval in the nucleation measurements, $n \pm 2\sqrt{n}$ is
816 displayed on each nucleation time course.

817 To calculate the percentage of γ-TuRCs that nucleate a MT, we visualized MT nucleation
818 from Alexa-568 labelled γ-TuRC in the presence of 21μM tubulin and 100nM XMAP215, or with
819 10.5μM tubulin. We counted the number of labelled γ-TuRC molecules attached in the field of
820 view and counted the number of MTs nucleated specifically from these molecules but excluded
821 spontaneous MT nucleation. For the reaction with 21μM tubulin and 100nM XMAP215, we
822 directly measured that 15% of γ-TuRC molecules nucleated a MT. For the reaction with 10.5μM
823 tubulin, a similar calculation was performed and using measured curves (Fig. 2C), we estimated
824 the percentage of γ-TuRC that will nucleate with 21μM tubulin as 11%.

825

826 **Power-law analysis of critical nucleus size on γ-TuRC**

827 We consider the following simplified model to determine the number of αβ-tubulin dimers in the
828 rate-limiting, transition state on γ-TuRC i.e. the critical nucleus. We consider a total number of γ-
829 TuRC molecules N_0 available to nucleate MTs at a specific αβ-tubulin concentration C. The total
830 number of MTs nucleated $N(t)$ from a total N_0 γ-TuRCs is a function of time t. If n tubulin
831 dimers assemble cooperatively on γ-TuRC for a successful MT nucleation, the rate of MT
832 nucleation from γ-TuRC molecules available to nucleated at time t, $N_0 - N(t)$ reads,

833 $$\frac{dN(t)}{dt} = k_{nucleate}(N_0 - N(t))C^n \quad (1)$$

834 Here we assume that tubulin does not get significantly depleted over time in the course of our
835 reactions as shown by previous calculations[68]. At the start of the reaction $t = 0$, no MTs have

836 nucleated $N(t=0)=0$, therefore at early times we assume $N_0 - N(t) \approx N_0$ to simplify the
837 calculation of the critical MT nucleus,

838 $$\left.\frac{dN}{dt}\right|_{t\to 0} = k_{nucleate} N_0 C^n \quad (2)$$

839 Converting into log scale,

840 $$ln\left(\left.\frac{dN}{dt}\right|_{t\to 0}\right) = n\, ln(C) + a \quad (3)$$

841 To obtain the number of αβ-tubulin dimers in the critical nucleus on γ-TuRC, a straight line was
842 fit to the initial, linear region of each nucleation curve $N(t)$ versus t curve for every tubulin
843 concentration C and the rate of nucleation $\left.\frac{dN}{dt}\right|_{t\to 0}$ was obtained from slope of this fit. A straight
844 line was then fit to $ln\left(\left.\frac{dN}{dt}\right|_{t\to 0}\right)$ versus $ln(C)$ for all concentrations, the slope of which provides
845 the size of critical nucleus n. Finally, the measured rate of nucleation depends on the total number
846 of γ-TuRC molecules available. As the total number of γ-TuRC molecules obtained from different
847 days purifications changes, the rate of nucleation from γ-TuRCs at 10.5μM tubulin was set to 1
848 (normalization factor) to allow pooling of all datasets for γ-TuRC-mediated nucleation.
849

850 **Spontaneous microtubule nucleation and data analysis**

851 Spontaneous MT assembly was visualized similar to γ-TuRC-mediated nucleation with the
852 following changes. The Pluronic, casein and NeutrAvidin incubations were performed identical to
853 γ-TuRC nucleation assay but instead of attaching γ-TuRCs, sucrose-based buffer (of the same
854 composition as used for γ-TuRC elution) was diluted 5-fold with BRB80, introduced in the flow
855 chamber and incubated for 10 minutes. Washes were performed with 1 vol of BRB80, nucleation
856 mix was added, and imaging was performed as described above. MTs nucleate spontaneously in
857 solution fall down on the coverslip due to depletion forces during the 10 minutes of visualizing the

858 reaction. The number of MTs nucleated in the field of view were counted manually and plotted in
859 Fig. 3B. 95% confidence interval is displayed assuming a Poisson distribution for theoretical field-
860 to-field heterogeneity as described above.

861 In the absence of any attached nucleation site, the spontaneously nucleated MTs are usually
862 not visualized from the time of their nucleation and the analysis used for γ-TuRC mediated
863 nucleation was adapted. Integrating the equation (2) above

864 $$N(t) = k_{nucleate} N_0 C^n t \quad (4)$$

865 Converting into log scale at time $t = \tau$,

866 $$ln(N(t = \tau)) = n\, ln(C) + b \quad (5)$$

867 To obtain the number of αβ-tubulin dimers in the critical nucleus in spontaneous assembly, the
868 number of MTs at a specified time t =7.5 min was measured, a straight line was then fit to
869 $ln(N(t = \tau))$ versus $ln(C)$ for all concentrations, the slope of which provides the size of critical
870 nucleus n. All datasets were pooled and reported.

871

872 **Preparation, microtubule assembly from blunt microtubule seeds and data analysis**

873 Blunt MTs were prepared with GMPCPP nucleotide in two polymerization cycles as described
874 recently[25]. Briefly, a 50 µl reaction mixture was prepared with 20 µM bovine brain tubulin with
875 5% Alexa-568 labeled tubulin and 5% biotin-labeled tubulin, 1mM GMPCPP (Jena Bioscience)
876 in BRB80 buffer, incubated on ice for 5 minutes, then incubated on 37°C for 30 minutes to
877 polymerize MTs, and MTs were pelleted by centrifugation at 126,000 xg for 8 minutes at 30°C in
878 TLA100 (Beckman Coulter). Supernatant was discarded, MTs were resuspended in 80% original
879 volume of BRB80, incubated on ice for 20 minutes to depolymerize MTs, fresh GMPCPP was
880 added to final 1mM, incubated on ice for 5 minutes, a second cycle of polymerization was

881 performed by incubating the mixture at 37°C for 30 minutes, and MTs were pelleted again by
882 centrifugation. Supernatant was discarded and MTs were resuspended in 200µl warm BRB80,
883 flash frozen in liquid nitrogen in 5µl aliquots, stored at -80°C and found to be stable for months.
884 To verify that these MT seeds have blunt ends, frozen aliquots were quickly thawed at 37°C,
885 diluted 20-fold with warm BRB80, and incubated at room temperature for 30 minutes to ensure
886 blunt ends as described previously[25]. MTs were pipetted onto CF400-Cu grids (Electron
887 Microscopy Sciences), incubated at room temperature for 60 seconds and then wicked away. 2%
888 uranyl acetate was applied to the grids for 30 seconds, wicked away, and the grids were air-dried
889 for 10 minutes. The grids were imaged using Phillips CM100 TEM microscope at 130000 x
890 magnification and most MT ends were found to be blunt.

891 To assay MT assembly from blunt MT seeds, MT assembly experiments similar to γ-TuRC
892 nucleation assays were performed with the following variation. A lower concentration 0.05 mg/ml
893 NeutrAvidin (A2666, ThermoFisher) was attached, and washes were performed with warm
894 BRB80 prior to attaching MTs. One aliquot of MT seeds was thawed quickly, diluted to 100-fold
895 with warm BRB80, incubated in the chamber for 5 minutes, unattached seeds were washed with 1
896 vol of warm BRB80, and the slide was incubated at room temperature for 30 minutes to ensure
897 blunt MT ends. Wide bore pipette tips were used for handling MT seeds to minimize the shear
898 forces that may result in breakage of MTs. Nucleation mix was prepared as described above and a
899 low αβ-tubulin concentration (1.4-8.7 µM) was used. MT assembly from blunt seeds was observed
900 immediately after incubating the slide on the objective heater. Imaging and analysis were
901 performed as described above for to γ-TuRC nucleation assays. The probability curves $p(t)$ for
902 MT assembly were obtained by normalizing for the total number of seeds observed in the field of
903 view $N(t)/N_0$, which allow for direct comparison across datasets. 95% confidence interval

904 represents the theoretical variation in the number of MTs assembled from seeds across fields of
905 view as described above. Rate of nucleation $\left.\frac{dp}{dt}\right|_{t\to 0}$ was obtained as the slope of a straight line fit
906 to the initial region of $p(t)$ versus t curve for every tubulin concentration C. Power-law analysis
907 was performed similar to γ-TuRC nucleation assays described above. However, as assembly from
908 seeds occur near minimal tubulin concentration needed for polymerization of the plus end C_*, the
909 governing equation reads,

910 $$\frac{dp(t)}{dt} = k_{nucleate}(1 - p(t))C^{n-1}(C - C_*) \quad (6)$$

911 At the start of the reaction $t = 0$, no MTs have nucleated $p(t = 0) = 0$, therefore at early times
912 we assume $1 - p(t) \approx 1$ to simplify the calculation of the critical MT nucleus. Converting
913 equation (6) in log scale with these simplifications,

914 $$ln\left(\left.\frac{dp}{dt}\right|_{t\to 0}\right) = (n-1)ln(C) + ln(C - C_*) + a \quad (7)$$

915 Critical tubulin concentration for polymerization C_* was obtained from the x-intercept of the
916 growth speed curve ($C_* = 1.4$μM) as described previously. Finally, observing the total number of
917 MT seeds for assembly allows for direct pooling of all datasets for MT assembly from seeds. From
918 fitting a straight line between $ln\left(\left.\frac{dp}{dt}\right|_{t\to 0}\right)$ versus $ln(C - C_*)$ for all concentrations, we found the
919 slope $n \approx 1$, which satisfies the above equation and provides the size of critical nucleus for MT
920 assembly from seeds $n \approx 1$.

921

922 **Size exclusion chromatography of γ-tubulin and αβ-tubulin**

923 Size exclusion chromatography of γ-tubulin and αβ-tubulin was performed as follows at 4°C.
924 Purified, human γ-tubulin was diluted to 300nM in γ-TB buffer (defined 50mM K-MES pH6.6,
925 5mM MgCl2, 1mM EGTA, 10mM thioglycerol, 10μM GDP) with additional 250mM KCl, and

926 αβ-tubulin individually diluted to 20μM or 70μM with BRB80 buffer. Protein aggregates were
927 pelleted by ultracentrifugation of the proteins individually at 80,000 rpm in TLA 100 (Beckman
928 Coulter) for 15 minutes. γ-tubulin and αβ-tubulin were mixed in 1:1 volume ratio to achieve final
929 concentrations 150nM γ-tubulin to 10μM or 35μM αβ-tubulin and incubated on ice for 10 minutes.
930 500μl of the mixture was loaded onto Superdex 200 Increase 10/300 column (GE Healthcare). The
931 column was equilibrated with γ-TB buffer containing 90 mM KCl and chromatography was
932 performed in this buffer. For control chromatography runs, equal volume of corresponding buffer
933 was used. Absorbance at 214 nm was recorded. 0.3ml fractions were collected and alternate
934 fractions eluted between 8.5ml and 16.6ml were analyzed via immunoblot against γ-tubulin, αβ-
935 tubulin and StrepII tag on γ-tubulin. Secondary antibody conjugated to 800nm IRDye (LI-COR)
936 was used and imaged with Odyssey CLx imaging station (LI-COR). High molecular weight gel
937 filtration standards (Thyroglobulin, Aldolase and Ovalbumin) were purchased from GE Healthcare
938 (Catalog #28403842) and used to estimate the Stokes' radii of eluted proteins in the same buffer
939 as used for corresponding SEC run[69].
940
941 **Measurement of affinity between γ-tubulin and αβ-tubulin with single molecule microscopy**
942 γ-TuRC nucleation assay was adapted as follows to measure the interaction affinity between γ-
943 tubulin and αβ-tubulin. The imaging channel was prepared by sequentially with 5% w/v Pluronic
944 F-127 incubation, casein buffer washes, 0.05 mg/ml NeutrAvidin incubation in casein buffer,
945 BRB80 washes as described above. 100-200nM of biotinylated αβ-tubulin or BRB80 buffer was
946 introduced in the flow chamber and incubated for 5 minutes on a cold block, and unbound αβ-
947 tubulin was washed with 50μl of BRB80. During the incubations, binding mix was prepared with
948 100nM of Alexa-568 or Alexa-488 labelled αβ-tubulin (24-50% labelling percentage) or with

949 100nM of labelled γ-tubulin with identical fluorophore (7% labelling percentage) in 1x assay
950 buffer, ultracentrifuged for 12 minutes in TLA100, oxygen scavengers were added, and reaction
951 mixture was introduced into the flow chamber.

952 Single molecule binding of fluorescent γ-tubulin or αβ-tubulin with biotinylated αβ-tubulin
953 was visualized with TIRF microscopy using the setup described above at 33.5°C. Images were
954 collected at 2-5 fps with EMCCD gain of 300 and exposure time of 200 ms each frame, and data
955 acquisition was started within 60-90 seconds after flowing fluorescent γ-tubulin or αβ-tubulin.
956 Minimal photobleaching was observed for the first 15 seconds of time series acquired, which was
957 used to extract the number by molecules bound by analyzing with the single molecule analysis
958 software ThunderSTORM[70]. Specifically, images were filtered with wavelet B-spline filter (scale
959 2-3 and order 3), molecules localized with 8-connected local maximum approach, threshold
960 selected as the standard deviation of the first wavelet level, and suggested settings for sub-pixel
961 localization by fitting an integrated Gaussian PSF model with maximum likelihood estimation was
962 performed. The number of single molecules identified for each frame were recorded. The results
963 from ThunderSTORM analysis were verified against manually identified molecules with a sample
964 dataset. To obtain how many molecules bind to biotin-αβ-tubulin for every frame, the number of
965 molecules of γ-tubulin or αβ-tubulin bound inspecifically to the coverslip were independently
966 subtracted from the number of molecules bound to biotin-αβ-tubulin, and this value was divided
967 by the known fluorescent labelling percentage. The calculated number of γ-tubulin or αβ-tubulin
968 bound were averaged for the first 14 seconds (28 frames) for each dataset, and their mean and
969 standard deviation was reported.

970 Interaction assays between αβ-tubulin and γ-tubulin were confirmed with biolayer
971 interferometry using Octet RED96e (ForteBio) instrument in an 8-channel plate format. The plate

972 temperature was held at 33°C and the protein samples were shaken at 400 rpm during the
973 experiment. First, Streptavidin coated biosensors (ForteBio) were rinsed in interaction buffer
974 (50mM K-MES pH 6.6, 100mM KCl, 5mM $MgCl_2$, 1mM EGTA, 0.05% Tween20, 1mM GTP).
975 100-400 nM biotin-labeled αβ-tubulin, or blank buffer, was bound to Streptavidin sensor until
976 loaded protein results in a wavelength shift (Δλ) of 3 nm. Unbound protein was removed by rinsing
977 the sensor in interaction buffer, and interaction with αβ-tubulin was measured by incubating the
978 sensor containing biotinylated αβ-tubulin with 0-35 μM unlabeled αβ-tubulin or 0-1 μM unlabeled
979 γ-tubulin in interaction buffer for 5 minutes. Δλ (nm) was recorded as a measure of the amount of
980 unlabeled αβ-tubulin that binds to the sensor.
981
982 **Nucleation of microtubules from purified γ-tubulin**
983 MT assembly experiments from purified γ-tubulin was performed similar to γ-TuRC nucleation
984 assays described above with following variation. No avidin was attached to the coverslips, and
985 varying concentration of γ-tubulin was prepared by diluting purified γ-tubulin in a high salt buffer
986 (50mM K-MES pH 6.6, 500mM KCl, 5mM $MgCl_2$, 1mM EGTA), centrifuging to remove
987 aggregates separately for 12 minutes in TLA100 before adding to the nucleation mix containing
988 15 μM αβ-tubulin (5% Cy5-labeled) with BSA, glucose oxidase and catalase as described above
989 to a final salt concentration of 44mM KCl. The reaction mixture was introduced into the flow
990 chamber and imaged via TIRF microscopy. A large number of MTs get nucleated immediately in
991 the presence of 250 nM-1000 nM γ-tubulin.
992
993 **Negative stain electron microscopy of γ-tubulin filaments**

994 Purified γ-tubulin was observed to form higher order oligomers previously using analytical gel
995 filtration[29]. γ-tubulin filaments were prepared by diluting pure γ-tubulin to 1μM to the buffer
996 50mM K-MES pH 6.6, 5mM $MgCl_2$, 1mM EGTA, 100mM KCl. 5 μl of γ-tubulin mixture was
997 pipetted onto EM grids (Electron Microscopy Sciences, Catalog number: CF400-Cu), which were
998 glow discharged for 25 seconds. 5 μl sample was incubated on the grid at room temperature for 60
999 seconds and wicked away with filter paper (cat #). Grids were washed with 5 μl of dH_2O 3 times,
1000 stained three times with 0.75% Uranyl formate, where the first two incubations were wicked away
1001 immediately while the last was incubated for 30 seconds. The grids were air-dried for 10 minutes.
1002 Data were collected on a Talos L120C TEM (FEI) equipped with a BM Ceta CCD camera, at a
1003 nominal magnification of 74,000x corresponding to a pixel size of 2.03 Å/pixel on the specimen
1004 with 1 second integration time, and a defocus range of 1-2 μm underfocus. Micrographs were
1005 acquired both in-plane with +0 degree tilt.

1006 Micrographs were converted to mrc file format with IMOD package and imported into
1007 RELION-3.0.6[71] where the data analysis was performed. Contrast transfer function (CTF)
1008 estimation of 370 micrographs performed using Gctf[72]. Segments along the length of thin filaments
1009 were picked manually. Filaments were boxed into helical segments with 50Å rise, and subjected
1010 to two rounds of 2D classification and particle selection. 1001 particles were selected and were
1011 used to generate an ab-initio 3D model. One round of refinement using 3D auto-refine was
1012 performed with all particles, followed by one round of 3D classification. 659 particles from the
1013 most populated 3D class were selected and another round of refinement was performed to generate
1014 a final map with the solvent mask. Analysis was performed in UCSF Chimera[73]. Longitudinal
1015 arrangement of αβ-tubulins (pink filament, Fig. 4-supplement 2E) was generated by isolating one
1016 protofilament from PDB: 6DPU[38] and elongating the protofilament with the super-position

1017 function in Coot. Lateral arrangement of γ-tubulin array (blue filament, Fig. 4-supplement 2E) was
1018 generated from the crystal contacts observed in the published P21 crystal array (PDB: 1Z5W[40]),
1019 as described previously[39]. An alternate γ-tubulin arrangement was also generated by isolating the
1020 other possible filament from this P21 symmetry group, where neighboring γ-tubulins neither
1021 arrange linearly nor show lateral contacts (green filament, Fig. 4-supplement 2E). Simultaneous
1022 docking of 4 copies each of longitudinal αβ-tubulin array, lateral γ-tubulin array, or alternate
1023 arrangement of γ-tubulin array, was performed by fitting each copy at 15Å resolution in UCSF
1024 Chimera using the fitmap function. Lateral γ-tubulin arrays, but not other filament arrangements,
1025 display good fit where the γ-tubulin spacing closely matches that of the reconstructed filaments.
1026

1027 **Monte Carlo simulations of microtubule nucleation by γ-TuRC**

1028 Simulation procedure

1029 Kinetic Monte Carlo simulations for MT nucleation and assembly by γ-TuRC were coded and run
1030 in MATLAB and were based on a previous stochastic model for the plus-end dynamics of a MT[41].
1031 A type-B MT lattice geometry with 13-protofilaments and a pitch of 3 tubulins at the seam was
1032 assumed, and a similar γ-TuRC geometry was encoded. On the blunt plus-end geometry, αβ-
1033 tubulin dimers in the MT lattice may have no neighbors, one or half a neighbor at the seam. Once
1034 the MT growth occurs into a tapered one, αβ-tubulin dimers can also have one or two neighbors.

1035 New αβ-tubulin dimers arrive with a constant on rate, k_{on} ($M^{-1}s^{-1}$) on each protofilament.
1036 This on rate is equal for each protofilament on the plus-end or on γ-TuRC and remains constant
1037 during the simulation. An input concentration of αβ-tubulin dimers was assumed to be constant
1038 and not be depleted as shown by previous calculations[68]. Therefore, the net on-rate at each time
1039 step is, $k_{on}C$ (s^{-1}), where C is the concentration of αβ-tubulin dimers. The interactions between

αβ-tubulins was assumed to occur with longitudinal and lateral bond energies, $\Delta G_{Long,\alpha\beta-\alpha\beta}$ and $\Delta G_{Lat,\alpha\beta-\alpha\beta}$, respectively. All αβ-tubulin dimers recruited to the MT lattice or γ-TuRC have a longitudinal bond, and the lateral bond energy depends on the arrangement of neighboring αβ-tubulin dimers. The longitudinal bond energy between γ-/αβ-tubulin on γ-TuRC is $\Delta G_{Long,\gamma-\alpha\beta}$. As a result, the dissociation rate (off-rate) of individual tubulin dimers from the lattice differs and is a function of total bond energy ΔG_{tot}. ΔG_{tot} is a sum of the longitudinal bond energy, $\Delta G_{Long,\alpha\beta-\alpha\beta}$ or $\Delta G_{Long,\gamma-\alpha\beta}$, plus the total lateral bond energy from all the neighbors, $m \times \Delta G_{Lat,\alpha\beta-\alpha\beta}$. Based on previous works, we also posit that when a tubulin dimer dissociates, all dimers above it in the protofilament dissociate as well. The off-rate of each dimer was then calculated from the following equation as derived previously[41],

$$lnK = ln\left(\frac{k_{on}}{k_{off}\ (s^{-1})}\right) = -\frac{\Delta G_{tot}}{k_B T} \quad (8)$$

An open conformation of native γ-TuRC was assumed as observed in recent cryo-EM structures[13–15]. The αβ-tubulins assembled on neighboring sites do not form lateral interactions in the open conformation. A possible transition to a closed γ-TuRC state was allowed with a thermodynamic penalty of $\Delta G_{\gamma TuRC-conf}$. However, if *n* lateral bonds form upon this transition from αβ-tubulins assembled on neighboring sites, that net energy for an open-to-closed transition is $\Delta G_{close} = \Delta G_{\gamma TuRC-conf} - n\Delta G_{Lat,\alpha\beta-\alpha\beta}$. At each time step in the simulation, the rate of this transition is calculated as, $k_{\gamma TuRC-conf} \times \exp\left(\frac{-\Delta G_{close}}{k_B T}\right)$, where $k_{\gamma TuRC-conf}\ (s^{-1})$ is the pre-factor of the Arrhenius equation. Hydrolysis of incorporated tubulin dimers was ignored because few catastrophe events were observed in our experiments.

To execute the stochastic simulations, we formulate a list of possible events at every time step, including association of a αβ-tubulin dimer, dissociation of a αβ-tubulin dimer, or transition

1062 of γ-TuRC to closed state. The forward rate of each event is calculated as described above. A
1063 uniform random number (R_i) from 0 to 1 is generated for each possible event in the list and a
1064 single realization of the exponentially distributed time is obtained for each event,

1065 $$t_i = \frac{-\ln(R_i)}{k_i\,(s^{-1})} \quad (9)$$

1066 The event with the shortest execution time is implemented and time elapsed during the simulation
1067 is advanced by t_i seconds. Each simulation was run with a maximum defined time, usually
1068 between 100-500 seconds, or were stopped once the MT grew a total of 2-5μm in length. The
1069 MATLAB code for simulations is provided in the Supplementary Materials.

1070

1071 Parameter estimation

1072 MT growth parameters were determined by fitting to experimental growth speed curves. Briefly,
1073 20 simulations were performed for each concentration from 2-20μM tubulin for 100 seconds each.
1074 MT length versus time was plotted. Growth speed was obtained from the slope of a linear curve
1075 fit of the polymerizing stretch of the length versus time plot. Parameter values of $k_{on} =$
1076 $1.3 \times 10^6\ (\mu M^{-1}s^{-1}), \Delta G_{Long,\alpha\beta-\alpha\beta} = -7.2k_BT, \Delta G_{Lat,\alpha\beta-\alpha\beta} = -6.5k_BT$ resulted in the best
1077 fit for all tubulin concentrations. These parameter values are similar to those obtained in previous
1078 reports[31,41]. With these polymerization parameters fixed, we varied the remaining parameters.
1079 $\Delta G_{Long,\gamma-\alpha\beta}$ was varied from $(0.7 - 1.3) \times \Delta G_{Long,\alpha\beta-\alpha\beta}$. $\Delta G_{\gamma TuRC-conf}$ was varied from $+(0 -$
1080 $30)k_BT$ and $k_{\gamma TuRC-conf}$ from $(1 - 0.001)\ s^{-1}$. For each parameter set, we performed 200-500
1081 simulations each at specific tubulin concentrations between 2-50μM. For each simulation, the time
1082 of γ-TuRC ring closure was recorded as the nucleation time as it represents the transition from
1083 zero MT length to a continuously growing MT. For the simulation where no MT nucleation
1084 occurred, a nucleation time of infinity was recorded. Cumulative probability distribution of

1085 nucleation ($p(t)$) versus time was generated from the log of nucleation times for each tubulin
1086 concentration. Rate of nucleation $\left.\frac{dp}{dt}\right|_{t\to 0}$ was obtained by a linear fit from the initial part of each
1087 nucleation fit, as described above. The slope of a straight line was fit to $ln\left(\left.\frac{dp}{dt}\right|_{t\to 0}\right)$ versus $ln(C)$,
1088 as outlined in equations (2-3) above, provide the size of critical nucleus n. The nucleation curves
1089 and power-law analysis was compared with experimental data for γ-TuRC-mediated nucleation.
1090 The best agreement was found with $\Delta G_{Long,\gamma-\alpha\beta} = 1.1 \times \Delta G_{Long,\alpha\beta-\alpha\beta}$, as supported by our
1091 biochemical measurements, $\Delta G_{\gamma TuRC-conf} = 10k_BT$ and $k_{\gamma TuRC-conf}$=0.01 s^{-1}.

1092 To analyze the arrangement of αβ-tubulins in the transition state, the state of γ-TuRC with
1093 αβ-tubulin dimers was recorded at the time of γ-TuRC ring closure for 2119 simulations. 3D-
1094 dimensional probability distribution of total number of αβ-tubulin dimers and number of lateral
1095 αβ-tubulin bonds was generated. The arrangement of αβ-tubulin dimers in the most frequently
1096 occurring transition states were displayed with schematics.

1097 To capture the dynamics of MT assembly from blunt seeds, we simulated nucleation
1098 assuming a closed γ-TuRC geometry as follows. Lateral bonds between αβ-tubulins assembled on
1099 the neighboring sites on γ-TuRC were allowed and $\Delta G_{Long,\gamma-\alpha\beta}$ was set equal to $\Delta G_{Long,\alpha\beta-\alpha\beta}$.
1100 Simulations were performed as described above with the following change. The time when the
1101 MT in each simulation grew to 50nm length was recorded to generate the probability distribution.
1102 Nucleation curves and power-law analysis was compared with experimental data for seed-
1103 mediated MT assembly.

1104

1105 **Measuring the effect of microtubule associated proteins on γ-TuRC-mediated nucleation**

1106 Effect of microtubule associated proteins (MAPs) was measured on γ-TuRC's nucleation activity.
1107 γ-TuRC was attached on the coverslips using the setup described above and a control experiment

1108 was performed with identical reaction conditions for each protein tested. Because CDK5RAP2's
1109 γ-TuNA motif and NME7 bind γ-TuRC, to test their activity γ-TuRC was additionally incubated
1110 6μM γ-TuNA motif or 6μM NME7 to γ-TuRC for 5 minutes prior to attachment to coverslips to
1111 maximize their likelihood of binding and the control γ-TuRC reaction was treated identically with
1112 the storage buffer for each protein. Nucleation mix was then prepared containing 10.5 μM αβ-
1113 tubulin concentration (5% Cy5-labeled tubulin) as specified along with 1mg/ml BSA and oxygen
1114 scavengers, and either buffer (control), 10nM GFP-TPX2, 3μM γ-TuNA motif from CDK5RAP2,
1115 6μM NME7, 5μM Stathmin or 10nM MCAK was added. To test NME7 or MCAK's effect, the
1116 assay buffer additionally contained 1mM ATP. The reaction mixture containing tubulin and MAP
1117 at specified concentration was introduced into the flow chamber containing γ-TuRC, and MT
1118 nucleation was visualized by imaging the Cy5-fluorescent channel at 0.5-1 frames per second. For
1119 TPX2, fluorescence intensity of the protein was simultaneously acquired.

1120 The number of MTs nucleated over time was measured as described above and the effect
1121 of protein on γ-TuRC's nucleation activity was assessed by comparing nucleation curves with and
1122 without the MAP. In order to normalize for the total number of γ-TuRC molecules obtained from
1123 different purifications and enable pooling results from all datasets, the number of MTs nucleated
1124 at a specified time point, mentioned in each figure legend, was set to 1 for γ-TuRC only (no MAP)
1125 control reactions. As before the shaded region represents 95% confidence interval ($n \pm 2\sqrt{n}$) in
1126 the number of MTs, n assuming a Poisson distribution that determines binding and subsequent
1127 nucleation from γ-TuRCs and was calculated and displayed on each nucleation time-course.

1128

1129 **Cooperative microtubule nucleation assay with purified XMAP215 and γ-TuRC**

1130 A similar set of experiments as above to characterize the effect of MAPs was performed to study
1131 the effect of XMAP215 on γ-TuRC-mediated nucleation with the single molecule assays with the
1132 following differences. 20nM of XMAP215-GFP-7xHis was added to nucleation mix prepared with
1133 3.5-7 μM αβ-tubulin concentration (5% Cy5-label) in XMAP assay buffer (80mM K-PIPES, 1mM
1134 $MgCl_2$, 1mM EGTA, 30mM KCl, 0.075% w/v methylcellulose 4000 cp, 1% w/v D-(+)-glucose,
1135 0.007% w/v Brij-35, 5mM BME, 1mM GTP). MTs nucleated from attached γ-TuRC with and
1136 without XMAP215 were measured to assess the efficiency of nucleation induced by XMAP215.
1137 To assess if N- or C-terminal domains of XMAP215 increases nucleation efficiency, wild-type
1138 XMAP215 was replaced with a C-terminal construct of XMAP215 (TOG5-Cterminus-GFP) or an
1139 N-terminal construct (TOGs1-4-GFP) in the described experiment.

1140 To measure the kinetics of cooperative nucleation XMAP215 and γ-TuRC, a constant
1141 density of γ-TuRC was attached as described above and nucleation mix nucleation mix was
1142 prepared with a range of αβ-tubulin concentration between 1.6-7 μM (5% Cy5-label) with 20-
1143 25nM of XMAP215-GFP-7xHis or XMAP215-TEV-GFP-7xHis-StrepII in XMAP assay buffer,
1144 introduced into reaction chamber and MT nucleation was imaged immediately by capturing dual
1145 color images of XMAP215 and tubulin intensity at 0.5 frames per second.

1146 Data analysis was performed as above for γ-TuRC mediated nucleation, theoretical field-
1147 to-field heterogeneity in the number of MTs nucleated was represented with a Poisson distribution
1148 as before and 95% confidence interval. Critical tubulin nucleus for cooperative nucleation from
1149 XMAP215 and γ-TuRC was obtained as described for γ-TuRC alone (equations (1-3)). A straight
1150 line was fit to log rate of nucleation $ln\left(\frac{dN}{dt}\Big|_{t\to 0}\right)$ versus log tubulin concentration $ln(C)$ and its
1151 slope provides the size of critical nucleus n. Finally, to normalize for the total number of γ-TuRC

1152 molecules obtained from different purifications, the rate of cooperative nucleation from XMAP215
1153 and γ-TuRC at 3.5μM tubulin was set to 1. All datasets were pooled and reported.
1154
1155 **Triple-color imaging of XMAP215, γ-TuRC and microtubules**
1156 For triple-color fluorescence assays, Alexa-568 and biotin-conjugated γ-TuRC was first attached
1157 to coverslips as described above with the following variation: 0.05 mg/ml of NeutrAvidin was
1158 used for attaching γ-TuRC. Nucleation mix was prepared with 7μM αβ-tubulin (5% Cy5-label),
1159 10nM Alexa-488 XMAP215-SNAP or XMAP215-GFP with BSA and oxygen scavengers in
1160 XMAP assay buffer (80mM K-PIPES, 1mM $MgCl_2$, 1mM EGTA, 30mM KCl, 0.075% w/v
1161 methylcellulose 4000 cp, 1% w/v D-(+)-glucose, 0.007% w/v Brij-35, 5mM BME, 1mM GTP)
1162 and introduced into the reaction chamber containing attached γ-TuRC. Three-color imaging per
1163 frame was performed with sequential 488, 568 and 647 nm excitation and images were acquired
1164 with EMCCD camera at 0.3 frames per second.

1165 **Figure legends**

1166

1167 **Figure 1. Single molecule microscopy of microtubule nucleation from γ-TuRC.**

1168 (A) Schematic for microtubule nucleation from γ-TuRC. Biochemical features of γ-TuRC
1169 including the γ-/αβ-tubulin interaction affinity and conformation of γ-TuRC determine to MT
1170 nucleation activity and transition state. (B) Purified, biotinylated γ-TuRC molecules were attached,
1171 incubated with αβ-tubulin and time-lapse of MT nucleation after is shown. MTs already nucleated
1172 in the first frame are marked with yellow arrow, while new MT nucleation events between the first
1173 and last frame with blue arrows. (C) Three representative kymographs of (left) unlabeled γ-TuRC
1174 nucleating MTs colored in grayscale, or (right) fluorescent γ-TuRC, pseudo-colored in green,
1175 nucleating MTs, pseudo-colored in red. Arrows point to nucleation sites. The experiments with
1176 unlabeled γ-TuRC were repeated more than ten times with independent γ-TuRC preparations,
1177 while those fluorescent γ-TuRC repeated were repeated six times with three independent γ-TuRC
1178 preparations. See Figure 1-figure supplement 1 and Videos 1-2.

1179

1180 **Figure 2. Molecular composition of transition state in γ-TuRC-mediated nucleation.**

1181 (A) Titrating tubulin concentration with constant the density of γ-TuRC. MT nucleation from γ-
1182 TuRC begins at 7μM tubulin. (B) MT plus-end growth speed increases linearly with tubulin
1183 concentration. Individual data points are plotted, and linear fit (red line) with shaded mean±2std
1184 (95% confidence interval) is displayed. Critical concentration for polymerization as $C^* = 1.4$ μM.
1185 Inset: Number of MTs nucleated by γ-TuRCs within 120 seconds varies non-linearly with tubulin
1186 concentration. (C) Number of MTs nucleated ($N(t)$) over time (t) is plotted for varying tubulin
1187 concentration to obtain rate of nucleation as the slope of the initial part of the curves. Shaded

1188 regions represent 95% confidence interval ($n \pm 2\sqrt{n}$) in the number of nucleated MTs (n)
1189 assuming a Poisson distribution as described in Methods. (D) Number of tubulin dimers (n) in the
1190 critical nucleus on γ-TuRC was obtained as 3.9±0.5 from the equation $\left.\frac{dN}{dt}\right|_{t\to 0} = kC_{tub}{}^{n}$ displayed
1191 on a log-log axis as detailed in Methods. The rate of nucleation at 10.5μM was set to 1 to normalize
1192 differences in γ-TuRC concentration from individual experiments. The experiments and analyses
1193 in (A-D) were repeated identically three times with independent γ-TuRC preparations. MT
1194 nucleation data, prior to normalization, from one representative dataset is displayed in (B-C).
1195 Analyses from all repeats was pooled and normalized as described above, and data points from 15
1196 nucleation-time curves are plotted in (D). See Video 3.
1197
1198 **Figure 3. Comparison of γ-TuRC-mediated, spontaneous and seed-templated nucleation.**
1199 (A) Spontaneous MT nucleation (schematized) was measured with increasing tubulin
1200 concentration and high concentrations. 14μM tubulin is required. (B) Number of MTs ($N(t=\tau)$)
1201 nucleated spontaneously were plotted against tubulin concentration. Power-law curve was fit as
1202 $N(t = \tau) = kC^n$ on a log-log axis, and linear scale in the inset. Tubulin cooperativity (exponent)
1203 of n = 8.1±0.9 was obtained as detailed in Methods. Experiments and analyses in (A-B) were
1204 repeated thrice independently, all data were pooled and data points from 11 nucleation curves are
1205 plotted in (B). In the inset, data is represented in linear plot, where shaded regions represent 95%
1206 confidence interval ($n \pm 2\sqrt{n}$) in the number of nucleated MTs (n) assuming a Poisson
1207 distribution as described in Methods. Scale bars, 10μm. (C) Schematic and an example micrograph
1208 of blunt, stabilized MT seeds is shown and MT assembly from them was observed (bottom) with
1209 varying tubulin concentration. (D) Cumulative probability of MT assembly from seeds ($p(t)$) over
1210 time (t) is plotted and rate of nucleation was obtained as the slope from initial part of the curves.

1211 Shaded regions represent 95% confidence interval ($n \pm 2\sqrt{n}$) in the number of MTs assembled
1212 (n) from seeds as described in Methods. (E) As described in Methods, the measurements fit well
1213 to equation $\left.\frac{dp}{dt}\right|_{t\to 0} = k(C - C^*)^n$ displayed on a log-log plot. n = 1±0.3 was obtained showing
1214 nearly non-cooperative assembly of tubulin dimers. The experiments and analyses in (C-E) were
1215 repeated three times independently. MT nucleation data, prior to normalization, from one
1216 representative dataset is displayed in (C-D). Analyses from all experiments was pooled, and data
1217 points from a total of 11 nucleation-time curves are reported in (E). See Figure 3-figure supplement
1218 1 and Videos 4-5.
1219
1220 **Figure 4. γ-tubulin binds to αβ-tubulin with a high affinity.**
1221 (A) Size-exclusion chromatography was performed with 150nM of γ-tubulin alone (i) and with
1222 35μM and 10μM αβ-tubulin in (ii) and (iii) respectively. Gel filtration fractions were analyzed via
1223 SDS–PAGE followed by immunoblot with γ-tubulin and αβ-tubulin antibodies. A shift in the γ-
1224 tubulin elution to fraction H was observed with both 35μM and 10μM αβ-tubulin, denoting
1225 complex formation with αβ-tubulin. See Fig. 4-figure supplement 1A. Stokes' radii of reference
1226 proteins: thyroglobulin (8.6 nm), aldolase (4.6 nm) and ovalbumin (2.8 nm), are marked at their
1227 elution peak. Size exclusion runs were repeated three times, with the exception of 10μM αβ-tubulin
1228 run that was performed twice. (B) Single molecule microscopy was performed with γ-tubulin and
1229 αβ-tubulin. Control buffer (left panels, (i) and (ii)) or biotinylated αβ-tubulin (right panels, (i) and
1230 (ii)) was attached to coverslips, incubated with fluorescent αβ-tubulin (i) or γ-tubulin (ii)
1231 molecules, set as 0 seconds, and their binding at 60-90 seconds. (C) Number of bound molecules
1232 were analyzed for the first 15 seconds of observation described in Methods. Experiments and
1233 analyses in (B-C) were repeated identically two times, pooled and reported. n =56 data points each

1234 were displayed as mean ± std in the bar graph in (C). Further confirmed with a third supporting
1235 experimental set where the observation began later at 180 seconds and was therefore, not pooled.
1236 See also Figure 4-figure supplements 1-2.
1237
1238 **Figure 5. Monte Carlo simulations of microtubule nucleation from γ-TuRC.**
1239 (A) Kinetic Monte Carlo simulations of MT nucleation were performed. Helical MT lattice was
1240 simulated with 13 protofilaments and a pitch of 3 tubulin monomers across the seam. Native γ-
1241 TuRC was simulated in an open conformation and was allowed transition into a closed
1242 conformation with a thermodynamic penalty of $\Delta G_{\gamma TuRC-conf}$. αβ-tubulin dimers form
1243 longitudinal bonds with energies, $\Delta G_{Long,\gamma-\alpha\beta}$ and $\Delta G_{Long,\alpha\beta-\alpha\beta}$ to γ-tubulin and other αβ-
1244 tubulins, respectively, and lateral bond with energy, $\Delta G_{Lat,\alpha\beta-\alpha\beta}$ with neighboring αβ-tubulin
1245 dimers. (B) MT length (μm) versus time (seconds) traces of two independent simulations are
1246 presented (bottom). MT nucleation occurs are variable time points for each model realization.
1247 Zoomed-in insets of the first simulation show the length of the tallest protofilament (nm) and total
1248 number of αβ-tubulin dimers assembled in the first 200 msec and 5 sec near the transition state of
1249 the simulation. (C) Simulations were performed with $k_{on} = 1.3 \times 10^6\ (M^{-1}s^{-1}pf^{-1})$,
1250 $\Delta G_{Long,\alpha\beta-\alpha\beta} = -7.2k_BT$, $\Delta G_{Lat,\alpha\beta-\alpha\beta} = -6.5k_BT$, $\Delta G_{Long,\gamma-\alpha\beta} = 1.1\Delta G_{Long,\alpha\beta-\alpha\beta}$,
1251 $k_{\gamma TuRC-conf} = 0.01s^{-1}$. $\Delta G_{\gamma TuRC-conf}$ was varied from $+(0-30)k_BT$. Tubulin concentration
1252 was varied from 2.5-50μM. 200 simulations were performed for a given tubulin concentration at
1253 every parameter set, except for $\Delta G_{\gamma TuRC-conf} = 10k_BT$ where 500 simulations were performed.
1254 From probability of MT nucleation ($p(t)$) versus time (t) curves, the initial rate of nucleation $\left.\frac{dp}{dt}\right|_{t\to 0}$
1255 was measured and plotted against concentration on a log-log axis as detailed in Methods. (D) With
1256 the parameters defined above and $\Delta G_{\gamma TuRC-conf} = 10k_BT$, the transition state at the time of γ-

1257 TuRC's conformational change was recorded for *n*=2119 simulations. Normalized histogram of
1258 total number of αβ-tubulin dimers is plotted (left). 3-dimensional probability distribution of total
1259 number of αβ-tubulin dimers (x) and number of lateral αβ-tubulin interactions (y) is plotted (right).
1260 The most populated transition states are denoted with coordinates (x,y) and schematized. See also
1261 Figure 5-figure supplements 1-2.
1262
1263 **Figure 6. Regulation of γ-TuRC-mediated nucleation by putative activation factors.**
1264 (A) A constant density of γ-TuRC molecules were attached without (left) and with (right) 6μM
1265 CDK5RAP2's γ-TuNA motif and 10.5μM tubulin ± 3μM additional γ-TuNA was added. Scale
1266 bar, 10μm. (B) MTs nucleated from γ-TuRC molecules were analyzed and 3-6μM CDK5RAP2's
1267 γ-TuNA motif (left) or 1-6μM NME7 (right). Experiments and analyses in (A-B) were individually
1268 repeated twice on different days of experimentation with independent or same γ-TuRC
1269 preparations. Number of MTs nucleated in control reactions at 200 seconds for γ-TuNA, and at
1270 150 seconds for NME7 was set to 1 to account for variable γ-TuRC concentration across
1271 purifications, all data was pooled and reported. Individual datasets with ±γ-TuNA and ±NME7 is
1272 represented with solid or dashed curves. Shaded regions represent 95% confidence interval ($n \pm$
1273 $2\sqrt{n}$) from each dataset in the number of nucleated MTs (n) assuming a Poisson distribution as
1274 described in Methods. (C-D) A constant density of γ-TuRC molecules were attached and 10.5μM
1275 tubulin ± 10-20nM GFP-TPX2 was added. Experiments and analyses were repeated thrice with
1276 independent γ-TuRC preparations. To account for the variable γ-TuRC concentration across
1277 purifications, the number of MTs nucleated in control reactions at 150 seconds was set to 1. All
1278 data was pooled and reported. Individual dataset with ±TPX2 is represented with solid, dashed or
1279 dotted curves. Shaded regions represent 95% confidence interval ($n \pm 2\sqrt{n}$) from each dataset in

1280 the number of nucleated MTs (n) assuming a Poisson distribution as described in Methods. See
1281 Figure 6-figure supplement 1 and Video 6.
1282
1283 **Figure 7. Role of XMAP215 and microtubule-associated proteins in microtubule nucleation**
1284 **with γ-TuRC.**
1285 (A) γ-TuRCs were attached and 7μM tubulin (pseudo-colored in red) ± 20nM XMAP215-GFP
1286 (pseudo-colored in green) was added. Scale bar, 10μm. Experiments and analyses in (A-B) were
1287 repeated thrice with independent γ-TuRC preparations. (B) Number of MTs nucleated ($N(t)$) over
1288 time (t) was measured and control reactions at 120 seconds was set to 1 to account for variable γ-
1289 TuRC concentration across purifications, all data was pooled and reported. Individual datasets with
1290 ±XMAP215 is represented with solid or dashed curves. Shaded regions represent 95% confidence
1291 interval ($n \pm 2\sqrt{n}$) from each dataset in the number of nucleated MTs (n) assuming a Poisson
1292 distribution as described in Methods. See also See Figure 7-figure supplement 1A-B. (C) Sequence
1293 of events during cooperative MT nucleation by γ-TuRC and XMAP215 was visualized using
1294 labeled γ-TuRC (blue), XMAP215 (red) and tubulin (green) represented in a time sequence and
1295 kymograph. γ-TuRC and XMAP215 form a complex prior to MT nucleation. XMAP215
1296 molecules reside on γ-TuRC for before MT nucleation. The experiment was repeated a total of 8
1297 times with two independent γ-TuRC preparations and independent XMAP215 purifications. Scale
1298 bar, 5μm. (D-E) Number of MTs nucleated ($N(t)$) over time (t) was measured after titrating tubulin
1299 with constant γ-TuRC and XMAP215 concentration. XMAP215/γ-TuRC molecules nucleate MTs
1300 from 1.6 μM tubulin. Shaded regions represent 95% confidence interval ($n \pm 2\sqrt{n}$) in the number
1301 of nucleated MTs (n) assuming a Poisson distribution as described in Methods. (E) Number of
1302 tubulin dimers (n) in the critical nucleus on cooperative nucleation by γ-TuRC/XMAP215 was

1303 obtained as 3.3±0.8 from the equation $\left.\frac{dN}{dt}\right|_{t\to 0} = kC_{tub}{}^{n}$ displayed on a log-log axis as detailed in

1304 Methods. The rate of nucleation at 3.5μM was set to 1 to normalize differences in γ-TuRC

1305 concentration from individual experiments. Experiment and analyses in (D-E) was repeated thrice

1306 over the entire concentration range with independent γ-TuRC preparations, and fewer

1307 concentration points were repeated another two times. All five datasets were pooled and data points

1308 from a total of 18 nucleation-time curves are reported in (E). Simulations were adapted to

1309 understand how XMAP215 changes the thermodynamics of γ-TuRC-mediated nucleation.

1310 Parameter values used: $k_{on} = 1.3 \times 10^{6}\ (M^{-1}s^{-1}pf^{-1})$, $\Delta G_{Long,\alpha\beta-\alpha\beta} = -8.64k_BT$,

1311 $\Delta G_{Lat,\alpha\beta-\alpha\beta} = -6.2k_BT$, $\Delta G_{Long,\gamma-\alpha\beta} = -9.5k_BT$, $k_{\gamma TuRC-conf} =$

1312 $0.01s^{-1}$and $\Delta G_{\gamma TuRC-conf} = 10k_BT$. Compared to simulations for γ-TuRC alone (Figure S6A),

1313 either $\Delta G_{Long,\alpha\beta-\alpha\beta}$ was increased 1.2-fold, as proposed previously[41], or both $\Delta G_{Long,\alpha\beta-\alpha\beta}$ and

1314 $\Delta G_{Long,\alpha\beta-\alpha\beta}$ were increased 1.2-fold. 200 simulations each were performed for a range of tubulin

1315 concentration 1.6-7μM. Probability of MT nucleation ($p(t)$) versus time (t) is displayed in (D). The

1316 initial rate of nucleation $\left.\frac{dp}{dt}\right|_{t\to 0}$ was measured at each tubulin concentration and plotted against

1317 concentration on a log-log axis in (E). Linear curve was fit for n=5 simulated data points, and

1318 critical nucleus of 3.8 ± 0.3 αβ-tubulins. Increasing all longitudinal bond energies reproduces the

1319 effect of XMAP215 on γ-TuRC-mediated nucleation. (F) Number of MTs nucleated was measured

1320 to assess the effect of inhibitory MAPs MCAK or Stathmin on γ-TuRC-mediated nucleation.

1321 10.5μM tubulin ± 10nM MCAK, or 7-10.5μM tubulin ± 2-5μM Stathmin was added to attached

1322 γ-TuRC- molecules, and MCAK and Stathmin were both found to inhibit γ-TuRC-mediated

1323 nucleation. Experiments and analyses for both MAPs were repeated thrice individually with

1324 independent γ-TuRC preparations. Number of MTs nucleated in control reactions at 200 seconds

1325 was set to 1 to account for variable γ-TuRC concentration across purifications, all data was pooled
1326 and reported. Individual dataset with ± MCAK are reported with solid, dashed or dotted curves.
1327 For Stathmin, two datasets for 10.5μM tubulin ± 5μM Stathmin are reported with solid and dashed
1328 lines, and one dataset for 7μM tubulin ± 2μM Stathmin in dotted line. Shaded regions represent
1329 95% confidence interval ($n \pm 2\sqrt{n}$) from each dataset in the number of nucleated MTs (n)
1330 assuming a Poisson distribution as described in Methods. See Figure 7-figure supplements 1-2 and
1331 Videos 7-9.

1332 **Supplementary Figure legends**

1333

1334 **Figure 1-figure supplement 1. Controls for γ-TuRC-mediated microtubule nucleation.**

1335 (A) Protein gel of purified γ-TuRC was stained with SYPRO Ruby stain (left). Biotinylated sites
1336 on γ-TuRC was visualized with alkaline phosphatase conjugated to avidin (middle), and Alexa-
1337 568 labelled subunits of γ-TuRC after additional fluorescent conjugation were visualized on an
1338 SDS-PAGE with Typhoon 9500 fluorescence imager (right). Major, known γ-TuRC components
1339 were detected in the purified protein and GCP2/3 are heavily biotinylated or Alexa-568 labelled
1340 during purification. The experiments were repeated thrice with independent γ-TuRC preparations,
1341 with the exception of Alexa-568 scan that was repeated twice. (B) Purified and biotinylated γ-
1342 TuRC was stained with uranyl acetate and visualized with transmission electron microscopy. Scale
1343 bar, 100nm. The experiments were repeated over ten times with independent γ-TuRC preparations.
1344 (C) Fluorescently-labelled and biotinylated γ-TuRC molecules (pseudo-colored as green) were
1345 attached, incubated with 10.5μM αβ-tubulin (pseudo-colored as red) and time-lapse of MT
1346 nucleation after is shown. γ-TuRCs denoted with yellow arrows have nucleated a MTs before 180
1347 seconds, while those labelled with gray arrows nucleated MTs between 180 and 330 seconds
1348 visualized in the time-lapse. Scale bar, 10μm. See Video 2. The experiment was repeated six times
1349 with three independent γ-TuRC preparations. (D) MTs were first nucleated from γ-TuRC with
1350 Alexa 568-labeled tubulin (pseudo-colored in cyan), followed by introduction of Cy5-labeled
1351 tubulin (pseudo-colored in magenta). New tubulin incorporates only on the freely growing, plus-
1352 end but not at the nucleated minus-end. Scale bar, 10μm. The experiment was performed three
1353 times with two independent γ-TuRC preparations. See also Figures 1-2 and Videos 1-2.

1354

1355 **Figure 3-figure supplement 1. Controls for spontaneous and blunt seed-mediated**
1356 **microtubule nucleation.**
1357 (A) Representative kymographs of spontaneously nucleated MT is displayed, demonstrating that
1358 MTs grow from both the minus-end (dotted line) and the plus-end (solid line) and can be
1359 distinguished from γ-TuRC-mediated nucleation. Scale bar, 10μm. Tens of kymographs were
1360 generated from at least three independent experiments. (B) Comparison of γ-TuRC-mediated with
1361 spontaneous MT nucleation and reactions where γ-TuRC was not attached. MTs were nucleated
1362 by attaching purified γ-TuRC (left), adding control buffer to allow for spontaneous MT nucleation
1363 (middle) or leaving avidin out to test the level of nucleation by non-specifically attached γ-TuRCs
1364 (right). Robust MT nucleation only occurs with γ-TuRC attached to coverslips and not in control
1365 reactions. Scale bar, 10μm. (C) MTs nucleation from γ-TuRCs or spontaneously were compared
1366 directly at 10.5μM tubulin concentrations. Shaded regions represent 95% confidence interval($n \pm$
1367 $2\sqrt{n}$) in the number of nucleated MTs (n) assuming a Poisson distribution as described in
1368 Methods. γ-TuRC nucleates significantly higher number of MTs than spontaneous assembly. The
1369 experimental set and analyses in (B-C) were repeated identically two times with independent γ-
1370 TuRC preparations. (D) MTs were assembled from blunt seeds. Tubulin concentration was titrated,
1371 and growth speed of MT plus-ends was measured from kymographs (blue circles). Critical
1372 concentration (C^* = 1.4 μM) was determined from the linear fit (blue line) with shaded 95%
1373 confidence intervals. The experiment and analyses in were repeated thrice with independent seed
1374 preparations. The growth speed of MTs assembled from seeds was overlaid with those nucleated
1375 from γ-TuRC (Fig. 2B, red circles and line) for comparison. See also Videos 3-5 and Figures 2-3.
1376

1377 **Figure 4-figure supplement 1. Purified γ-tubulin binds αβ-tubulin with high affinity *in vitro*.**

1378 (A) Size-exclusion chromatography was performed with 35μM and 10μM αβ-tubulin alone in (i)
1379 and (ii) respectively. Gel filtration fractions were analyzed via SDS–PAGE followed by
1380 immunoblot with αβ-tubulin antibodies. At high concentration (35μM), αβ/αβ-tubulin self-
1381 interaction occurs, and oligomeric species elutes in fractions B-C, as seen via the immunoblot and
1382 absorbance reading. Oligomeric species is not observed at 10μM αβ-tubulin. Stokes' radii of
1383 reference proteins: thyroglobulin (8.6 nm), aldolase (4.6 nm) and ovalbumin (2.8 nm), are marked
1384 at their elution peak. Size exclusion runs was repeated three times for 35μM αβ-tubulin and twice
1385 for 10μM αβ-tubulin. (B) Molecular interaction between γ/αβ-tubulin was verified with bio-layer
1386 interferometry. Buffer ((i) and (ii), left curves) or biotin-tagged αβ-tubulin ((i) and (ii), right
1387 curves) was loaded on the probe as bait. Untagged αβ-tubulin (i) at 0-35μM or γ-tubulin (ii) at 0-
1388 1μM were used as prey. Wavelength shift, $\Delta\lambda$ (nm) was recorded to estimate the mass of bound
1389 protein on the probe. More than 2μM of αβ-tubulin was needed to observe significant binding to
1390 biotin-αβ-tubulin. While γ-tubulin non-specifically associates with the probe to a low extent,
1391 significant association with biotin-αβ-tubulin over this non-specific binding was observed at
1392 significantly lower concentrations. (300nM). The experiments in (i) and (ii) were repeated two
1393 times independently. See also Figure 4.
1394
1395 **Figure 4-figure supplement 2. Purified γ-tubulin nucleates microtubules and assembles**
1396 **laterally into filaments.**
1397 (A) MTs nucleate from high concentration of purified γ-tubulin efficiently and (B) minus-ends of
1398 γ-tubulin-nucleated MTs remain capped while the plus-ends polymerize. The experiments were
1399 repeated twice for all concentration points, with one additional supporting experimental set with
1400 fewer γ-tubulin concentrations. (C) γ-tubulin self-assembles into filaments of variable widths at

1401 high concentration (1-2μM) and physiological salt (100mM KCl) as observed with negative-stain,
1402 transmission electron microscopy. Scale bar, 100nm. (D) 3D reconstructions of negatively stained
1403 γ-tubulin filaments with thin width shows 4 linearly arrays of interacting γ-tubulins. Repeat
1404 distance of approximately 54Å was observed between each γ-tubulin within a linear array. (E)
1405 Longitudinal arrangement of αβ-tubulins (pink filament), generated by isolating one protofilament
1406 from PDB: 6DPU[37,38], docked into map (see Methods). Repeat distance between longitudinally-
1407 interacting αβ-tubulins (40Å) does not match the map spacing (54Å). Lateral arrangement of γ-
1408 tubulin array (blue filament) was generated from the crystal contacts observed in the crystal lattice
1409 of PDB: 1Z5W[39,40]. An alternate γ-tubulin arrangement was also generated (green filament) was
1410 isolated from the other possible filament in this P21 crystal lattice of PDB: 1Z5W. In this
1411 arrangement, neither do neighboring γ-tubulins arrange into straight filaments nor do they show
1412 lateral contacts (green filament). Both filaments were docked into the one position in the map.
1413 Laterally-associated γ-tubulin array (blue filament) display a good fit where the γ-tubulin spacing
1414 closely matches that of the reconstructed filament. In the arrangement displayed in the green
1415 filament, not only are the alternate γ-tubulins farther apart (61Å) and do not make a direct contact,
1416 the alternate γ-tubulins also place off-axis and do not form a linear array. This arrangement does
1417 not recapitulate the linear γ-tubulin arrangement where all γ-tubulins are 54Å apart, as observed
1418 in the map. Thus, our filaments are composed of laterally-associated, linear γ-tubulin arrays.
1419

1420 **Figure 5-figure supplement 1. Parameter variation in Monte Carlo simulations of γ-TuRC-**
1421 **mediated nucleation.**

1422 (A) MT plus-end assembly was simulated. Parameter values used: $k_{on} = 1.3 \times$
1423 $10^6\ (M^{-1}s^{-1}pf^{-1})$, $\Delta G_{Long,\alpha\beta-\alpha\beta} = -7.2k_BT$, $\Delta G_{Lat,\alpha\beta-\alpha\beta} = -6.5k_BT$. 20 simulations each

1424 were performed at tubulin concentration 2-20μM. MT growth speed was obtained from each MT
1425 length versus time trace and overlaid on experimental data. (B) MT nucleation from γ-TuRC was
1426 simulated with input polymerization parameters defined above, $\Delta G_{\gamma TuRC-conf} = 10k_BT$ and
1427 $\Delta G_{Long,\gamma-\alpha\beta} = 1.1\Delta G_{Long,\alpha\beta-\alpha\beta}$. $k_{\gamma TuRC-conf}$ was varied from $(1-0.001)s^{-1}$. Tubulin
1428 concentration was varied from 5-30μM. 200 simulations were performed for a given tubulin
1429 concentration at every $k_{\gamma TuRC-conf}$ value, except for $k_{\gamma TuRC-conf} = 0.01s^{-1}$ where 500
1430 simulations were performed. Probability of MT nucleation ($p(t)$) versus time (t) curves at 15μM
1431 tubulin are displayed in (i). The initial rate of nucleation $\left.\frac{dp}{dt}\right|_{t\to 0}$ was measured and plotted against
1432 concentration on a log-log axis in (ii). The critical nucleus size does not change significantly while
1433 the absolute rate of nucleation decreases with decreasing $k_{\gamma TuRC-conf}$. (C) MT nucleation from γ-
1434 TuRC was simulated with input polymerization parameters defined above, $\Delta G_{\gamma TuRC-conf} =$
1435 $10k_BT$ and $k_{\gamma TuRC-conf} = 0.01s^{-1}$. $\Delta G_{Long,\gamma-\alpha\beta}$ was varied from $(0.7-1.3)\times\Delta G_{Long,\alpha\beta-\alpha\beta}$.
1436 200 simulations were performed for every $\Delta G_{Long,\gamma-\alpha\beta}$ value at tubulin concentrations between
1437 2.5-30μM, except for $\Delta G_{Long,\gamma-\alpha\beta} = 1.1\Delta G_{Long,\alpha\beta-\alpha\beta}$ where 500 simulations were performed.
1438 Probability of MT nucleation ($p(t)$) versus time (t) curves at 20μM tubulin are displayed in (i). The
1439 initial rate of nucleation $\left.\frac{dp}{dt}\right|_{t\to 0}$ was measured and plotted against concentration on a log-log axis
1440 in (ii). For $0.7, 0.9, 1.3\Delta G_{Long,\alpha\beta-\alpha\beta}$, either few MTs nucleate or nucleation occurs immediately,
1441 and critical nucleus size could not be accurately measured. See also Figure 5.
1442
1443 **Figure 5-figure supplement 2. Simulations of microtubule nucleation from γ-TuRC and from**
1444 **blunt seeds.**

1445 (A) Simulations recapitulated experimental data for γ-TuRC-mediated MT nucleation. Parameter
1446 values used: $k_{on} = 1.3 \times 10^6\ (M^{-1}s^{-1}pf^{-1})$, $\Delta G_{Long,\alpha\beta-\alpha\beta} = -7.2k_BT$, $\Delta G_{Lat,\alpha\beta-\alpha\beta} =$
1447 $-6.5k_BT$, $\Delta G_{Long,\gamma-\alpha\beta} = 1.1\Delta G_{Long,\alpha\beta-\alpha\beta}$, $k_{\gamma TuRC-conf} = 0.01s^{-1}$ and $\Delta G_{\gamma TuRC-conf} =$
1448 $10k_BT$. 500 simulations each were performed for a range of tubulin concentration 5-25μM.
1449 Probability of MT nucleation (*p*(*t*)) versus time (*t*) is displayed in (i). The initial rate of nucleation
1450 $\left.\frac{dp}{dt}\right|_{t\to 0}$ was measured at each tubulin concentration and plotted against concentration on a log-log
1451 axis in (ii). Linear curve was fit for *n*=5 simulated data points, and critical nucleus of 4 ± 0.4 αβ-
1452 tubulins. See Figure 2C-D for comparison with experimental results. (B) MT nucleation dynamics
1453 from a closed γ-TuRC were simulated to compare with experimental data for blunt-seed mediated
1454 MT assembly. Parameter values used: $k_{on} = 1.3 \times 10^6\ (M^{-1}s^{-1}pf^{-1})$, $\Delta G_{Long,\alpha\beta-\alpha\beta} =$
1455 $-7.2k_BT$, $\Delta G_{Lat,\alpha\beta-\alpha\beta} = -6.5k_BT$, $\Delta G_{Long,\gamma-\alpha\beta} = 1.0\Delta G_{Long,\alpha\beta-\alpha\beta}$. An input for $k_{\gamma TuRC-conf}$
1456 or $\Delta G_{\gamma TuRC-conf}$ were not required because γ-TuRC does not undergo an open-to-closed
1457 transition. 200 simulations each were performed for a range of tubulin concentration 2-8μM. For
1458 each simulation, time point where over 50nm length of MT has assembled was recorded.
1459 Probability of MT nucleation (*p*(*t*)) versus time (*t*) is displayed in (i). The initial rate of nucleation
1460 $\left.\frac{dp}{dt}\right|_{t\to 0}$ was measured at each tubulin concentration and plotted against concentration, *C*-*C** on a
1461 log-log axis in (ii). Critical concentration of polymerization, *C**=1.4μM. Linear curve was fit for
1462 *n*=7 simulated data points, and critical nucleus of 1.1 ± 1 αβ-tubulins. See Figure 3D-E for
1463 comparison with experimental results. See also Figure 5.
1464

1465 **Figure 6-figure supplement 1. Effect of putative activation factor NME7 on γ-TuRC-**
1466 **mediated nucleation.**

1467 (A) A constant density of γ-TuRC molecules were attached without (left) and with (right) 6μM
1468 NME7 and 10.5μM tubulin ± 1μM additional NME7 was added. Experiments were repeated twice
1469 on different experimental days with the same γ-TuRC preparation. See also Figure 6 and Video 6.
1470

1471 **Figure 7-figure supplement 1. Role of XMAP215 on γ-TuRC-mediated microtubule**
1472 **nucleation.**

1473 (A) γ-TuRCs were attached and 3.5-7μM tubulin ± 20nM XMAP215-GFP was added. Experiment
1474 was repeated identically two times with independent γ-TuRC purifications. One additional
1475 replicated was performed with 7μM tubulin. (B) Number of MTs nucleated ($N(t)$) over time (t) is
1476 plotted and shaded regions represent 95% confidence interval $(n \pm 2\sqrt{n})$ in the number of
1477 nucleated MTs (n) assuming a Poisson distribution as described in Methods. Analyses were
1478 repeated twice with independent γ-TuRC purifications, and representative dataset is reported to
1479 highlight the absolute increase in the number of MTs nucleated by XMAP215. One additional
1480 supporting replicate was obtained only at 7μM tubulin. (C) Titrating tubulin with constant γ-TuRC
1481 and XMAP215 concentration. XMAP215/γ-TuRC molecules were observed to nucleate MTs at
1482 low tubulin concentrations of 1.6-3.5μM. Experiments were repeated at three times with
1483 independent γ-TuRC preparations, and fewer concentration points were repeated another two
1484 times. (D) The role of C-terminal region of XMAP215 or N-terminal region was tested in the
1485 cooperative nucleation with purified γ-TuRC. MTs nucleated by γ-TuRC alone (top-left panel), γ-
1486 TuRC with 20nM full-length XMAP215 (top-right panel), γ-TuRC with 20nM C-terminal domain
1487 containing TOG5 and C-terminus of XMAP215 (bottom-left panel), or γ-TuRC with 20nM N-
1488 terminal domain containing TOG1-4 domains (bottom-right). While the N-terminus is not
1489 sufficient for MT nucleation, C-terminal domain of XMAP215, which binds γ-TuRC directly, also

1490 does not stimulate MT nucleation from γ-TuRC. (E) MT nucleation was measured, and number of
1491 MTs nucleated with wild-type XMAP215 reactions at 150 seconds was set to 1 to account for
1492 variable γ-TuRC concentration across purifications. Individual dataset with ±wt XMAP215,
1493 TOG5-CT or TOG1-4 are reported with solid, dashed or dotted curves. The number of times the
1494 experiment in (D-E) was repeated independent γ-TuRC preparations is as follows: buffer (3), wild-
1495 type XMAP215 (3), TOG1-4 (2), TOG5-CT (2). All data was pooled and reported in (E). Shaded
1496 regions represent 95% confidence interval $(n \pm 2\sqrt{n})$ in the number of nucleated MTs (n)
1497 assuming a Poisson distribution as described in Methods. Scale bars, 10μm. See also Figure 7 and
1498 Videos 7-8.
1499
1500 **Figure 7-figure supplement 2. MCAK and Stathmin inhibit γ-TuRC-mediated nucleation.**
1501 (A) γ-TuRC molecules were attached to coverslips and either 10.5μM tubulin alone (left panels),
1502 10μM tubulin + 10nM MCAK (top-right) or 10μM tubulin + 5μM Stathmin (bottom-right) was
1503 added to the reaction. Both MCAK and Stathmin were observed to decrease the number of MTs
1504 nucleated. For MCAK, the experiment and control were repeated three times with independent γ-
1505 TuRC preparations. For Stathmin, the experiment and control were repeated identically two times
1506 with independent γ-TuRC preparations and an additional, supporting experiment was performed
1507 at a slightly different concentration (7μM tubulin ± 2μM Stathmin). See also Figure 7 and Video
1508 9.

1509 **Video Legends**

1510

1511 **Video 1. Microtubule nucleation from γ-TuRC complexes**

1512 γ-TuRC was attached to functionalized coverslips and MT nucleation was observed upon
1513 introducing fluorescent αβ-tubulin (gray). MTs nucleated from individual γ-TuRC molecules from
1514 zero length at 14μM αβ-tubulin and the plus-end of nucleated MTs polymerized, but not its minus-
1515 end. Elapsed time is shown in seconds, where time-point zero represents the start of reaction. Scale
1516 bar, 10 μm.

1517

1518 **Video 2. Microtubule nucleation from fluorescent, single γ-TuRC molecules**

1519 Alexa-568 labelled γ-TuRC (green) was attached to functionalized coverslips and MT nucleation
1520 was observed upon introducing fluorescent αβ-tubulin (red). MTs nucleated from single γ-TuRC
1521 molecules at 10.5μM αβ-tubulin. Elapsed time is shown in seconds, where time-point zero
1522 represents the start of reaction. Scale bar, 10 μm.

1523

1524 **Video 3. γ-TuRC molecules nucleate microtubules efficiently**

1525 Constant density of γ-TuRC was attached while concentration of fluorescent αβ-tubulin was
1526 titrated (3.5-21μM) and MT nucleation was observed. γ-TuRC molecules nucleated MTs starting
1527 from 7μM tubulin and MT nucleation increased non-linearly with increasing tubulin concentration.
1528 Elapsed time is shown in seconds, where time-point zero represents the start of reaction. Scale bar,
1529 10 μm.

1530

1531 **Video 4. Spontaneous microtubule nucleation occurs at high tubulin concentration**

1532 Concentration of fluorescent αβ-tubulin was titrated (7-21μM) and spontaneous MT nucleation
1533 was assayed. MTs nucleated spontaneously starting from high concentration of 14μM tubulin and
1534 MT nucleation increased non-linearly with tubulin concentration. Both plus- and minus-ends of
1535 the assembled MTs polymerize. Elapsed time is shown in seconds, where time-point zero
1536 represents the start of reaction. Scale bar, 10 μm.
1537
1538 **Video 5. Microtubule assembly from blunt plus-ends resembles polymerization**
1539 MTs with blunt ends (seeds, cyan) were generated and attached to functionalized coverslips.
1540 Varying concentration of fluorescent αβ-tubulin was added (1.4-8.7μM, pseudo-colored as
1541 magenta) and MT assembly from seeds was assayed. MTs assembled at concentration above
1542 1.4μM tubulin, which is the minimum concentration needed for polymerization of MT plus-ends
1543 (*C**). Elapsed time is shown in seconds, where time-point zero represents the start of reaction.
1544 Scale bar, 10 μm.
1545
1546 **Video 6. γ-TuNA motif from CDK5RAP2, NME7 and TPX2 do not significantly increase γ-**
1547 **TuRC-mediated microtubule nucleation**
1548 Top panels: γ-TuRC was immobilized on coverslips with control buffer (left) or with 6μM γ-TuNA
1549 motif from CDK5RAP2 (right) and MT nucleation was observed upon introducing fluorescent
1550 10.5μM αβ-tubulin (gray) without or with 3μM γ-TuNA, respectively.
1551 Middle panels: γ-TuRC was immobilized on coverslips with control buffer (left) or with 6μM
1552 NME7 (right) and MT nucleation was observed upon introducing fluorescent 10.5μM αβ-tubulin
1553 (gray) without or with 1μM NME7, respectively.

1554 Bottom panels: γ-TuRC was immobilized on coverslips and MT nucleation was observed upon
1555 introducing fluorescent 10.5μM αβ-tubulin (pseudo-colored as red) without or with 10nM GFP-
1556 TPX2 (right, labelled as green). TPX2 bound along the nucleated MTs but did not significantly
1557 increase the MT nucleation activity of γ-TuRC molecules.
1558 Elapsed time is shown in seconds, where time-point zero represents the start of reaction. Scale bar,
1559 10 μm.
1560
1561 **Video 7. XMAP215 increases microtubule nucleation activity of γ-TuRC**
1562 γ-TuRC was immobilized on coverslips and MT nucleation was assayed with low concentration
1563 of fluorescent αβ-tubulin (3.5μM and 7μM) without (top panels) or with 20nM XMAP215-GFP
1564 (bottom panels). XMAP215 induces MT nucleation from γ-TuRC. Elapsed time is shown in
1565 seconds, where time-point zero represents the start of reaction. Scale bar, 10 μm.
1566
1567 **Video 8. Synergistic microtubule nucleation by γ-TuRC and XMAP215**
1568 Triple-color fluorescence microscopy was performed to observe the molecular sequence of events
1569 during MT nucleation from γ-TuRC and XMAP215. γ-TuRC (blue) and XMAP215 (red) formed
1570 a complex before MT nucleation occurred (pseudo-colored as green). For 50% of these events,
1571 XMAP215 remains on the nucleated minus-end. Elapsed time is shown in seconds, where time-
1572 point zero represents the start of reaction. Scale bar, 10 μm.
1573
1574 **Video 9. MCAK and Stathmin inhibit γ-TuRC-mediated microtubule nucleation**
1575 Top panels: γ-TuRC was immobilized on coverslips and MT nucleation was observed upon
1576 introducing fluorescent 10.5μM αβ-tubulin without (left) or with 10nM MCAK (right).

1577 Bottom panels: γ-TuRC was immobilized on coverslips and MT nucleation was observed upon
1578 introducing fluorescent 10.5μM αβ-tubulin without (left) or with 5μM Stathmin (right).
1579 Elapsed time is shown in seconds, where time-point zero represents the start of reaction. Scale bar,
1580 10 μm.
1581

Source Data files.

Figure 2-Source Data 1. Source data for Figure 2B-D. Each excel sheet is labelled with individual figure panel. For Figure 2C, all three experimental replicates are supplied, and dataset 1 is plotted.

Figure 3-Source Data 1. Source data for Figure 3 panels B, D, E and Figure 3-supplement 1C-D. Each excel sheet is labelled with individual figure panel. For Figure 3D, all three experimental replicates are supplied, and dataset 1 is plotted.

Figure 4-Source Data 1. Source data for Figure 4C.

Figure 6-Source Data 1. Source data for Figure 6 panels B, D.

Figure 7-Source Data 1. Source data for Figure 7 panels B, D, E, F and Figure 7-supplement 1 panels B, E. Each excel sheet is labelled with individual figure panel. For Figure 7D, all five experimental replicates are supplied, and dataset 1 is plotted.

1599 **Source Code.**

1600 MATLAB code for Monte Carlo simulations used to model the dynamics of γ-TuRC-mediated
1601 nucleation. Methods section details how the simulation was set up and performed. Figure 6-
1602 supplements 2 provide the parameters used to model our experimental data.

1603

Figure 1

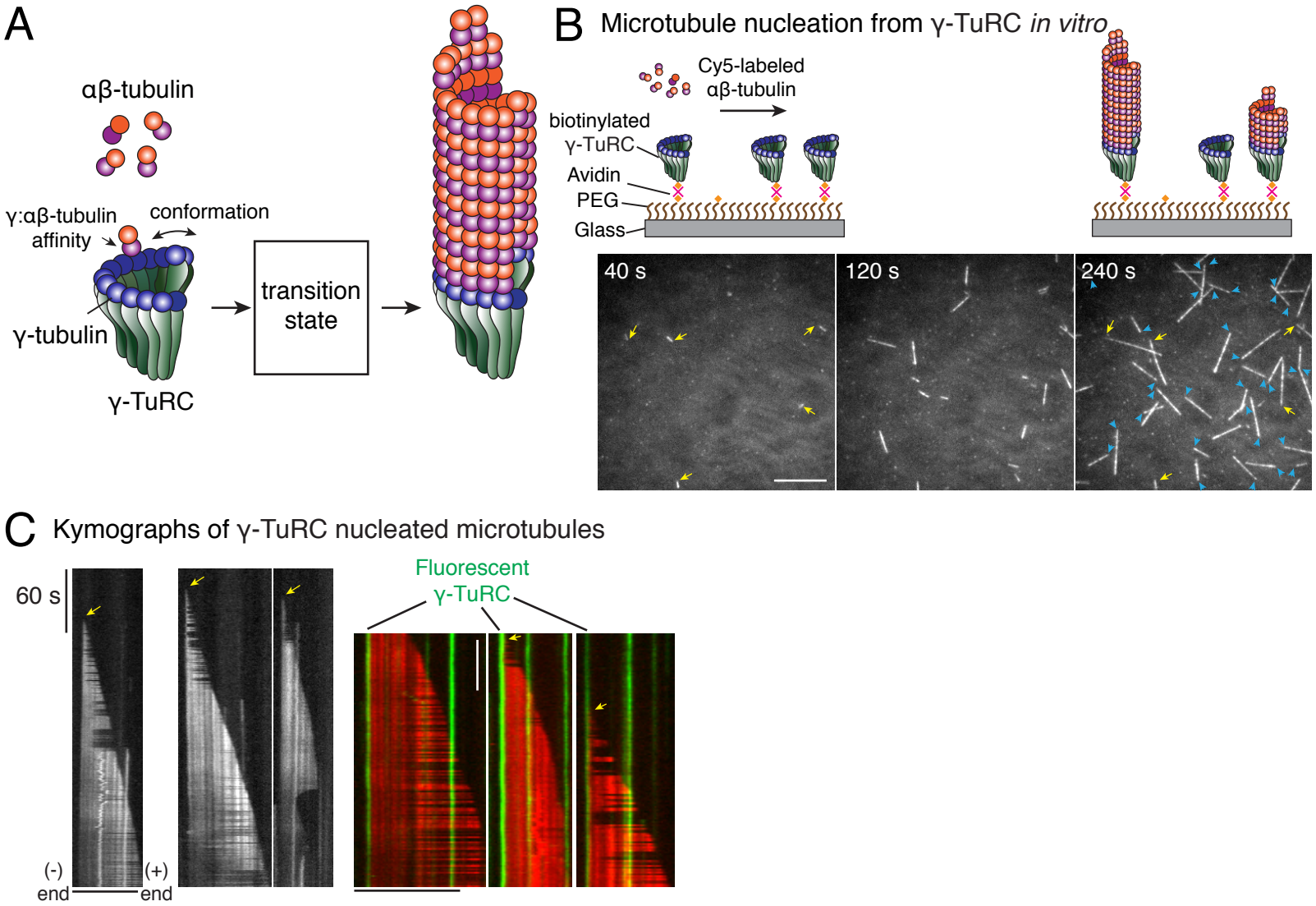
A
αβ-tubulin
γ:αβ-tubulin
affinity
conformation
γ-tubulin
γ-TuRC
transition
state
B
Microtubule nucleation from γ-TuRC *in vitro*
Cy5-labeled
αβ-tubulin
biotinylated
γ-TuRC
Avidin
PEG
Glass
40 s
120 s
240 s
C
Kymographs of γ-TuRC nucleated microtubules
60 s
(-)
end
(+)
end
Fluorescent
γ-TuRC

Figure 1-figure supplement 1

γ-TuRC purification and quality control reactions

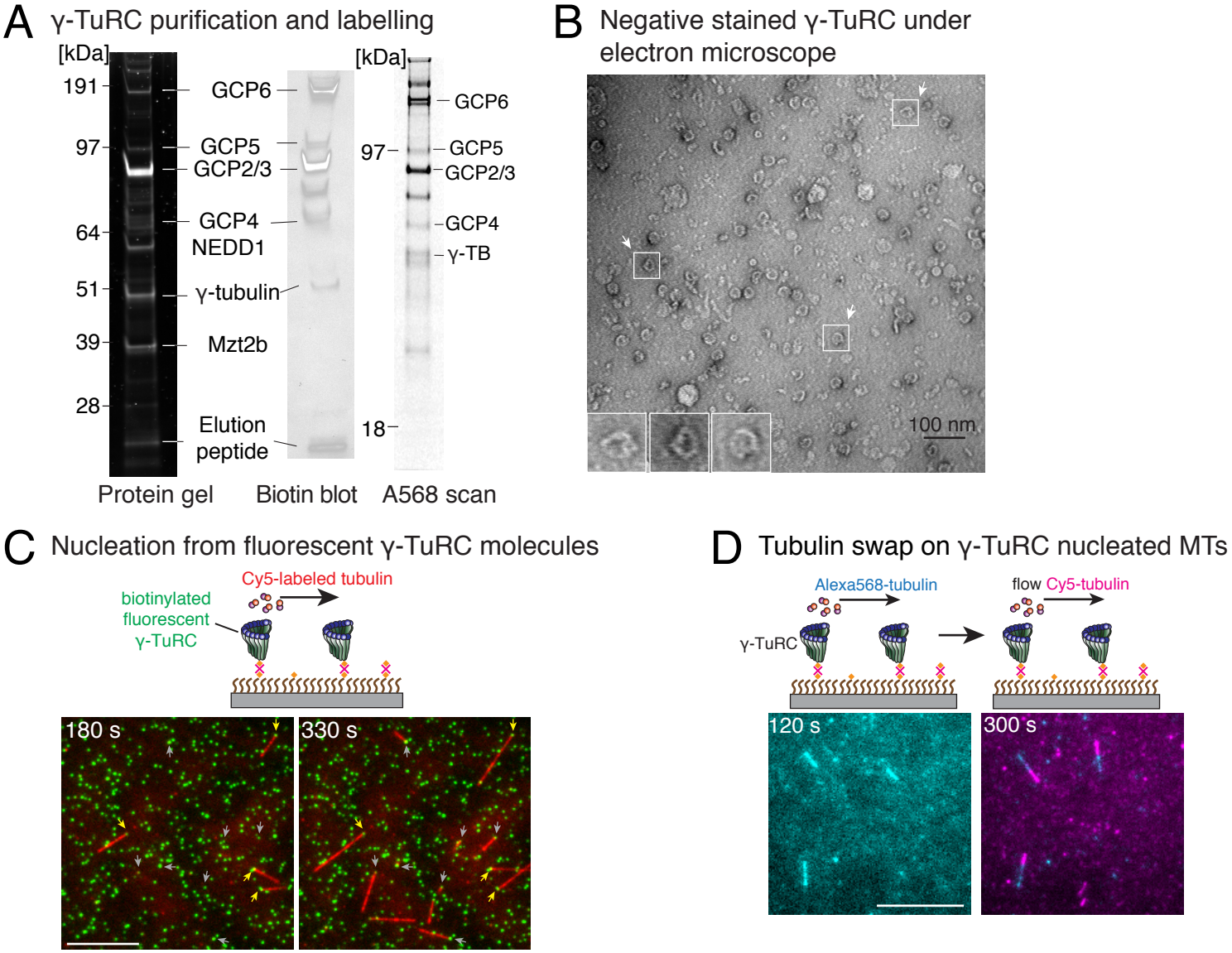

Figure 2

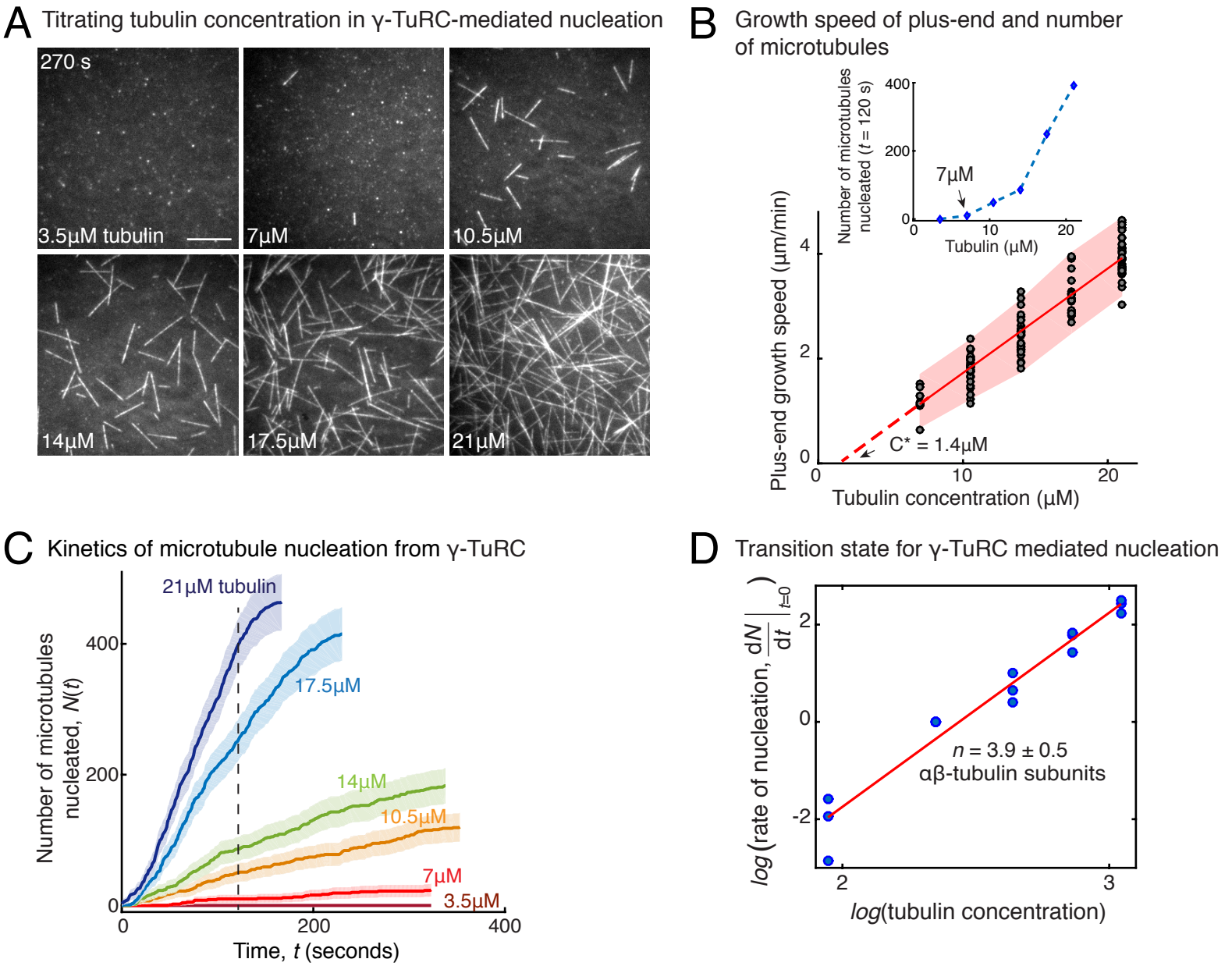
A
Titrating tubulin concentration in γ-TuRC-mediated nucleation
270 s
3.5μM tubulin
7μM
10.5μM
14μM
17.5μM
21μM
B
Growth speed of plus-end and number of microtubules
Number of microtubules nucleated (t = 120 s)
400
200
0
0
10
20
Tubulin (μM)
7μM
Plus-end growth speed (μm/min)
4
2
0
C* = 1.4μM
0
10
20
Tubulin concentration (μM)
C
Kinetics of microtubule nucleation from γ-TuRC
21μM tubulin
17.5μM
14μM
10.5μM
7μM
3.5μM
Number of microtubules nucleated, N(t)
400
200
0
0
200
400
Time, t (seconds)
D
Transition state for γ-TuRC mediated nucleation
log (rate of nucleation, dN/dt |t=0)
2
0
-2
n = 3.9 ± 0.5
αβ-tubulin subunits
2
3
log(tubulin concentration)

Figure 3

A Spontaneous microtubule nucleation

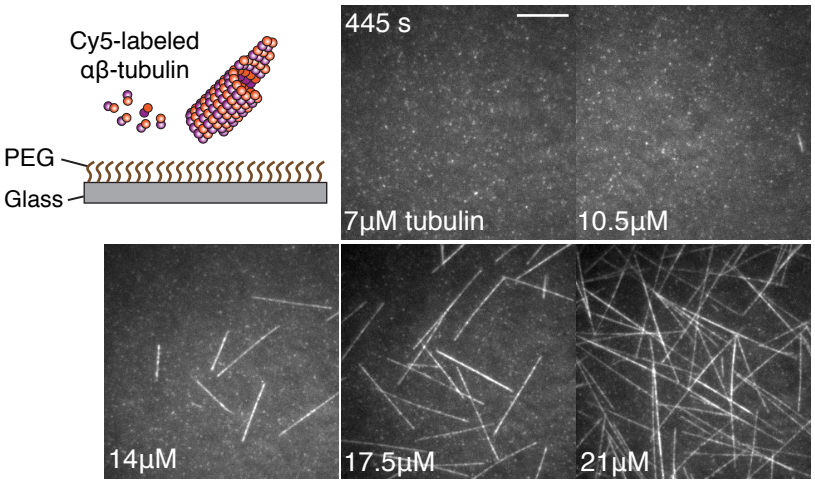

B Transition state for spontaneous nucleation

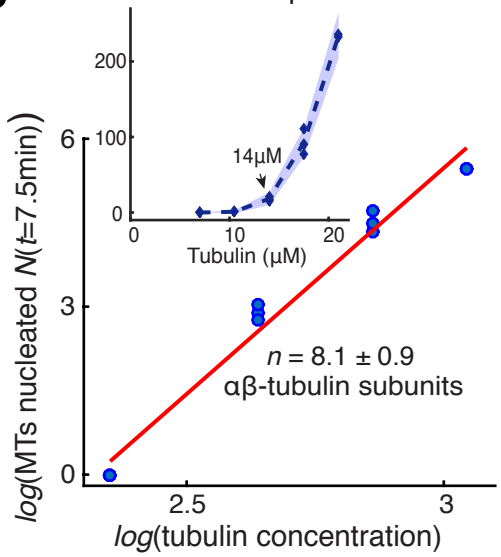

C Microtubule assembly from blunt seeds *in vitro*

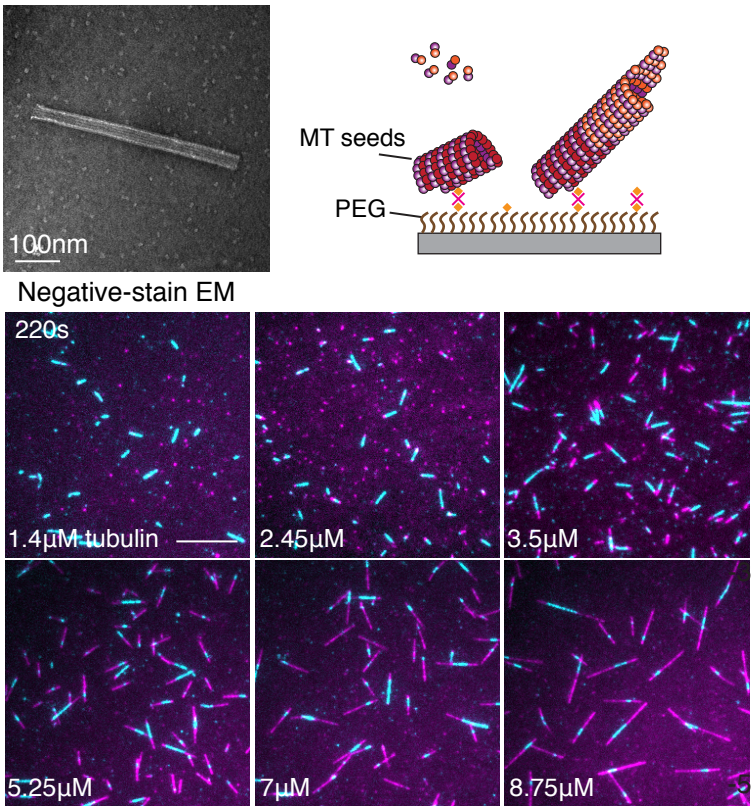

D

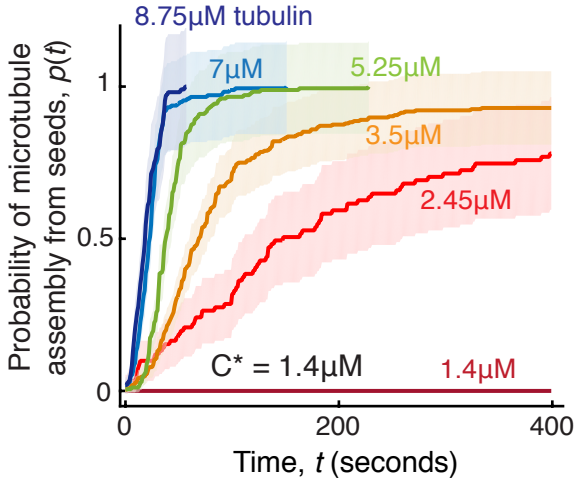

E Transition state for nucleation from blunt seeds

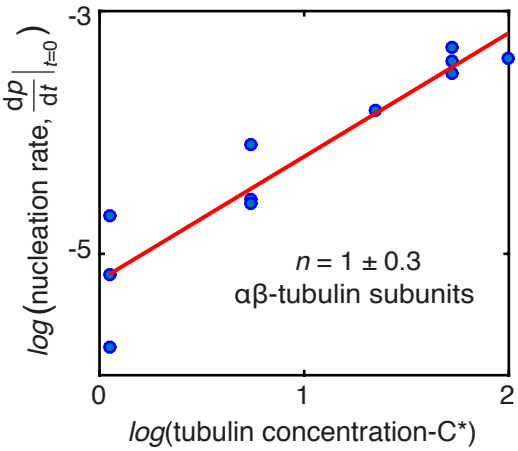

Figure 4

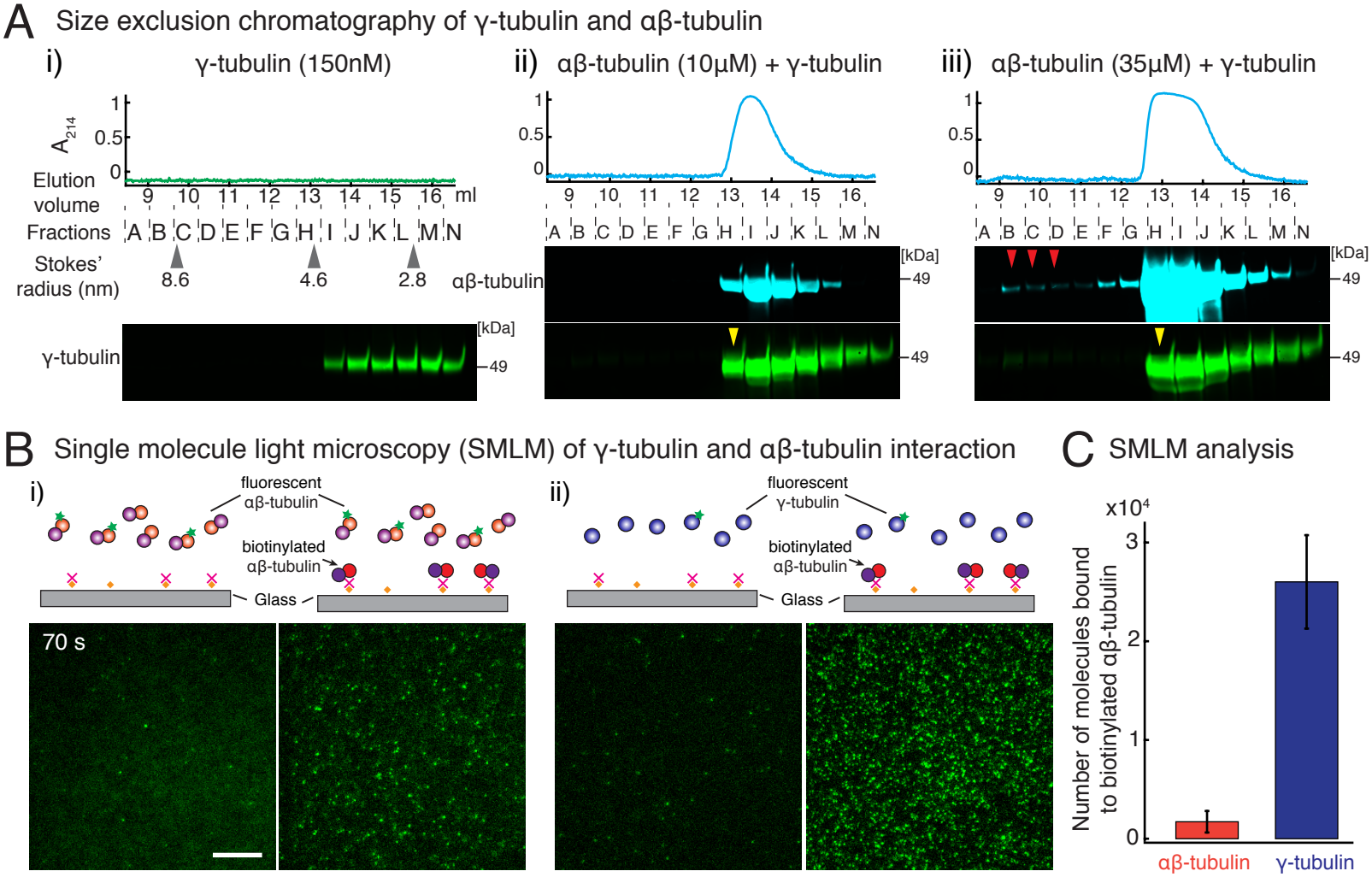
A Size exclusion chromatography of γ-tubulin and αβ-tubulin
i) γ-tubulin (150nM)
ii) αβ-tubulin (10μM) + γ-tubulin
iii) αβ-tubulin (35μM) + γ-tubulin
A214
Elution volume
ml
Fractions
Stokes' radius (nm)
8.6
4.6
2.8
αβ-tubulin
γ-tubulin
[kDa]
49
B Single molecule light microscopy (SMLM) of γ-tubulin and αβ-tubulin interaction
i)
fluorescent αβ-tubulin
biotinylated αβ-tubulin
Glass
70 s
ii)
fluorescent γ-tubulin
biotinylated αβ-tubulin
Glass
C SMLM analysis
x10⁴
Number of molecules bound to biotinylated αβ-tubulin
αβ-tubulin
γ-tubulin

Figure 3-figure supplement 1

Comparison of γ-TuRC-mediated and spontaneous nucleation

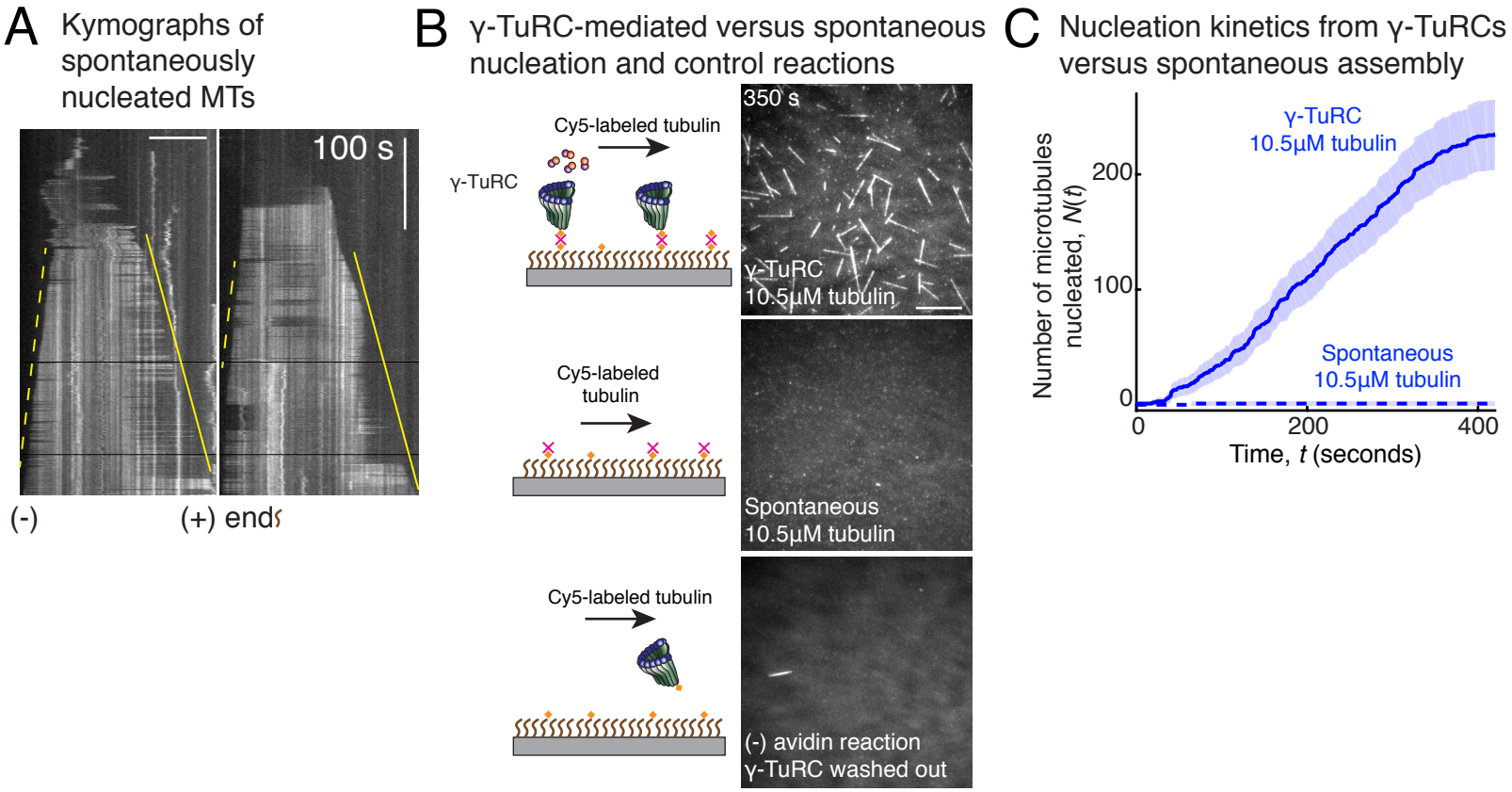

Growth speed of microtubule plus-ends assembled from blunt seeds and γ-TuRCs

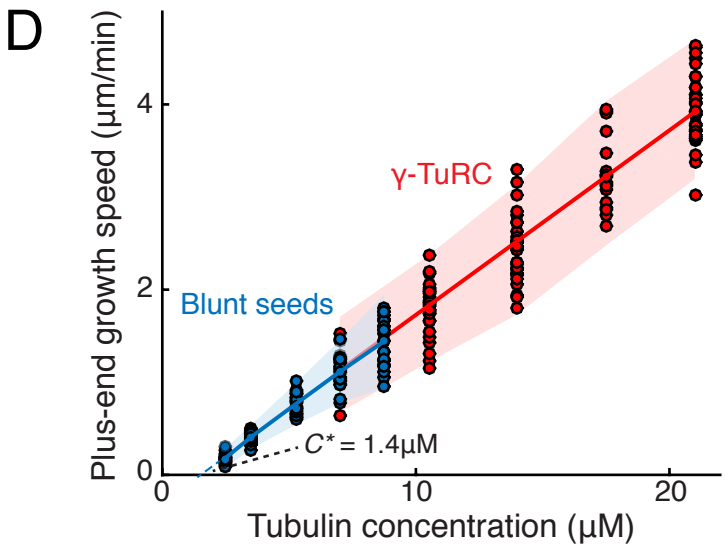

Figure 4

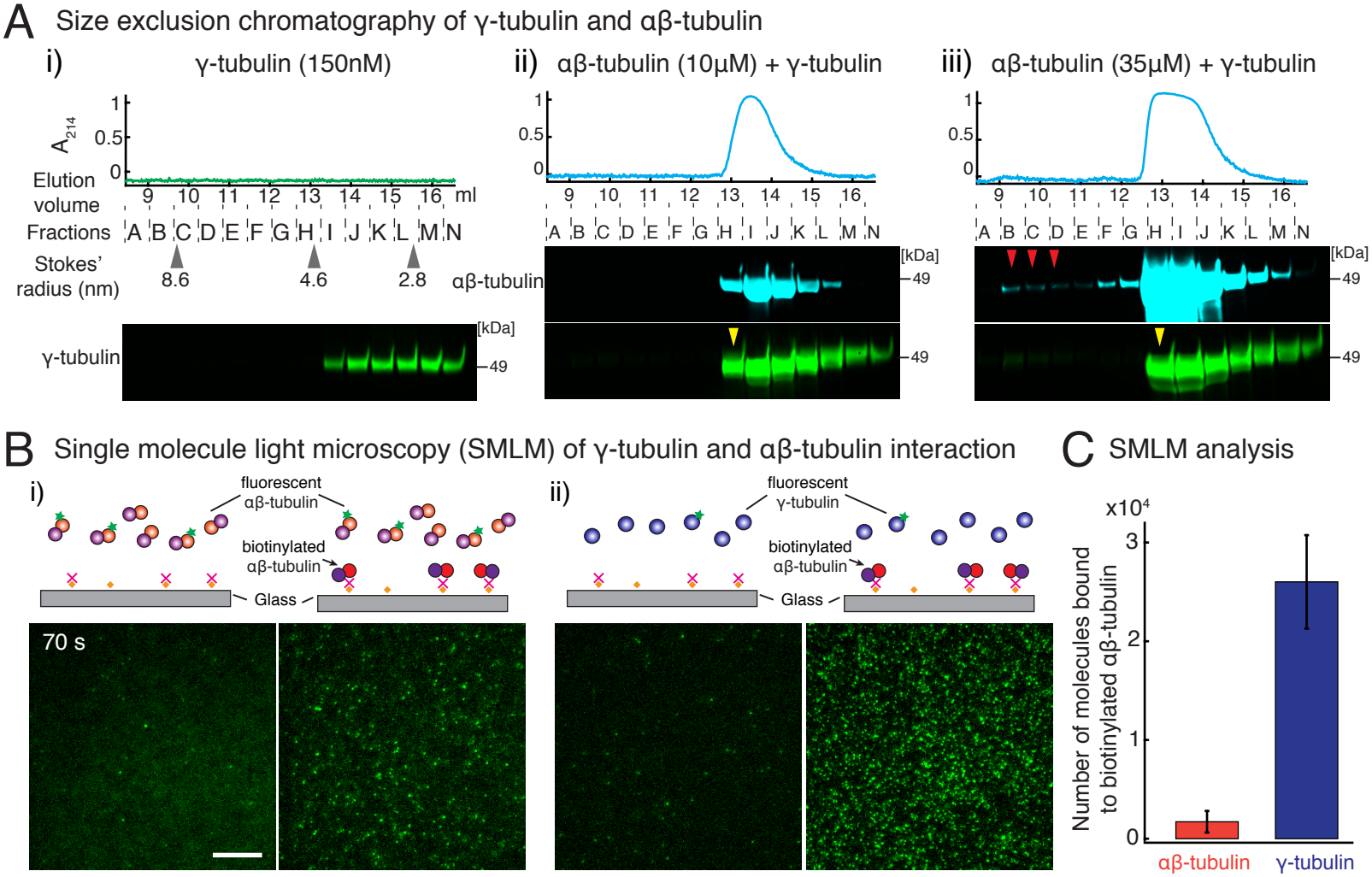
A Size exclusion chromatography of γ-tubulin and αβ-tubulin
i) γ-tubulin (150nM)
ii) αβ-tubulin (10μM) + γ-tubulin
iii) αβ-tubulin (35μM) + γ-tubulin
A214
Elution volume
ml
Fractions
Stokes' radius (nm)
8.6
4.6
2.8
αβ-tubulin
γ-tubulin
[kDa]
49
B Single molecule light microscopy (SMLM) of γ-tubulin and αβ-tubulin interaction
i)
fluorescent αβ-tubulin
biotinylated αβ-tubulin
Glass
70 s
ii)
fluorescent γ-tubulin
biotinylated αβ-tubulin
Glass
C SMLM analysis
x10⁴
Number of molecules bound to biotinylated αβ-tubulin
αβ-tubulin
γ-tubulin

Figure 4-figure supplement 1

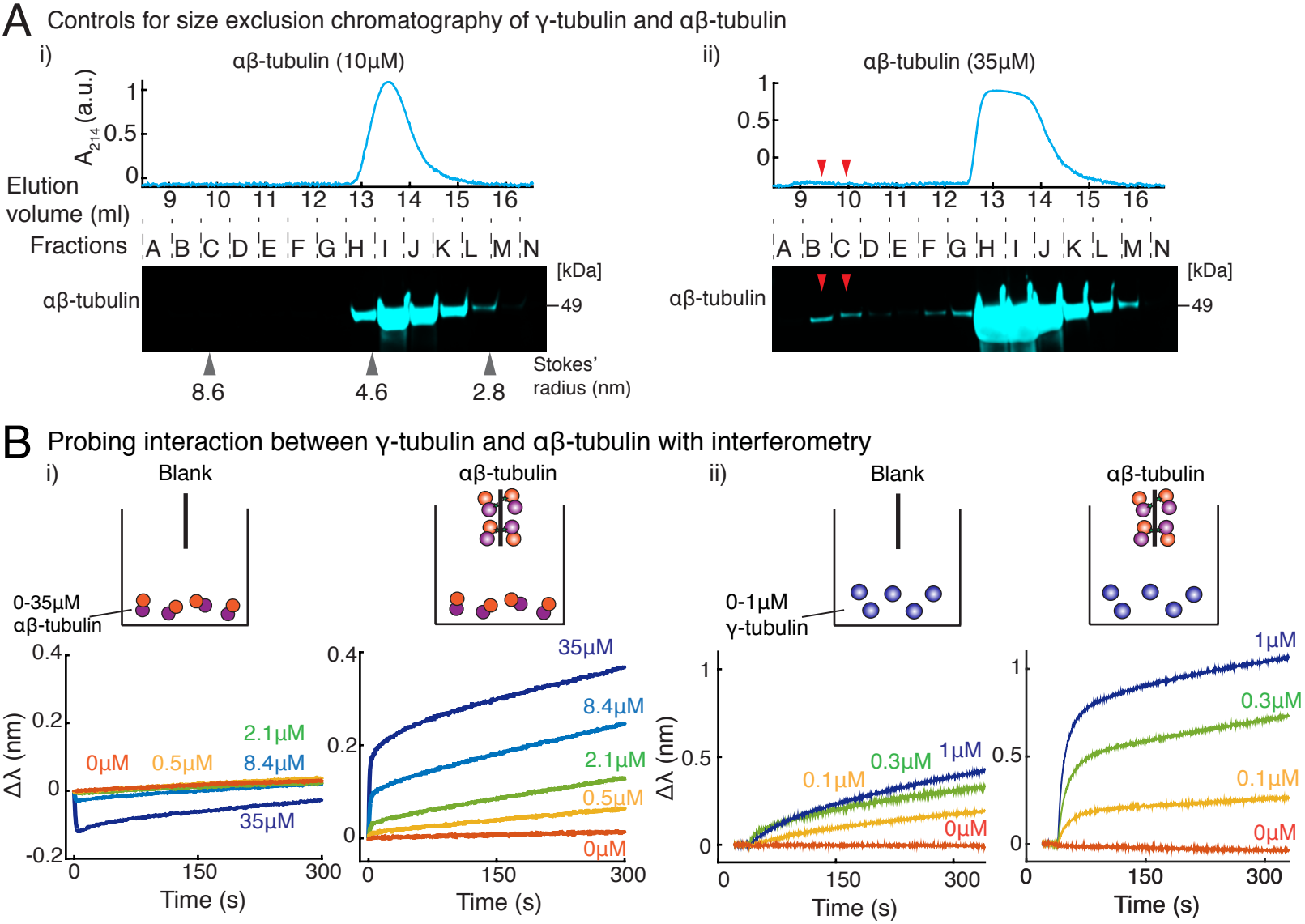

Figure 4-figure supplement 2

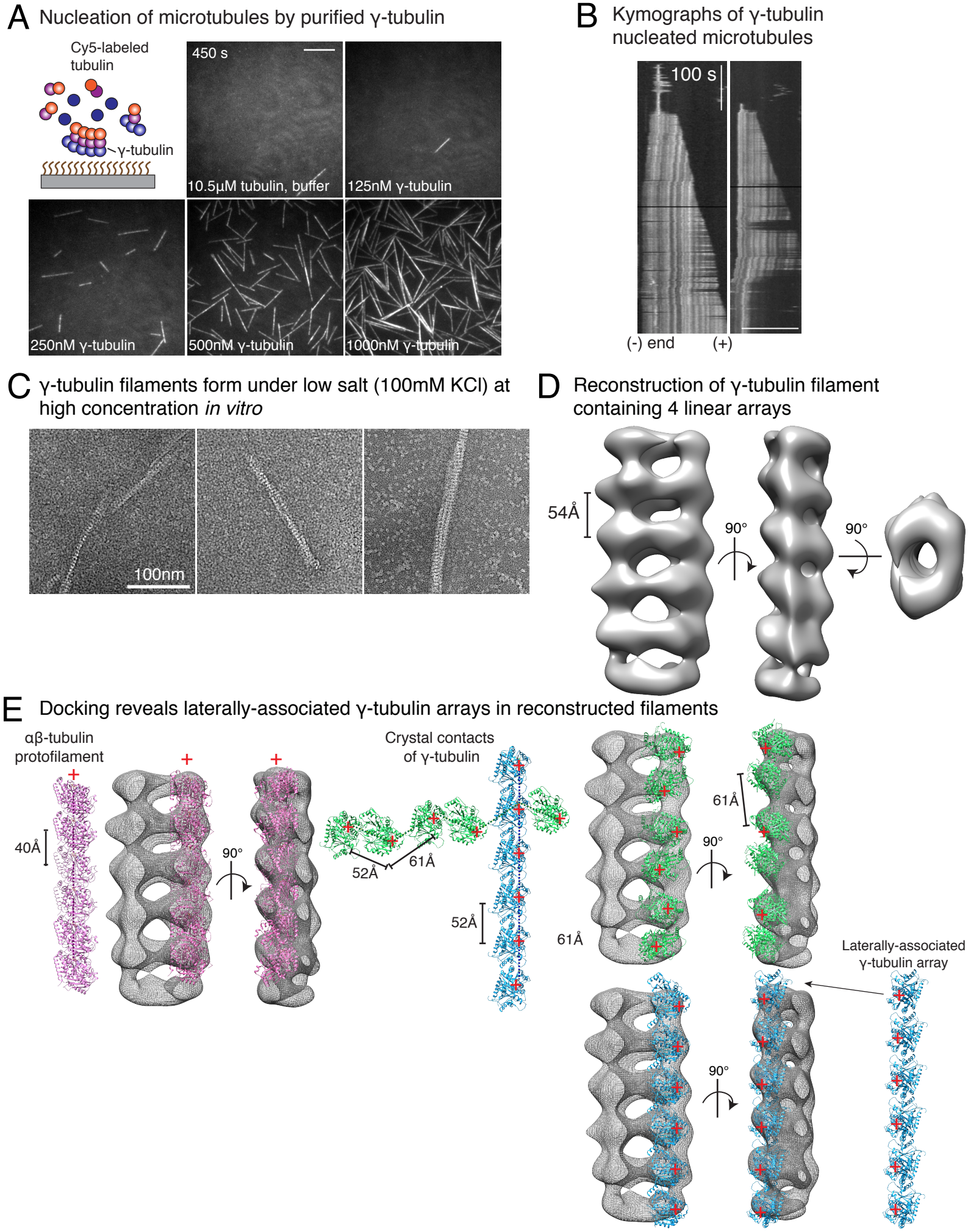

Figure 5

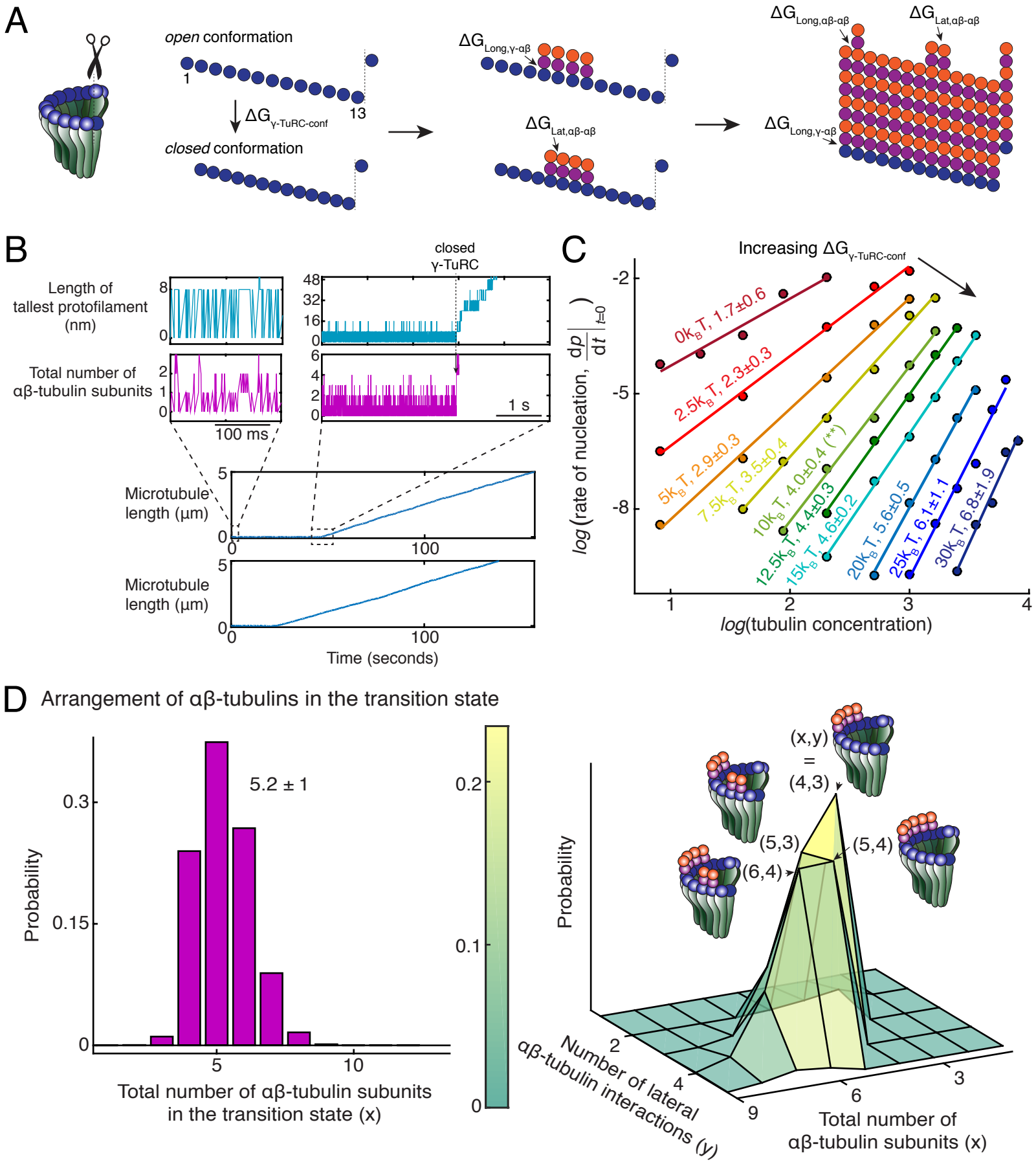
A
open conformation
closed conformation
ΔG γ-TuRC-conf
ΔG Long,γ-αβ
ΔG Lat,αβ-αβ
ΔG Long,αβ-αβ
B
Length of tallest protofilament (nm)
Total number of αβ-tubulin subunits
closed γ-TuRC
100 ms
1 s
Microtubule length (μm)
Time (seconds)
C
Increasing ΔG γ-TuRC-conf
0kBT, 1.7±0.6
2.5kBT, 2.3±0.3
5kBT, 2.9±0.3
7.5kBT, 3.5±0.4
10kBT, 4.0±0.4 (**)
12.5kBT, 4.4±0.3
15kBT, 4.6±0.2
20kBT, 5.6±0.5
25kBT, 6.1±1.1
30kBT, 6.8±1.9
log(rate of nucleation, dp/dt |t=0)
log(tubulin concentration)
D Arrangement of αβ-tubulins in the transition state
5.2 ± 1
Probability
Total number of αβ-tubulin subunits in the transition state (x)
(x,y) = (4,3)
(5,3)
(5,4)
(6,4)
Number of lateral αβ-tubulin interactions (y)
Total number of αβ-tubulin subunits (x)

Figure 5-figure supplement 1

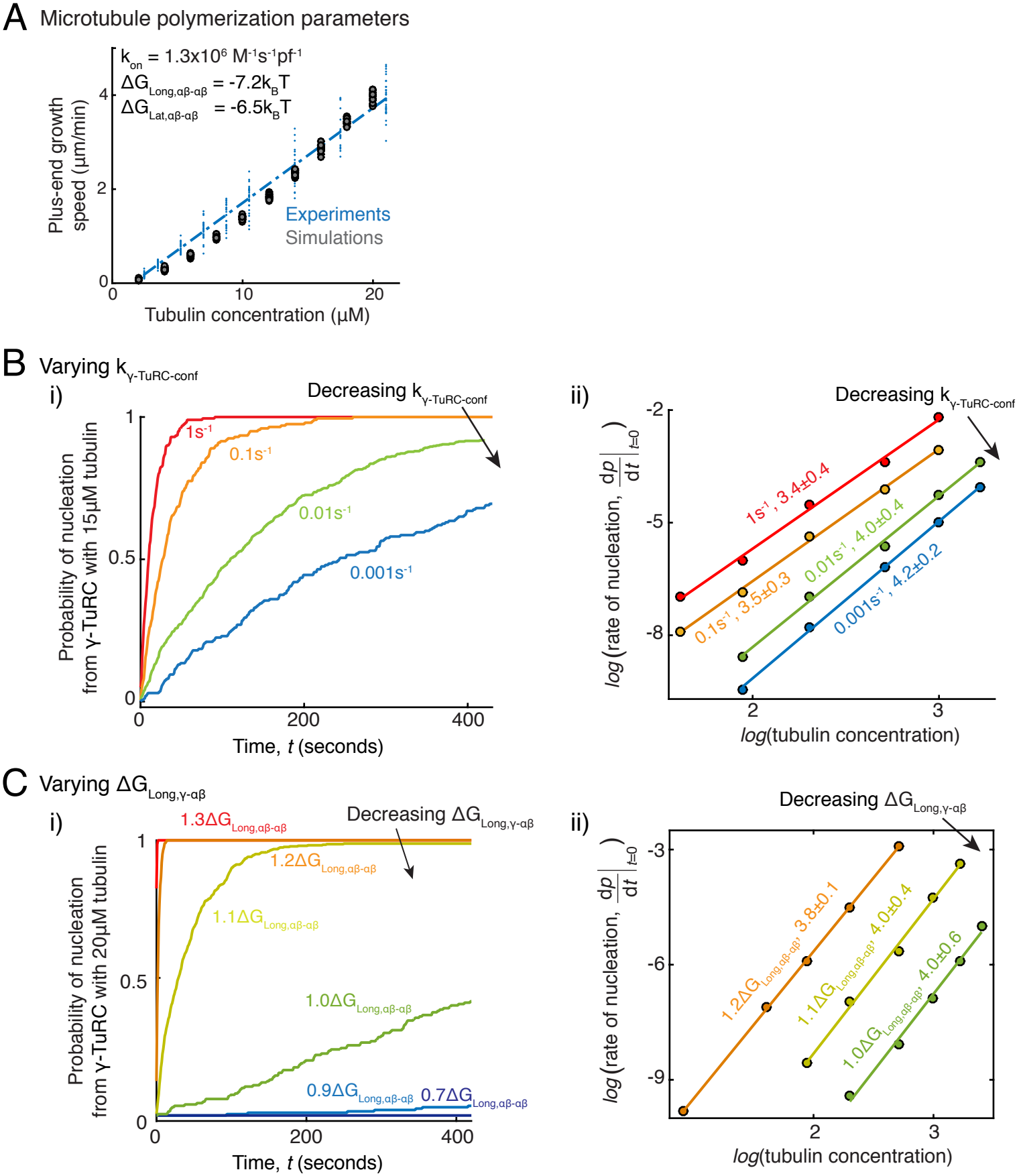

Figure 5-figure supplement 2

A Simulated kinetics of microtubule nucleation from γ-TuRC

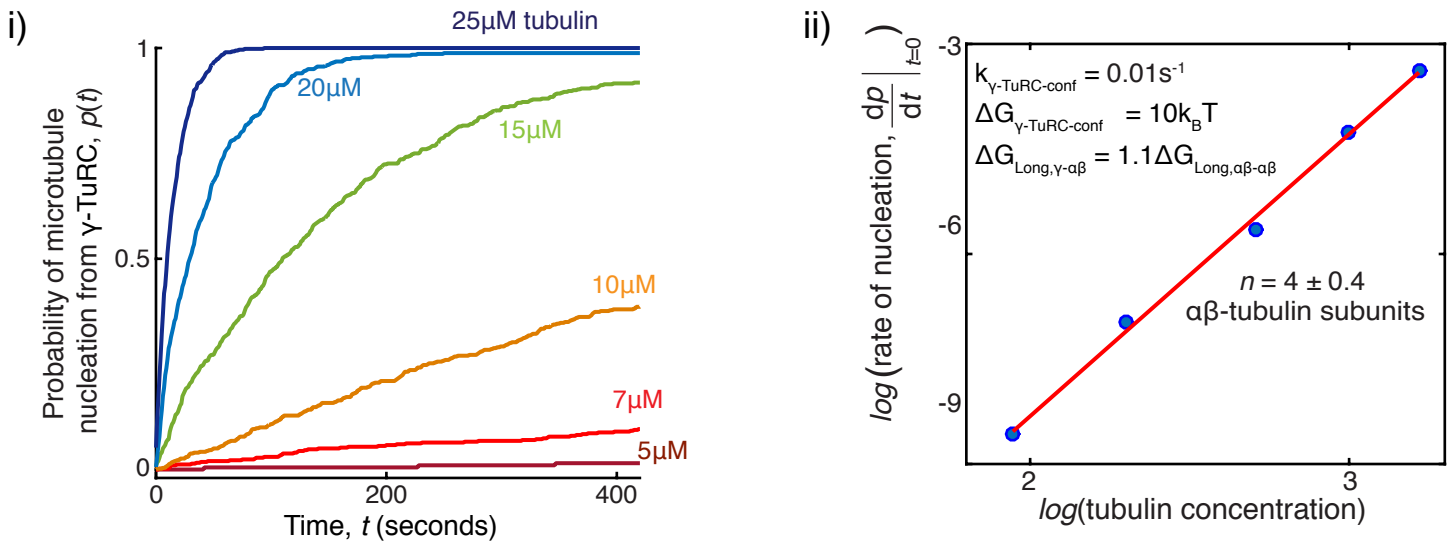

B Simulated kinetics of nucleation from *closed* γ-TuRC conformation

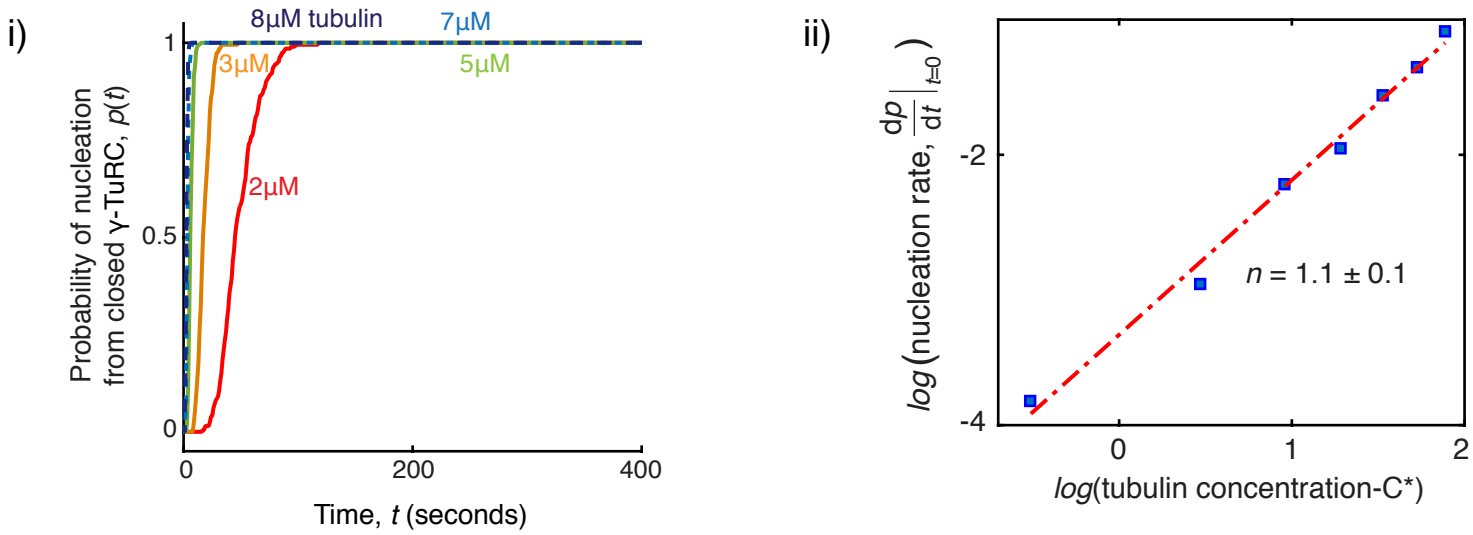

Figure 6

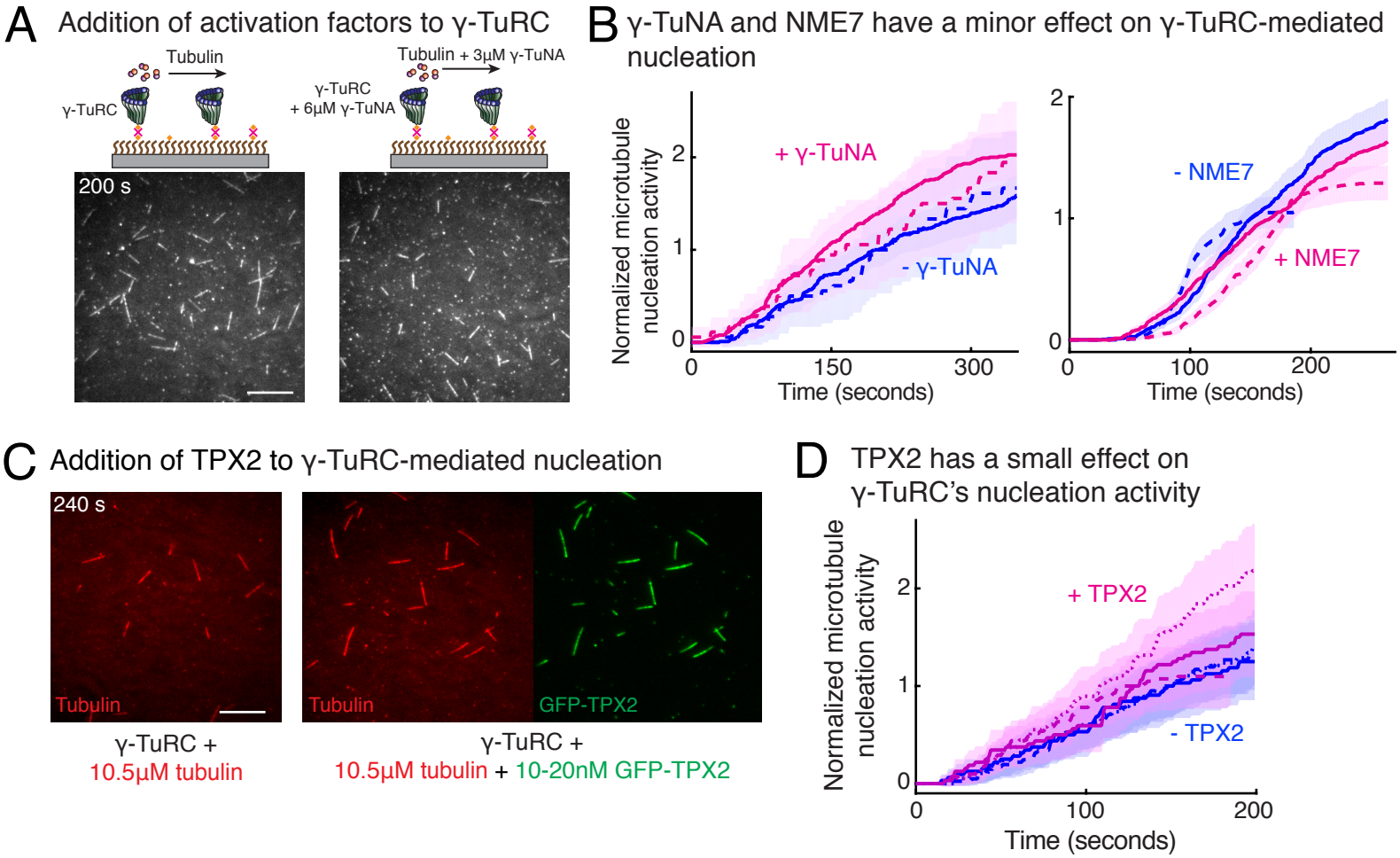
A
Addition of activation factors to γ-TuRC
Tubulin
γ-TuRC
Tubulin + 3μM γ-TuNA
γ-TuRC
+ 6μM γ-TuNA
200 s
B
γ-TuNA and NME7 have a minor effect on γ-TuRC-mediated nucleation
Normalized microtubule nucleation activity
+ γ-TuNA
- γ-TuNA
Time (seconds)
- NME7
+ NME7
Time (seconds)
C
Addition of TPX2 to γ-TuRC-mediated nucleation
240 s
Tubulin
Tubulin
GFP-TPX2
γ-TuRC +
10.5μM tubulin
γ-TuRC +
10.5μM tubulin + 10-20nM GFP-TPX2
D
TPX2 has a small effect on γ-TuRC's nucleation activity
Normalized microtubule nucleation activity
+ TPX2
- TPX2
Time (seconds)

Figure 6-figure supplement 1

Addition of NME7 to γ-TuRC

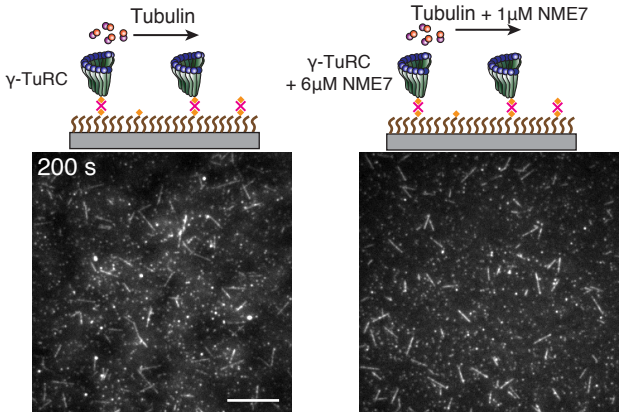

Figure 7

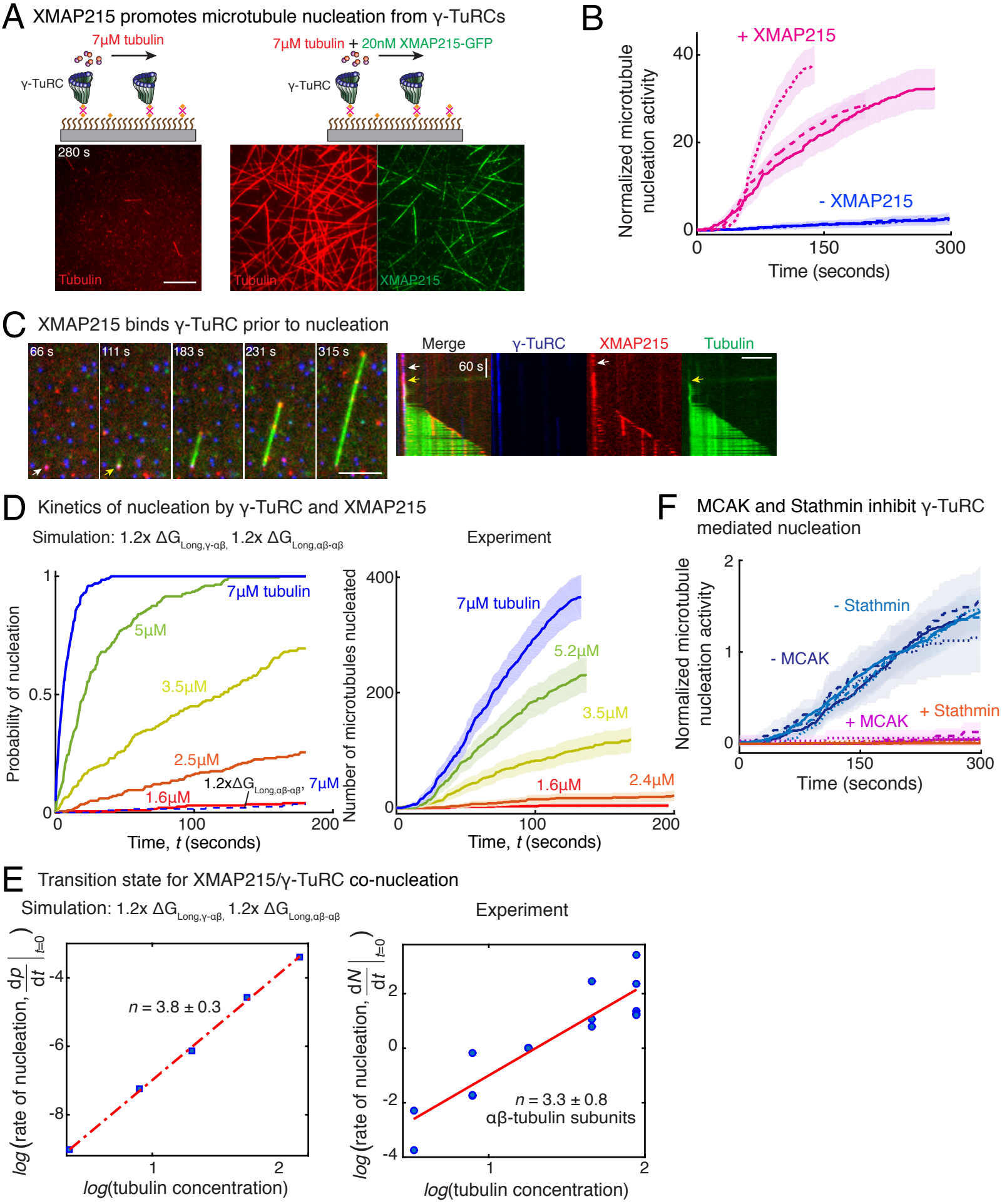
A XMAP215 promotes microtubule nucleation from γ-TuRCs
7μM tubulin
γ-TuRC
280 s
Tubulin
7μM tubulin + 20nM XMAP215-GFP
γ-TuRC
Tubulin
XMAP215
B
+ XMAP215
- XMAP215
Normalized microtubule nucleation activity
Time (seconds)
C XMAP215 binds γ-TuRC prior to nucleation
66 s
111 s
183 s
231 s
315 s
Merge
γ-TuRC
XMAP215
Tubulin
60 s
D Kinetics of nucleation by γ-TuRC and XMAP215
Simulation: 1.2x ΔG Long,γ-αβ, 1.2x ΔG Long,αβ-αβ
Experiment
Probability of nucleation
Number of microtubules nucleated
7μM tubulin
5μM
3.5μM
2.5μM
1.6μM
1.2xΔG Long,αβ-αβ, 7μM
5.2μM
2.4μM
Time, t (seconds)
F MCAK and Stathmin inhibit γ-TuRC mediated nucleation
- Stathmin
- MCAK
+ MCAK
+ Stathmin
Normalized microtubule nucleation activity
Time (seconds)
E Transition state for XMAP215/γ-TuRC co-nucleation
Simulation: 1.2x ΔG Long,γ-αβ, 1.2x ΔG Long,αβ-αβ
Experiment
log (rate of nucleation, dp/dt |t=0)
n = 3.8 ± 0.3
log(tubulin concentration)
log (rate of nucleation, dN/dt |t=0)
n = 3.3 ± 0.8
αβ-tubulin subunits
log(tubulin concentration)

Figure 7-figure supplement 1

A XMAP215 decreases the nucleation barrier from γ-TuRCs

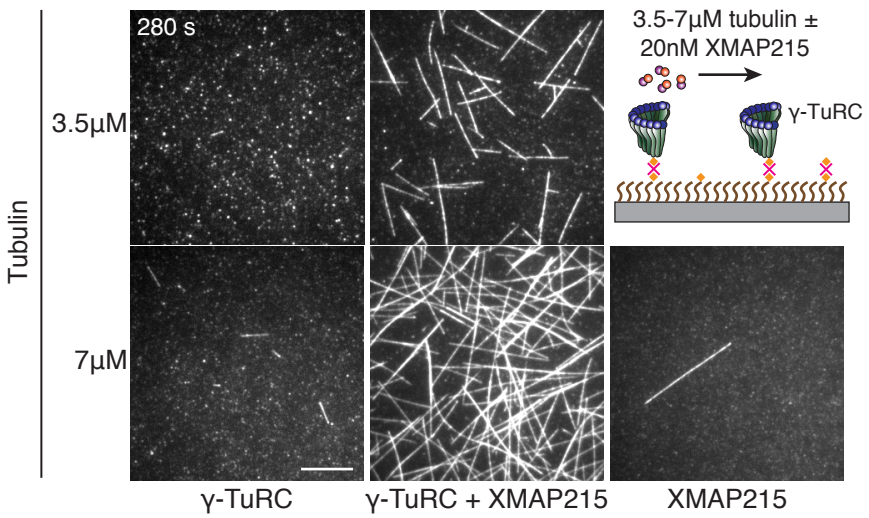

B

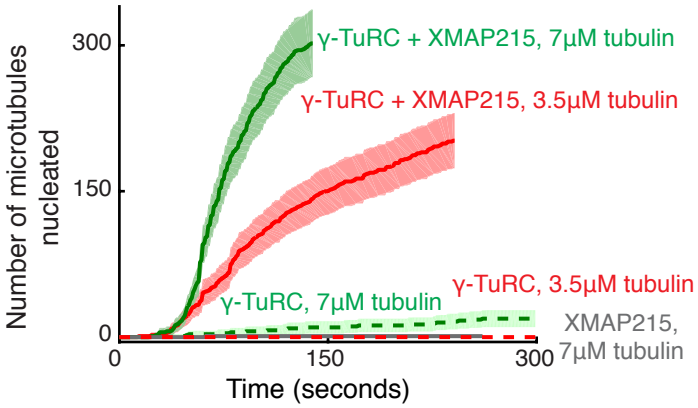

C Titrating tubulin concentration in γ-TuRC/XMAP215-mediated co-nucleation

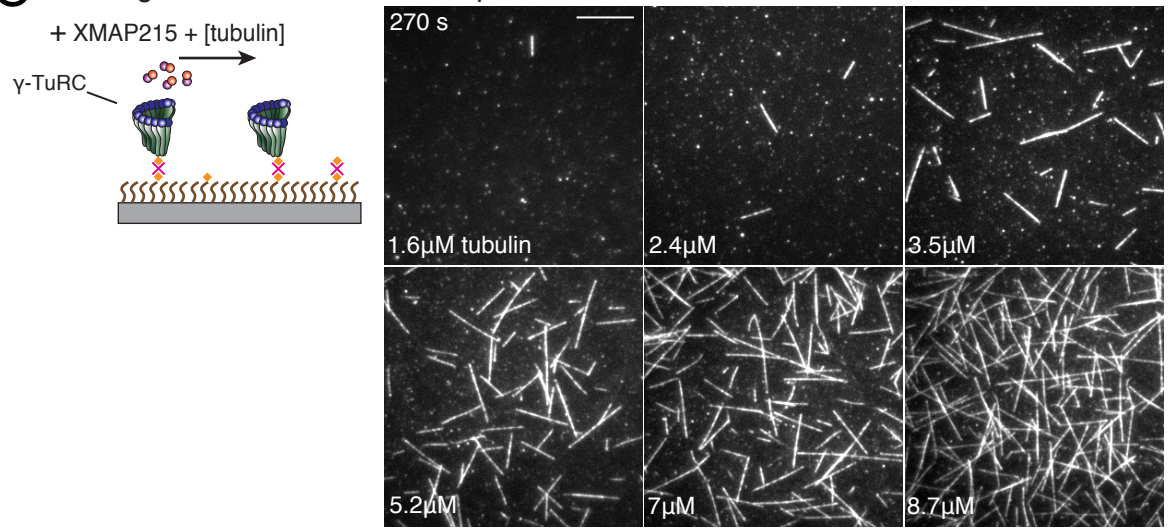

D Addition of XMAP215 truncations to γ-TuRC nucleation assay

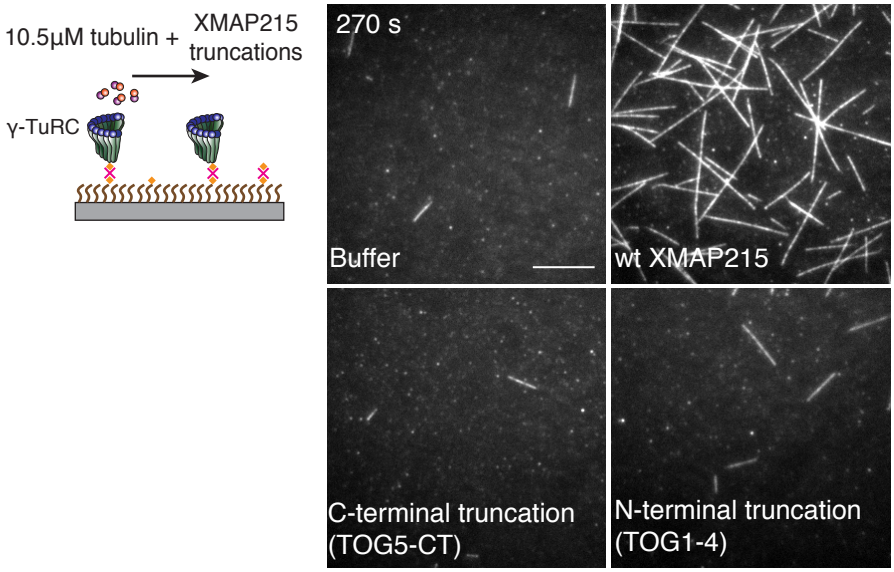

E C-terminal region of XMAP215 does not stimulate nucleation from γ-TuRC

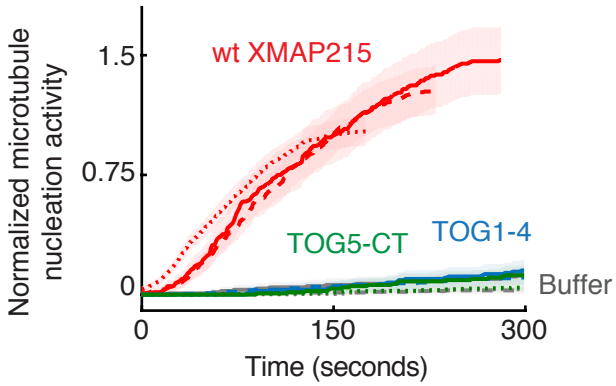

Figure 7-figure supplement 2
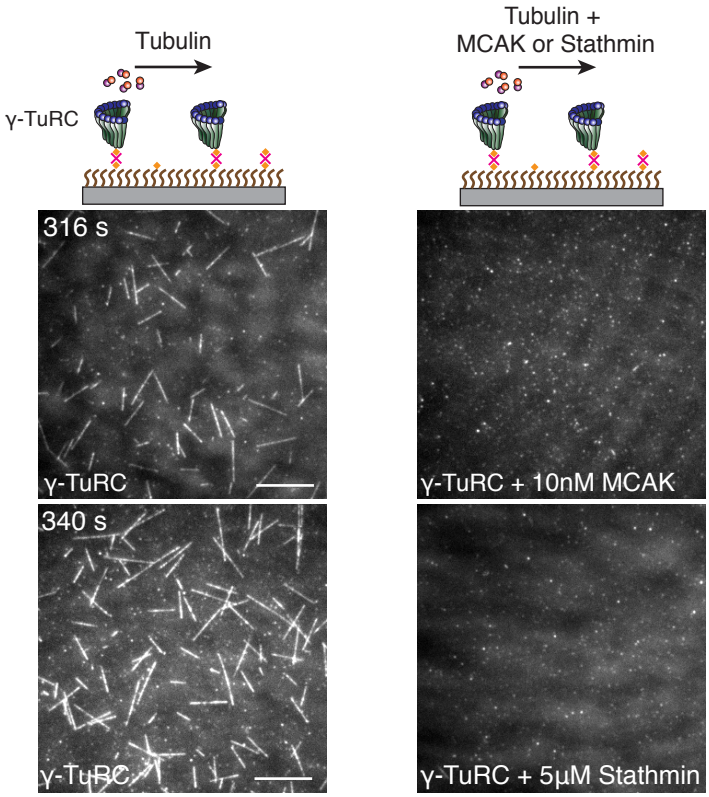
Addition of MCAK and Stathmin to γ-TuRC nucleation